Study of Interfacial Crack Propagation In Flip Chip Assemblies With Nano-Filled Underfill Materials

A Dissertation
Presented to
The Academic Faculty

By

Sakethraman Mahalingam

In Partial Fulfillment
of the Requirements for the Degree
Doctor of Philosophy in
G. W. Woodruff School of Mechanical Engineering

Georgia Institute of Technology
August 2005

© Copyright 2005 by Sakethraman Mahalingam

Study of Interfacial Crack Propagation In Flip Chip Assemblies With Nano-Filled Underfill Materials

Approved:

Prof. Suresh K. Sitaraman, Chairman
G. W. Woodruff School of Mechanical Engineering

Prof. Jianmin Qu
G. W. Woodruff School of Mechanical Engineering

Prof. Charles Ume
G. W. Woodruff School of Mechanical Engineering

Prof. Rao Tummala
The School of Electrical and Computer Engineering
& The School of Materials Science and Engineering

Dr. George White
Jacket Micro Devices

Dr. Sandeep Tonapi
General Electric Global Research

Date: 27 June 2005

"*It is not the mountain but ourselves we conquer*"

Tensing Norgay, on climbing Mount Everest

Dedicated to…

my late father, who taught me to be patient

my mother, for her unconditional love

and to my wife, for standing by my side.

ACKNOWLEDGEMENTS

I must admit that my enthusiasm during the course of this work was at times reduced to a mere hope. I would like to acknowledge all the people who have directly and indirectly helped me translate this hope into reality.

First of all, I would like to thank my advisor, Dr. Suresh Sitaraman for giving me the opportunity to study at Georgia Tech. In the aftermath of my father's sudden demise in October 2002, he urged me to continue my Ph.D. and I sincerely thank him for his encouragement and support. Much of the research presented in this thesis was done during my tenure at the General Electric Global Research Center in Bangalore, India and Dr. Sitaraman's patient, sincere and insightful reviews during this time have helped in steering this effort in the right direction.

I would like to thank Dr. Jianmin Qu, Dr. Charles Ume, Dr. Rao Tummala and Dr. George White for spending their valuable time serving on my committee and for their helpful suggestions. Besides serving on my committee, Dr. Sandeep Tonapi has been a great friend and I thank him for all his support, personal and professional.

On the personal side, I would like to first thank my late father for making countless sacrifices for my sake. Through his own life, he taught me the value of perseverance and it gives me great joy in fulfilling his dream. My mother's unconditional love has always motivated me to give my best and I thank her for being my inspiration. I am grateful to my grandparents for nurturing me as a kid, even though I was too young to realize its value. My aunts, Mrs. Rama and Mrs. Lakshmi and my uncles, Mr. Narayanan and Mr. Venkatasubramanian have rendered invaluable help in a time of need and I will be forever indebted to them. Over the course of my Ph.D., my wife Sunitha has bravely endured with me all the hardships that life has thrown at us and I dedicate my Ph.D. to our future together. My parents-in-law have been very kind to me and I thank them

wholeheartedly for their unflinching support. I would like to acknowledge all the immediate members of my family for having helped me in small ways that have made a big difference in the end. I would like to thank Mr. Mohan and Mrs. Saraswathi for their genuine affection and support.

My good friends, Dr. Ananth Prabhakumar and Kunal Goray at the General Electric Global Research Center have played a big part in my success and I would like to thank them. I would like to appreciate Dr. Om Prakash for offering valuable suggestions during all our technical discussions. I would like to thank Donald Buckley, Prameela Susarla, Bansi Phansalkar and Dr. Somakumar at GE for all their help. I would like to thank the people at the Microsystems Packaging Research Center (PRC) for their support during my early days at Georgia Tech. I have always enjoyed my discussions with Dr. Pucha and I thank him for his inputs. All my mates in CASPaR Lab were an integral part of my experience at Georgia Tech. and I thank them for their friendship. My friends - Manas Bajaj, Arnab Choudhury, Kunal Singh, Jitesh Panchal and Sriram Kanvah have been wonderful companions throughout my stay in Atlanta and I would not have made it without them.

Finally, I would like to thank God for giving me the opportunity and strength to succeed at this level.

TABLE OF CONTENTS

ACKNOWLEDGEMENTS.. v

LIST OF TABLES x

LIST OF FIGURES xi

SUMMARY xv

CHAPTER 1…INTRODUCTION 1

CHAPTER 2…LITERATURE REVIEW 8

2.1 Flip Chip Reliability 8

2.2 Underfill Design.. 10

2.3 Finite Element Modeling of Underfill Delamination.................................... 11

2.4 Fracture Toughness Characterization.. 12

2.5 Fatigue Crack Propagation 15

2.6 Cohesive Zone Modeling 17

CHAPTER 3…OBJECTIVES, APPROACH AND OUTLINE 18

3.1 Gaps in Existing Research.. 18

3.2 Research Objectives.. 19

3.3 Thesis Outline.. 20

3.3.1 Characterization of Mechanical Properties of the Underfill................. 20

3.3.2 Interfacial Fracture Toughness Determination.................................... 20

3.3.3 Cohesive Zone Modeling.. 21

3.3.4 Fatigue Crack Propagation.. 21

3.3.5 Reliability of Flip Chip Assemblies with NFU 22

3.3.5 Design Guidelines 22

CHAPTER 4…MATERIAL CHARACTERIZATION 23
4.1 Synthesis of NFU Materials 23
4.2 Material Properties 26
CHAPTER 5…INTERFACIAL FRACTURE TOUGHNESS CHARACTERIZATION 35
5.1 Introduction 35
5.2 Single Leg Bending Test 37
5.2.1 Specimen Fabrication 38
5.2.3 Experimental Results 40
5.2.3 Extraction of Fracture Parameters 41
5.3 Residual Stress Induced Decohesion (RSID) Test 46
5.3.1 Specimen Fabrication 47
5.3.2 Experimental Results 50
5.3.3 Extraction of Fracture Parameters 52
5.4 Discussion 57
CHAPTER 6…COHESIVE ZONE MODELING 59
6.1 Introduction 59
6.2 Derivation of the Cohesive Law 64
6.2.1 Characterization of Normal Cohesive Element using RSID Test 65
6.2.2 Characterization of Tangential Cohesive Element using SLB Test 67
CHAPTER 7…EXPERIMENTAL CHARACTERIZATION OF FATIGUE CRACK PROPAGATION 70
7.1 Experiment 70
7.2 Results 73
7.3 Analysis 74

CHAPTER 8…RELIABILITY OF FLIP CHIP ASSEMBLIES WITH NANO-FILLED UNDERFILL MATERIAL........ 83

8.1 Experiment........ 83

8.2 Analysis of Delamination in Flip Chip Assembly........ 86

8.2.1 Monotonic Loading........ 88

8.2.2 Fatigue Loading........ 89

CHAPTER 9…GUIDELINES OF UNDERFILL DESIGN........ 92

9.1 Interfacial Delamination........ 92

9.2 Chip-Fillet Interface........ 94

9.3 Crack Deflection........ 96

9.4 L Crack........ 98

9.5 Corner Crack........ 99

9.6 Underfill Fillet Crack........ 101

9.7 Design Guidelines........ 102

CHAPTER 10…CONCLUSIONS, RESEARCH CONTRIBUTIONS AND FUTURE WORK........ 104

10.1 Conclusions........ 104

10.2 Research Contributions........ 107

10.3 Recommendations for Future Work........ 108

APPENDIX A…INTERFACIAL FRACTURE MECHANICS........ 110

APPENDIX B…CRACK IN A BILAYER UNDER UNIFORM TEMPERATURE CHANGE........ 114

APPENDIX C…CRACK IN A TRILAYER UNDER UNIFORM TEMPERATURE CHANGE........ 118

REFERENCES........ 121

LIST OF TABLES

Table 5.1 Properties of Materials Used in the SLB Test 42

Table 5.2 Fracture Toughness of the SiN-NFU Interface – SLB Test................. 45

Table 5.3 Material Properties.. 53

Table 5.4 Fracture Toughness of the SiN-NFU Interface – Residual Stress Induced Decohesion Test... 55

Table 7.1 Material Properties.. 75

Table 7.2 Energy Release Rate and Mode Mixity in Fatigue Testing 77

Table 8.1 Material Properties.. 88

LIST OF FIGURES

Figure 1.1 Conventional Flip Chip Assembly Process 3

Figure 1.2 Flip Chip Assembly Using No-Flow Underfill 4

Figure 1.3 Wafer Level Underfilling 5

Figure 1.4 Excellent Soldering Achieved Using Nano-filled No Flow Underfill [Prabhakumar, 2004] 6

Figure 2.1 Underfill Fillet Cracking and Corner Delamination [Mahalingam, 2001] 9

Figure 2.2 Delamination of the Fillet from the Die Edge [Mahalingam, 2001] 10

Figure 2.3 Delamination Around the Solder Joints [Mahalingam, 2001] 10

Figure 2.4 Four Bending Specimens [Qu et al, 2000 ; Matos et al, 1989] 13

Figure 2.5 Compact Mixed Mode Specimen [Pang et al, 2002] 14

Figure 4.1 Functionalization of Nano-sized Silica [Liu et al, 2003] 25

Figure 4.2 TEM of NFU Showing Uniform Dispersion of Functionalized Silica Fillers 25

Figure 4.3 Effect of Filler Content on Underfill Material Properties 26

Figure 4.4 Effect of Underfill Viscosity and Assembly Parameters on Dwell Time 30

Figure 4.5 Temperature Dependent CTE of the Nano-filled Underfill 32

Figure 4.6 Temperature Dependent Modulus of the Nano-filled Underfill 32

Figure 4.7 Glass Transition Temperature Measured by TMA 33

Figure 5.1 Single Leg Bending Test 38

Figure 5.2 SLB Specimen Fabrication 40

Figure 5.3 Typical Load-Displacement Curve 41

Figure 5.4 Single Leg Bending Test Specimen Before and After Testing 41

Figure 5.5 Boundary Conditions for Cooling Down from Cure Temperature to Room Temperature 42

Figure 5.6 Contour Plot of Residual Shear Stresses Showing the Path for J Integral 43

Figure 5.7 Contour Plot of Residual Peel Stresses........ 43

Figure 5.8 Deformed Shape of the SLB Specimen under Three-Point Bending. 44

Figure 5.9 Peel Stresses Due to Three-Point Bending 44

Figure 5.10 Residual Stress Induced Decohesion Test........ 48

Figure 5.11 Fabrication of Residual Stress Induced Decohesion Test Specimen 49

Figure 5.12 Residual Stress Driven Interfacial Delamination........ 50

Figure 5.13 Residual Stress Test Setup 51

Figure 5.14 Residual Stress Test - Temperature Vs. Voltage........ 52

Figure 5.15 Boundary Conditions in the Finite-Element Model........ 53

Figure 5.16 Peel Stresses Close to the Crack Tip 53

Figure 5.17 Vertical Displacement Due to Residual Stresses........ 54

Figure 5.18 Effect of PC Layer Thickness on ERR........ 57

Figure 6.1 Cohesive Zone 60

Figure 6.2 Traction Displacement Curve Used by [Cui et al, 1993] 61

Figure 6.3 Trapezoidal Traction-Displacement Law 63

Figure 6.4 Triangular Traction-Displacement Law 64

Figure 7.1 Fatigue Testing Specimen........ 71

Figure 7.2 Fatigue Specimen Fabrication........ 72

Figure 7.3 Progress of Delamination 74

Figure 7.4 Optically Visible Delamination 74

Figure 7.5 Finite Element Model of the Fatigue Specimen 75

Figure 7.6 Peel Stresses Around the Crack Tip at -55°C.................................. 76

Figure 7.7 Comparison Between Finite-Element Model and Analytical Model ... 78

Figure 7.8 Rate of Crack Propagation 80

Figure 7.9 Paris Law for Underfill Delamination.. 81

Figure 8.1 Test Vehicle.. 84

Figure 8.2 Underfill Fillet Cracking... 85

Figure 8.3 Delamination of the Underfill-Passivation Interface 86

Figure 8.4 Finite Element Model of Flip Chip Assembly 87

Figure 8.5 Model of Underfill Delamination.. 87

Figure 8.6 Elastic-Plastic Properties of Eutectic Solder..................................... 87

Figure 8.7 Growth of Delamination in Flip Chip Assembly................................. 90

Figure 8.8 NFU-SiN Interfacial Delamination in Flip Chip Assemblies................ 91

Figure 9.1 Delamination Patterns 93

Figure 9.2 Finite Element Model of the Chip-Fillet Crack 94

Figure 9.3 Effect of Underfill Properties on the ERR for the Chip-Fillet Crack.... 95

Figure 9.4 Effect of Underfill Properties on the Mode Mixity for the Chip-Fillet Crack.. 95

Figure 9.5 Paths for Crack Deflection... 97

Figure 9.6 Comparison of ERR for Different Crack Paths 97

Figure 9.7 Effect of Underfill Properties on the ERR for the L Crack.................. 98

Figure 9.8 Effect of Underfill Properties on the Mode Mixity for the L Crack 99

Figure 9.9 Effect of Underfill Properties on the ERR for the Corner Crack 100

Figure 9.10 Effect of Underfill Properties on the Mode Mixity for the Corner Crack 100

Figure 9.11 3D Model of a Flip Chip with a Fillet Crack at the Corner 101

Figure 9.12 Effect of Underfill Properties on the ERR for the Corner Fillet Crack 102

Figure A2.1 Crack between Two Elastic Layers – Superposition [Suo and Hutchinson, 1990]... 114

Figure A3.1 Crack in a Tri-layer Structure [Gaudette et al, 2000] 118

SUMMARY

No-flow underfill materials that cure during the solder reflow process is a relatively new technology. Although there are several advantages in terms of cost, time and processing ease, there are several reliability challenges associated with no-flow underfills. When micron-sized filler particles are introduced in no-flow underfills to enhance the solder bump reliability, such filler particles could prevent the solder bumps making reliable electrical contacts with the substrate pads during solder reflow, and therefore, the assembly yield would be adversely affected. The use of nano-sized filler particles can potentially improve assembly yield while offering the advantages associated with filled underfill materials.

The objective of this thesis is to study the thermo-mechanical reliability of nano-filled epoxy underfills (NFU) through experiments and theoretical modeling. In this work, the thermo-mechanical properties of NFU's with 20-nm filler particles have been measured. An innovative residual stress test method has been developed to measure the interfacial fracture toughness. Using the developed residual stress method and the single-leg bending test, the mode-mixity-dependent fracture toughness for NFU-SiN interface has been determined. In addition to such monotonic interfacial fracture characterization, the interface crack propagation under thermo-mechanical fatigue loading has been experimentally characterized, and a model for fatigue interface crack propagation

has been developed. A test vehicle comprising of several flip chips was assembled using the NFU material and the reliability of the flip-chip assemblies was assessed under thermal shock cycles between -40°C and 125°C. The NFU-SiN interfacial delamination propagation and the solder bump reliability were monitored. In parallel, numerical models were developed to study the interfacial delamination propagation in the flip chip assembly using conventional interfacial fracture mechanics as well as cohesive zone modeling. Predictions for interfacial delamination propagation using the two approaches have been compared. Based on the theoretical models and the experimental data, guidelines for design of NFUs against interfacial delamination have been developed.

CHAPTER 1

INTRODUCTION

The packaging of silicon into smaller devices has resulted in marked miniaturization of electronic products. However, this trend is not fully over, or as many say, not yet started. As more functionality gets built into a given size of silicon, packaging the silicon into smaller devices will continue to be a major challenge will require the development of high density interconnect techniques. Predictions are that by 2016, a high performance silicon chip will have more than 7000 solder joints at a spacing of 50 microns [ITRS roadmap, 2002].

Flip chip packaging, first developed by IBM in 1964 [Prasad, 1997], continues to be a very attractive technique to achieve electrical and mechanical connection between the chip and the substrate at small pitches. Originally known as Controlled Collapsible Chip Connection or C4, it was primarily done using ceramic substrates and the solder joints were arranged along the perimeter of the chip. Today, this technology passes the benefits of large-scale integration at the silicon level by allowing an array of solder joints that cover the entire area of the chip, commonly known as area array packaging. In addition, the chips are assembled on cheaper organic substrates using smaller solder joints.

The use of organic substrates for flip chip packaging results in the well-known problem of thermal mismatch between the chip and the substrate. The

Coefficient of Thermal Expansion (CTE) of silicon is about 3ppm/^{o}C and is closely matched to that of ceramic substrates, which is about 6ppm/^{o}C. On the other hand, organic substrates have a relatively higher CTE, about 16-17ppm/^{o}C. This means that as the assembly is heated (mostly due to its operation) the substrate expands about 5-6 times more than the silicon and the stresses on the solder joints reach fatal proportions [Suryanarayana et al, 1991]. As the solder joint pitch reduces, the standoff of the assembled solder joint reduces and this translates into lower thermo-mechanical reliability.

The thermal mismatch between the substrate and the chip is alleviated by the introduction of an underfill material (Figure 1.1). This adhesive material couples the chip and the substrate and has been shown to enhance the reliability of flip chips by over 30 times [Darbha et al, 1999]. However, underfilling introduces an additional step in the assembly of flip chip packages. This process (Figure 1.1) involves the capillary flow of the underfill through the gap between the substrate and the chip and hence is time consuming.

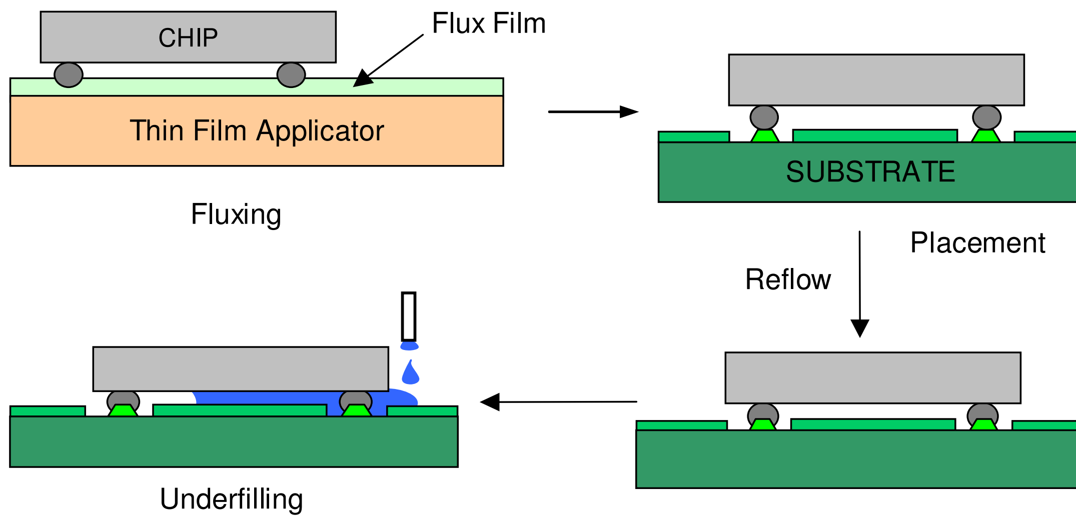

Figure 1.1 Conventional Flip Chip Assembly Process

The no-flow underfilling process (Figure 1.2) was developed to avoid the time consuming capillary flow at the end of reflow [Wang and Wong, 1996]. In this process, a special no-flow underfill is first dispensed on the substrate. Subsequently, the chip is placed on top of the substrate with sufficient force to displace the underfill. As the assembly passes through reflow, the no-flow underfill material acts as flux for the soldering process and is also cured by the end of reflow. Many no-flow underfill materials require some additional curing after the reflow process to completely harden them.

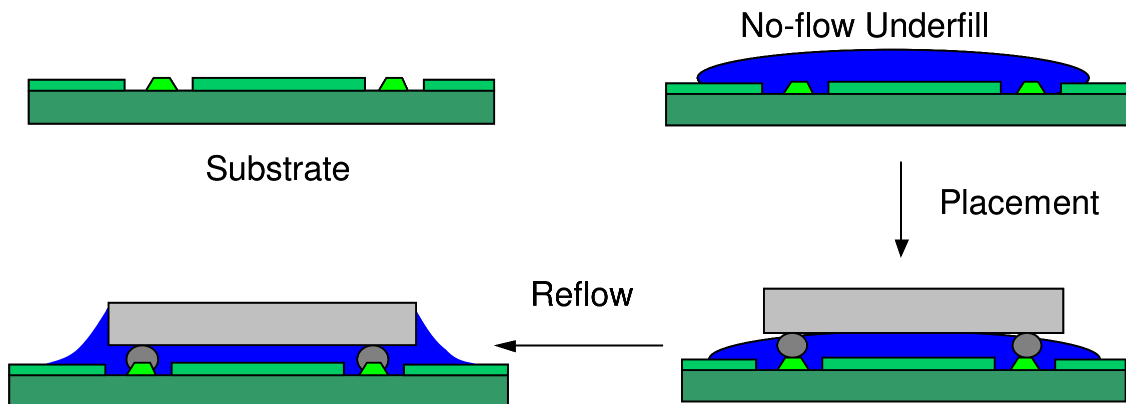

Figure 1.2 Flip Chip Assembly Using No-Flow Underfill

Wafer level underfilling [Prabhakumar et al, 2004] is a process in which the process of underfilling is accomplished immediately after wafer bumping (Figure 1.3). In this setup, the bumped wafer is coated with a layer of underfill material such that the solder bumps just stick out of the underfill layer. The underfill is then partially cured or B-staged. Later, the wafer is diced and assembled onto the substrate. Since the underfill is only partially cured, it starts to flow during reflow and an underfilled chip is obtained at the end of reflow. However, the partially cured underfill lacks the fluxing capacity of the uncured material and hence the chip has to be fluxed using a thin film applicator before placement (Figure 1.3).

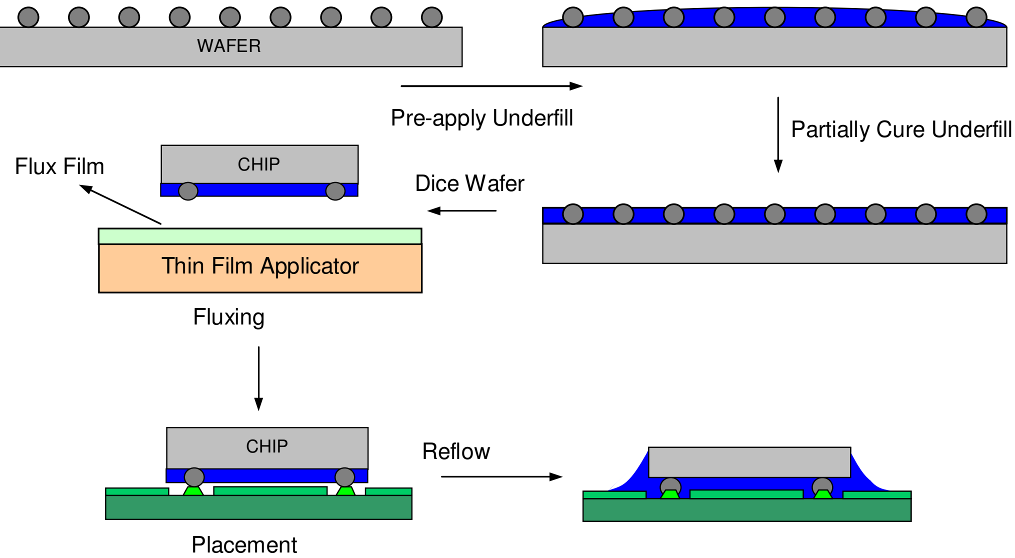

Figure 1.3 Wafer Level Underfilling

The underfill material is typically a resin material filled with ceramic particles such as silica or alumina. The modulus and viscosity of the underfill material increase with increase in filler content whereas the CTE decreases with increase in filler content [Qu and Wong, 2002]. As a general rule, underfills with higher modulus and lower CTE are preferred for good reliability while a low viscosity is useful in reducing the time spent in underfilling [Mahalingam, 2001]. A tradeoff between the three is achieved to get the correct filler content in the underfill. The size of the filler particles can vary from a few microns to about 25 microns and a standard capillary underfill will have about 40-65% filler particles by weight [Mahalingam, 2001].

Nano-filled underfills (NFU) [Prabhakumar et al, 2003; Gross et al, 2003; Rubinsztajn et al, 2003], as the name suggests, use nano-sized filler particles

instead of the micron sized ones. NFU possess a number of advantages over the conventional underfills. Most of the current no flow underfills are unfilled, as the filler particles tend to interfere with the soldering process. Further, unfilled materials tend to have a high CTE and a low modulus and reliability of such materials is poorer than conventional underfills [Mahalingam, 2001]. Compared to conventional micron sized fillers, NFU use nano-sized fillers that do not interfere with the soldering process [Prabhakumar, 2004] (Figure 1.4). However, they serve to reduce of the CTE and increase the modulus of the underfill. Further, previously unattainable combinations of underfill material properties are also made possible by using nano-sized fillers. In addition, NFU is optically transparent, making it an excellent choice for the wafer level underfilling process (Figure 1.3). The dicing of the wafer into individual chips requires the recognition of fiducials and an opaque underfill will not suit the process.

Figure 1.4 Excellent Soldering Achieved Using Nano-filled No Flow Underfill [Prabhakumar, 2004]

The underfill material has an important part in the reliability of flip chip devices. It is important to understand the performance of the nano-filled underfill materials in the context of reliability.

CHAPTER 2

LITERATURE REVIEW

The performance of the underfill material is crucial to the reliability of a flip chip package. The mechanical properties of the underfill such as the elastic modulus, coefficient of Thermal Expansion (CTE) and the adhesion of the underfill to silicon, passivation and other packaging materials are important factors that determine the performance of the underfill material. Underfill delamination, especially from passivation interface is the first step in the failure of an underfilled flip chip package. In this chapter, literature pertaining to interfacial delamination in general and underfill delamination in particular is presented.

2.1 Flip Chip Reliability

It would be fair to say that most electronic packaging problems are about getting the correct material combinations. Given this, it is not easy to change any one material in the system and expect the system to behave in the same fashion. It is therefore not surprising that underfilling does change the issues involved in flip chip packaging, not amongst the least of them is the reliability of the underfilled flip chip. Therefore, the design of the underfill material must be done with proper consideration of the failure modes of flip chips.

Two types of failures occur in an underfilled flip chip assembly, delamination and solder joint fatigue [Mahalingam, 2001; Smith et al, 2000]. Though both of these

mechanisms ultimately involve failure of the solder joint, the manner in which it is achieved is different. Corner delamination (Figure 2.1) is strongly correlated to cracking of the fillet at the corner of the flip chip package. It has been observed that thicker fillets tend to crack sooner in thermal cycling than thin ones. Once the fillet is cracked, delamination between the passivation and the underfill is initiated. As this delamination grows towards the solder joints, deformation of the solder reaches fatal proportions and premature failure of the joint is assured. Fillet cracks are also observed along the edges of the chip causing delamination between the vertical chip edge and the underfill fillet (Figure 2.2). This later could lead to delamination between the passivation and the underfill and result in solder joint failure. Solder joint fatigue occurs when delamination is initiated around the solder joint, mostly due to the presence of residues of the soldering process (Figure 2.3). Such a delamination causes a delayed failure of the solder joint and the solder ‘dies a more natural death’.

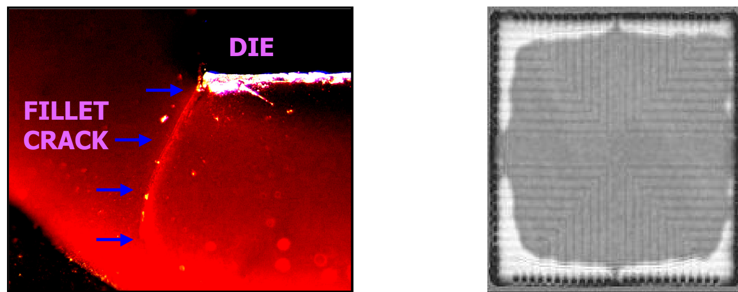

Figure 2.1 Underfill Fillet Cracking and Corner Delamination [Mahalingam, 2001]

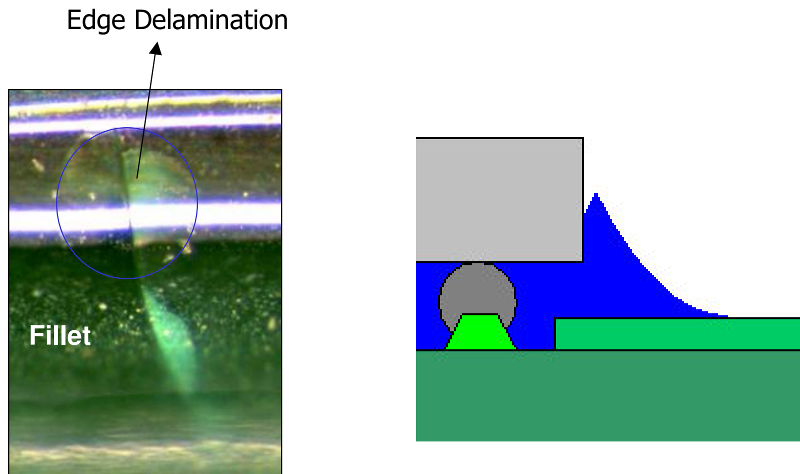

Figure 2.2 Delamination of the Fillet from the Die Edge [Mahalingam, 2001]

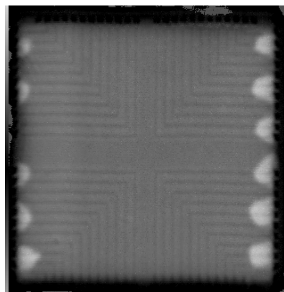

Figure 2.3 Delamination Around the Solder Joints [Mahalingam, 2001]

2.2 Underfill Design

Flip chip reliability and the design of the underfill material for the same has been the subject of many technical publications. Many of them do not include the presence of delamination in the different forms that were discussed above. There is a wide variety in the approaches that have been taken resulting in equally varied results. For example, [Okura et al, 2000] prefer a higher modulus and higher CTE underfill for good solder joint reliability. [Popelar, 1998] claims lower CTE and higher modulus is preferable. While [Okura et al, 2000] consider the

effect of hydrostatic stresses on the solder, [Popelar, 1998] is more conventional and does not consider hydrostatic stresses. The following papers consider the effect of underfill material properties such as CTE, modulus, adhesion strength and glass transition temperature on flip chip reliability [Shi et al, 2000; Smith, et al, 2000; Shim et al, 2000; Pearson et al, 2000; Dudek et al, 2000; Darbha et al, 1999; Goh, 2000; Zhang et al, 2000; Lu et al, 2000; Tsukada et al, 2000; Xu et al, 2000; Suryanarayana et al, 1991; Lau et al, 2000; Popelar, 1998; Okura et al, 2000].

2.3 Finite Element Modeling of Underfill Delamination

[Le Gall et al, 1996] were one of the first to publish results on a fracture mechanics analysis to understand cracking along the chip-fillet interface. Using linear elastic fracture mechanics, they showed that the energy release rate for an underfill with a modulus of 6GPa and CTE of 30ppm/^{o}C increased and subsequently decreased with crack length. [Lau et al, 2000a, b] presented a similar approach to delamination along the passivation-underfill interface. The equivalent plastic strain in the solder increases as the crack grew closer to the solder joint. While the study presented results for different underfill material properties, the effect of modulus and CTE of the underfill is inconclusive. [Mercado et al, 2000] have shown that the energy release rate for the delamination along the passivation-underfill interface decreases with crack length. [Zhai et al, 2004] have analyzed the passivation-underfill interface using Frac3D for different thermo-mechanical properties of the underfill. The energy

release rate increased with both modulus and CTE of the underfill material. [Fan et al, 1999] have reported stress intensity factors for the underfill-passivation interface. [Saitoh et al 2000a, b] have presented results on the effect of geometry and material parameters on the delamination between the silicon chip and encapsulant/die bonding material in a J-leaded package. [Ayhan et al, 1998], [Ayhan et al, 1999] and [Ayhan et al, 2001] have used enriched crack tip elements to understand cracks along the die-underfill, passivation-underfill and substrate-underfill interfaces. [Gu et al, 2001] have looked at delamination of the underfill from the passivation initiating at the root of the solder joint. The delamination of the underfill from the surface of the solder joint and subsequent delamination from the substrate is also considered. [Harries et al, 2001] have looked at the delamination between the chip and the encapsulant in a Very Small Peripheral Array package (VSPA). Energy release rate increases with increase in modulus and CTE of the encapsulant.

2.4 Fracture Toughness Characterization

The energy release calculated from the above models must be compared against the critical energy release rate or the fracture toughness of the interface to determine whether crack propagation would occur. There are a number of options to determine the fracture toughness of a given bimaterial interface.

Three point bend specimens such as End Notched Flexure (ENF), Unsymmetrical End Notched Flexure (UENF), Single Leg Bending (SLB),

Symmetrical Three Point Bending (S3PB), Asymmetric Three Point Bending (A3PB) and Mixed Mode Bending (MMB) have been developed [Auersperg, et al, 2002; O'Dowd, et al, 1992; Davidson, et al, 1996; Sundararaman, et al, 1998; Klingbeil et al, 1997; Yeung, et al, 2000; Lam et al, 2000].

Two variants of the four point bending specimen exist (Figure 2.4) [Matos et al, 1989; Yao et al, 1999a; Qu et al, 2000]. Standard Double Cantilever Beam (DCB) and Unsymmetrical Double Cantilever Beam (UDCB) are the two variants of the cantilever beam [Guo et al, 2001; Swadener et al, 1999; Sundararaman, 1997; Gurumurthy et al, 1998a]. Sandwich specimens [Suo, et al, 1989] are very useful to characterize the mixed-mode fracture toughness of interfaces. In general, different mode mixities can be achieved either by changing the geometry or by changing the loading direction. Sandwich specimens rely on the latter to achieve different mode mixities. Brazil Nut Sandwich, Modified Compact Test Specimen (MCTS) and Compact Mixed Mode (CMM) (Figure 2.5) are some of the typical sandwich specimens that have been reported [Awaji et al 1978; Wang et al, 1990; Huang et al, 1996; O' Dowd et al, 1992; Pang et al, 2002; Pang et al 2000; Madhusudhana et al, 2002; De et al, 1998; Mercado et al, 2000].

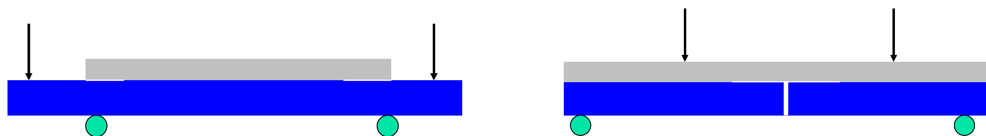

Figure 2.4 Four Bending Specimens [Qu et al, 2000 ; Matos et al, 1989]

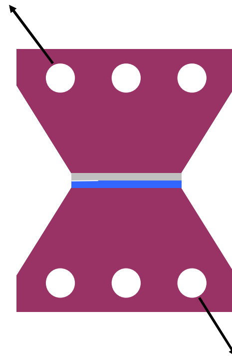

Figure 2.5 Compact Mixed Mode Specimen [Pang et al, 2002]

Theoretically, the bending specimens can produce a wide range of mode mixities and this is achieved by changing the dimensions of the specimen. The sandwich specimens are quite robust since they rely on changing the loading angle to get different mode mixities. This means that the specimen preparation can be standardized. However, not many analytical solutions exist for the sandwich specimens and calculation of mode mixity and stress intensity factors involve extensive finite element modeling.

[Qu et al, 2000] and [Yao et al, 1999a,b] report the use of a four point bending specimen to determine the fracture toughness of underfill-substrate interface. The fact that residual stresses have not been considered and that the experimental results give the 'apparent' fracture toughness of the interface is emphasized in these papers. [Yeung et al, 2000] and [Auersperg et al, 2002] discuss different specimen geometries that are suitable for interfacial fracture toughness testing in electronic packaging. [Lam et al, 2000] report the use of

ENF specimen to test interfacial fracture toughness while [Wang et al, 1999] use the actual flip chip in a three point bending configuration to obtain interfacial fracture toughness. [Pang et al, 2002] use the CMM test specimen (Figure 2.5) to estimate the fracture toughness of aluminum-underfill interface. It is important to note that none of these papers correct for the residual stresses that occur in the process of fabricating the test specimen.

2.5 Fatigue Crack Propagation

Fatigue crack propagation in bulk materials is well described by the Paris law. It has widely been demonstrated that such a behavior applies to fatigue crack propagation along interfaces as well [Xie, 2000; Ritter et al, 2002; Cheng et al, 2001; Gurumurthy et al, 1998b; Nagarajan et al, 2002; Kook et al, 1998].

$$da/dN = k(\Delta G)^m$$

where da/dN is the crack growth rate, ΔG is the range of energy release rate for the fatigue cycle and k & m are empirically fitted constants.

[Zhang, 2001] has tested fatigue crack propagation in homogenous underfill CT specimens under both ambient as well as 85^oC/85% R.H. conditions. As expected, crack propagation rates were faster under moisture laden conditions. Filler particle debonding from the epoxy matrix was the primary mode of crack propagation and materials with larger and more irregular particles were seen to

perform better. Under moist conditions, cracks grew below the threshold established under dry conditions and no clear threshold could be established [Zhang, 2001]. [Snodgrass et al, 2002] have studied the sub-critical debonding of a 3μm BCB layer from SiO_2 under both dry and moist conditions. While the Paris law exponent under dry conditions was 4-6, it was in the order of 17-34 under moist conditions. [Gurumurthy et al, 1998b] have used a thermo-mechanical approach to test the fatigue crack propagation between an underfill material and polyimide using a DCB specimen. In this approach, the fatigue load is applied by applying a temperature load and the energy release rate and mode mixity are calculated based on the deflection observed in the specimen. Underfills that did well in the fatigue propagation tests did well in actual flip chip packages as well.

Literature related to adhesives reveal a number of issues pertaining to interfacial fatigue crack propagation studies. One of them concerns the metric to be used to judge the severity of loading on a propagating mixed-mode crack. The range of the total energy release rate (ΔG_T) and the range of the mode I energy release (ΔG_1) seem to be popular [Xu et al, 1995]. Among the other options, [Kenane et al, 1997] has outlined

$\Delta G_{eff} = [1 + 2G_{II}/(G_I+G_{II})]\Delta G_I$

as a metric. This parameter, in fact, places more emphasis on mode I than mode II, which is clear because ΔG_{eff} goes to zero as ΔG_I diminishes.

One other feature that is striking about lap adhesive joints is that they exhibit cracks along the adhesive fillet just as an underfilled flip chip package though the shape of the fillet are completely different [Cheuk et al, 2002]. Adhesive joints have convex fillets while the underfill fillets are concave. However, the presence of fillet has been shown to enhance fatigue life of the lap joint [Dessureault et al, 1997] just as it has been for flip chip packages [Borgesen, 2000].

2.6 Cohesive Zone Modeling

The use of models having a cohesive zone or a damage zone is becoming more and more popular in the simulation of fracture processes [Zou et al, 2003; Petrossian et al, 1998; Needleman, 1988; Mohammed et al, 2000; Rahul Kumar, 1999; Borg et al, 2001]. The basic idea for such models can be traced back to [Dugdale, 1962] and [Barenblatt, 1960]. These models relate traction to the relative displacement at an interface where a crack may occur. Crack initiation is related to interfacial strength i.e. the maximum traction that can be sustained by the body. When the area under the traction-displacement curve equals the critical fracture energy, the tractions reduce to zero and the crack is said to have initiated or progressed. Various traction-displacement laws have been explored – cubic/exponential [Needleman, 1989], bilinear [Reedy et al, 1997; Mi et al, 1998], trapezoidal [Tvergaard et al, 1992] and perfectly plastic [Cui et al, 1993]. The advantage of this approach is that crack initiation and propagation can be combined into a single model. Moreover, the cohesive zone model can easily be implemented into finite element code.

CHAPTER 3

OBJECTIVES, APPROACH AND OUTLINE

3.1 Gaps in Existing Research

Based on the detailed survey of literature, the following gaps were observed.

i) There are only limited studies on no-flow underfill reliability; practically there is no study on nano-filled no-flow underfill reliability.

ii) While extensive work has been done on the measurement of fracture toughness of FR4-underfill, solder mask-underfill and aluminum-underfill interfaces, there exists very limited work on the measurement of the fracture toughness of the die passivation (SiN)-underfill interface. Most specimens involve tedious fabrication and residual stresses are usually ignored.

iii) There is practically no empirical model for the propagation of delamination in underfill/passivation interface under thermo-mechanical fatigue loading. A lot of work in open literature focuses on delamination under monotonic loading.

iv) Conventional fracture mechanics is typically used in studying interfacial delamination propagation in electronic packages. Although such interfacial fracture mechanics models are popular, they require 1) pre-existing crack and 2) extensive calculations for mode mixity. Therefore, there is a need to explore alternate approaches.

v) Limited work that combines both numerical models and experiments. Practically no work exists that correlates the experimental underfill delamination data to numerical predictions. Most of the work in open literature focuses on either modeling or on experimentation.

vi) Inadequate design guidelines for nano-filled underfill material development. Most guidelines focus on formulating underfills for solder joint fatigue reliability without considering underfill delamination.

3.2 Research Objectives

The objectives of this research are, therefore, to study the thermo-mechanical reliability of nano-filled epoxy underfills (NFU) through experiments and theoretical modeling. In particular, this work aims to

- characterize the mechanical properties of nano-filled underfills,
- develop a test methodology to measure the interfacial fracture toughness and use the methodology to measure the interfacial fracture toughness of SiN-underfill interface,
- conduct experiments and develop models for thermo-mechanical fatigue delamination propagation,
- explore the application of cohesive zone models to study interfacial fracture
- validate the developed models by using experimental data from NFU flip chip assemblies subjected to thermal cycling and

- to develop design guidelines against interfacial delamination propagation in flip chip assemblies through experiments and theoretical models.

3.3 Thesis Outline

To achieve the objectives, the following systematic approach was employed in this work:

3.3.1 Characterization of Mechanical Properties of the Underfill

The underfill material was prepared by using nano-sized silica particles as filler material. The reduction in size of the filler particles leads to some unique advantages and disadvantages. One of the advantages is that the properties of the underfill, especially the CTE, can be engineered to a level not previously attainable using micron sized filler particles. However, the properties of the underfill have to be tailored to meet competing requirements of low underfill viscosity and low CTE. The challenges in underfill material preparation are described in Chapter 4. Based on various considerations, a no-flow, nano-filled underfill material was synthesized and its temperature dependent thermo-mechanical properties are characterized.

3.3.2 Interfacial Fracture Toughness Determination

Under monotonic loading conditions, the propagation of delamination will occur if the energy release rate is higher than or equal to the fracture toughness of the underfill-passivation interface. Interfacial cracks are inherently mixed mode due

to the elastic mismatch between the materials and the fracture toughness of interface needs to be specified at a given mode mixity. In Chapter 5, the fracture toughness of the underfill-passivation interface is evaluated at two different mode mixities by using two different experiments. First, an innovative residual stress induced decohesion (RSID) test was developed and used to evaluate the mode I fracture toughness of the NFU-SiN interface. Second, a single-leg bending specimen is used to evaluate the fracture toughness at a mode mixity of -32°.

3.3.3 Cohesive Zone Modeling

As mentioned earlier, much of work in open literature focuses on using conventional fracture mechanics to understand underfill delamination. Cohesive zone models are an alternate way of studying fracture processes. Unlike conventional fracture mechanics, these models do not need require a pre-existing crack and do not involve complex mathematical computations for mode mixity. In Chapter 6, a cohesive zone model (CZM) is formulated for the underfill delamination problem using available experimental results.

3.3.4 Fatigue Crack Propagation

The propagation of delamination in a flip chip package occurs under thermo-mechanical fatigue loading. In Chapter 7, a Paris law for underfill delamination propagation is developed based on a thermo-mechanical fatigue crack growth study of the NFU-SiN interface.

3.3.5 Reliability of Flip Chip Assemblies with NFU

The qualification of an underfill materials for flip chip assembly is done using accelerated thermal cycling. In Chapter 8, a reliability study of a test vehicle comprising of several flip chip assemblies assembled using NFU material is presented. Two dimensional finite-element models are developed for underfill delamination propagation under monotonic as well as fatigue loading. In addition, the cohesive zone model developed in Chapter 6 is employed to study underfill delamination under monotonic thermal loading.

3.3.5 Design Guidelines

In Chapter 9, a comprehensive study of different types of delamination occurring in a flip chip assembly is presented. The effect of underfill material properties is particularly emphasized. Based on numerical modeling and the results from experimental test results, guidelines for the design of nano-filled underfill materials against underfill delamination are presented.

CHAPTER 4

MATERIAL CHARACTERIZATION

Nano-filled underfill (NFU) materials possess some unique properties that make them attractive candidates for the no-flow and wafer level underfilling processes. It is necessary to tailor the properties of the NFU such that the reliability of flip-chip assemblies is good, and at the same time, the properties are consistent with standard flip-chip assembly processes. In this chapter, work done on the characterization of the NFU material and the relevance of the results to the assembly process are presented.

4.1 Synthesis of NFU Materials

Organic-inorganic composites offer an excellent range of material properties and are commonly used in electronic packaging. The underfill material is a good example of such a composite. In the underfill material, the inorganic part is the filler particles. As the size of the filler particles is reduced, better dispersion of the filler particles in the organic matrix occurs and the intended effect of the filler particle is more easily achieved. For example, [Sun and Wong, 2004] report that the CTE of an underfill material reduces from 40ppm/^{o}C to about 26ppm/^{o}C when the size of the fillers were reduced from 30μm to about 7μm, even when the filler weight fraction in the underfill composite was maintained at 70%. At a given filler weight fraction, there are fewer 30μm particles than 7μm particles in a given quantity of underfill. Therefore, the effect of the filler is more pronounced with the

7μm particles and there is a further reduction in CTE. In the same vein, the use of nano-sized filler particles should offer a wider range of mechanical properties for the underfill material that were previously difficult to attain. However, there are some significant challenges in the synthesis of nano-filled underfills.

One of the challenges in the synthesis of NFU materials is the homogenous dispersion of the nano-sized filler particles. In this research, nano-sized silica particles were used as fillers. The silica particles do not have any particular affinity to the organic matrix and tend to agglomerate easily [Liu et al, 2003; Sun and Wong, 2004]. Surface modification of the filler particles is needed to increase the compatibility of the inorganic filler with the organic matrix by using alkoxysilanes [Prabhakumar et al, 2003; Lewis et al, 1995]. In this step, organic functional groups are introduced on the silica filler surface by the condensation reaction between the silanol group (Si-OH) on the silica surface and the alkoxysilanes (Figure 4.1). However, some silanol groups can remain in the final product of this reaction due to incomplete dehydration [Liu et al, 2003]. These silanol groups tend to be highly reactive and can cause further condensation during storage of the blend. This problem is especially severe in the case of epoxy resins and the condensation reactions during storage results in dramatic increase in viscosity. In the extreme case, premature curing of the blend can occur [Prabhakumar et al, 2003].

To overcome this problem, the stability of the blend was first enhanced by removing traces of acid that may be present. Additionally, the use of hexamethyldisilazane (HMDZ) results in the conversion of unreacted silanol groups into the unreactive trimethylsiloxy functionality. The stability of the blend was dramatically improved by these steps and no additional condensation was observed even after 6 weeks of storage. The underfill was then prepared by combining the functionalized silica blend with a standard set of epoxy, hardener, flow promoters and catalyst. The uniform dispersion of the nano-particles is confirmed by Transmission Electron Microscopy (Figure 4.2).

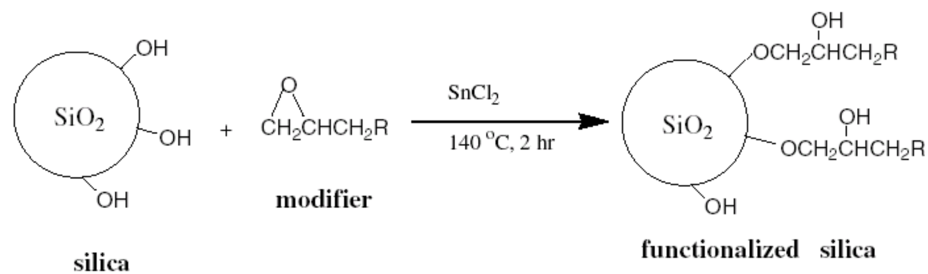

Figure 4.1 Functionalization of Nano-sized Silica [Liu et al, 2003]

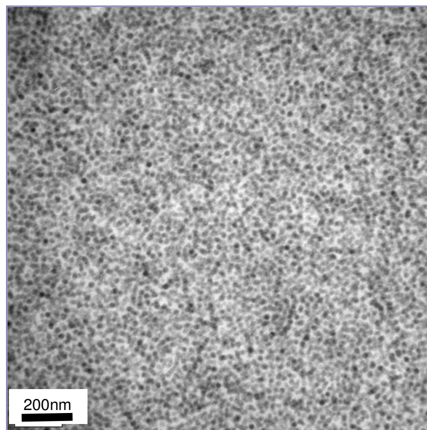

Figure 4.2 TEM of NFU Showing Uniform Dispersion of Functionalized Silica Fillers

4.2 Material Properties

In this work, nano-colloidal silica with an average diameter of 20nm was used in the preparation of the underfill. The CTE and viscosity of the NFU with filler contents varying from 0 to 55% by weight was evaluated. Thermo-mechanical analysis (TMA) was used to determine the coefficient of thermal expansion (CTE) and the glass transition (Tg) of the underfills. Specimens were prepared by casting the NFU material in a stainless steel mold (5 cm x 1.25 cm x 2 mm cavity) and curing it under a temperature profile approximating a eutectic reflow profile. In order to fully cure the samples, they were placed in a hot air oven at 150°C for 1 hour. TMA specimens measuring at least 2 mm in each dimension were cut from these cast samples.

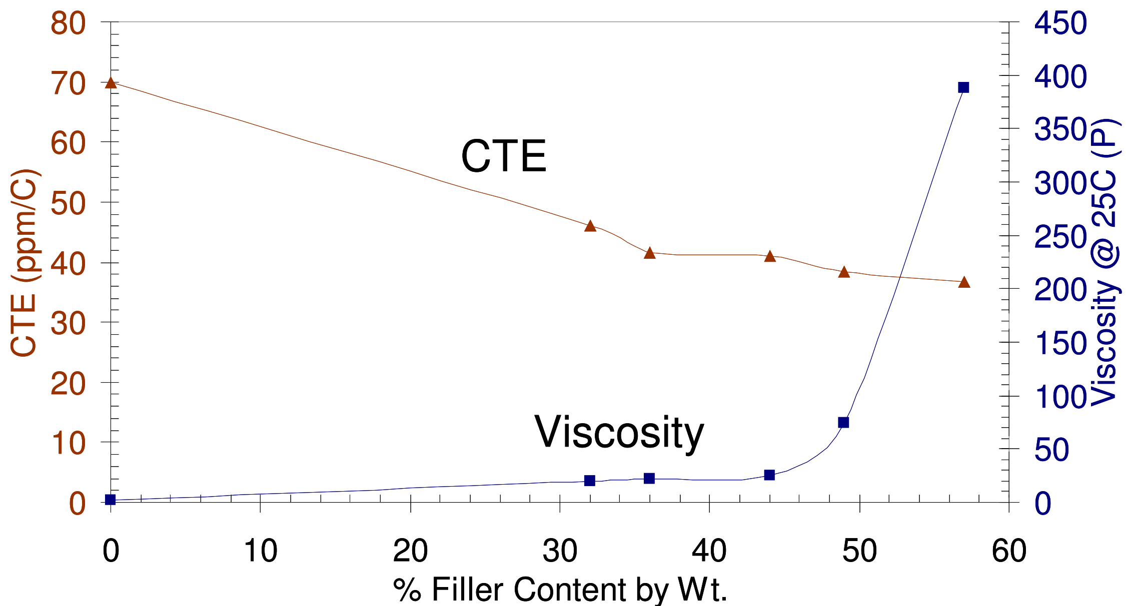

Figure 4.3 Effect of Filler Content on Underfill Material Properties

TMA was performed on a Perkin Elmer® TMA 7 Instrument. The sample temperature was first ramped at 5℃/min from 25℃ to 250℃ then cooled at 5℃/min to 0℃. The second heat, used for analysis, ramped from 0℃ at 5℃/min to 250℃. An initial vertical probe force of 0.05N was used. Viscosity was measured at room temperature by a standard Brookfield® viscometer using spindle #52 at 50rpm.

Figure 4.3 shows the variation in CTE and viscosity with the filler content. The weight fraction of filler content has opposite effects on CTE and viscosity and it is clear that beyond 50% filler content by weight, the viscosity increases dramatically. Even with 30% weight fraction of the fillers, there is a significant decrease in the CTE of the NFU material.

Viscosity of the NFU material is critical to the yield of the no-flow assembly process. The viscosity must be low enough such that the underfill can be displaced by the chip during the assembly process resulting in good solder joint formation. A typical sequence of steps involved in the no-flow assembly process is as follows [Thorpe et al, 2001]. The underfill is first dispensed on the substrate and is guided into place in the automated chip placement machine. The chip is carefully placed on the dispensed liquid underfill and pushed towards the substrate at a constant velocity until a preset force is reached. Once the force is reached, it is maintained for a certain dwell time until the solder balls on the chip touch the pads on the substrate. The key parameters in this process are the

placement velocity and the force. For a given underfill, both these parameters need to be optimized in order to achieve good assembly yield.

According to [Thorpe et al, 2001], the force exerted by the underfill on the chip is given by the Stefan equation.

$F_{fluid} = \frac{3\pi R^4 \mu(-\dot{h})}{h_o^3}$ where

$R = \sqrt{\frac{A}{\pi}}$ is the effective radius of a chip have an area, A

μ is the viscosity of the underfill

$\dot{h}$ is the velocity

h_o is the distance between the chip and the substrate

The head that holds the chip during the placement process starts at a certain height above the substrate and moves towards the substrate at a constant velocity. As the chip comes in contact with the underfill, the placement head measures the resistance offered by the fluid. Using the Stefan equation, the distance (h_o) at which the fluid resistance equals the preset force is reached can be determined by equating

$F_{fluid} = F_{placement}$

As mentioned earlier, from this point, the placement force is maintained until the solder bumps on the chip touch the pads on the substrate. Since the height of the

solder bumps on the chip is known, the dwell time can be calculated by solving the Stefan equation.

$$\tau = \frac{3\pi R^4 \mu}{2F_{placement}}\left[\frac{1}{h_f^2} - \frac{1}{h_o^2}\right]$$ where

h_f = height of solder bumps on the chip

Using this equation, the dwell time that would be needed to assemble a PB08 chip measuring 5mm x 5mm using nano-filled underfills with 30, 50 and 55% weight fraction was evaluated. The effect of placement velocity and placement force was also evaluated (Figure 4.4). Clearly, the dwell time needed for assembly increases with underfill viscosity. There is a dramatic increase in the dwell time for underfills with more than 50% weight fraction due to the sudden increase in viscosity of these materials. However, the dwell time needed for chip assembly decreases with placement force and velocity. The effect of the placement velocity is not as strong as the effect of placement force.

As mentioned earlier, one of the motivations for using nano-fillers is to tailor the mechanical properties of the underfill material to levels that were previously difficult to attain. A lower CTE would be preferred for good solder bump reliability, which can be achieved by increasing the weight fraction of the filler material. However, increasing the weight fraction of the filler increases the viscosity of the NFU material and a larger placement force would be needed in order to reduce

the dwell time needed for assembly. Since a large placement force can potentially damage the flip chip, there is a limit to which the placement force can be increased. As a result, it may be difficult for the chip to displace viscous NFU materials completely and the chances that the solder bumps on the chip would not touch the substrate pads increases.

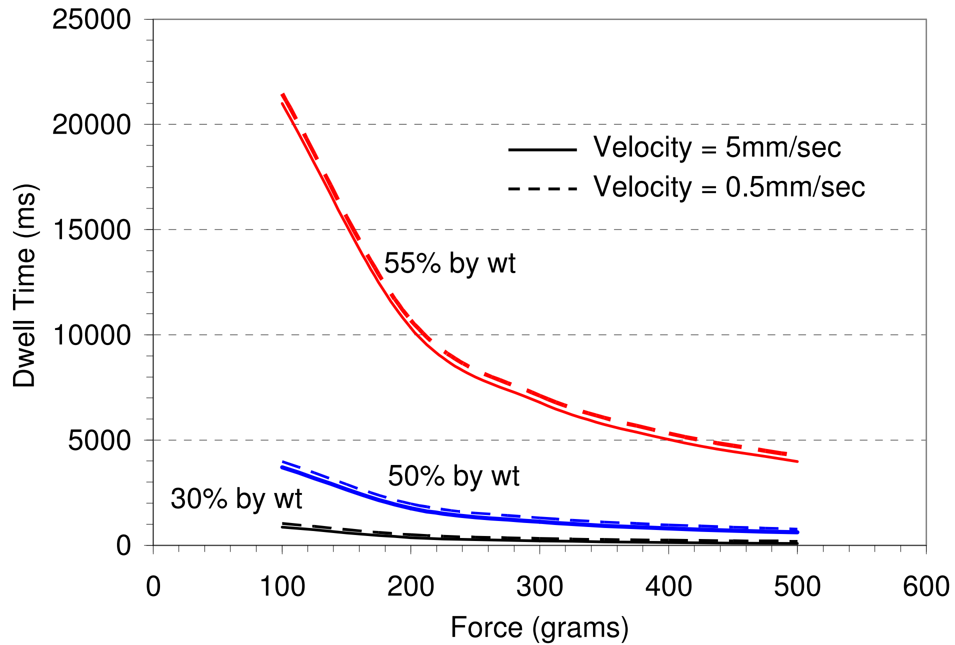

Figure 4.4 Effect of Underfill Viscosity and Assembly Parameters on Dwell Time

A tradeoff between CTE and viscosity of the NFU material is needed to decide the weight fraction of the fillers in the NFU material. As shown in Figure 4.3, the reduction in CTE was substantial even with 30% weight fraction of the nano-fillers. However, the reduction in CTE of the underfill with additional filler loading was not as significant. On the other hand, the increase in viscosity of the NFU as the weight fraction of the nano-fillers approached 50% was substantial. Therefore, a weight of 30% appears to be a suitable value considering the constraints of

lower CTE and viscosity. When flip chips were assembled using a no-flow NFU material with 30% filler particles by weight, excellent solder bump contact and reflow were achieved. A placement force of 150g with a dwell time of 500ms [Prabhakumar, 2004] was used in the process. These results are in good agreement with the predictions made using the Stefan equation.

Based on the tradeoff between CTE and viscosity, 30% weight fraction of the fillers in the NFU material appeared to be most suitable. The rest of this thesis is focused on studying the reliability of flip chip assemblies with a NFU material has 30% nano-silica particles by weight.

As a first step to understanding the thermo-mechanical behavior of the NFU material, the temperature dependent CTE and modulus of this underfill were evaluated using the Thermo-Mechanical Analyzer (TMA) and Dynamic Mechanical Analyzer (DMA) respectively. As discussed before, the CTE of the NFU material was measured on a fully cured underfill sample using a temperature scan from $0^{o}C$ to $250^{o}C$ (Figure 4.5) on a Perkin Elemer® TMA 7 instrument. DMA analysis was done using cured underfill bars measuring 10mm x 30mm x 1.7mm from $0^{o}C$ to $200^{o}C$ in a single cantilever mode at a heating rate of $3^{o}C/min$ and multiple frequencies (1, 2, 5, 10Hz) [Rubinsztajn et al, 2003] (Figure 4.6).

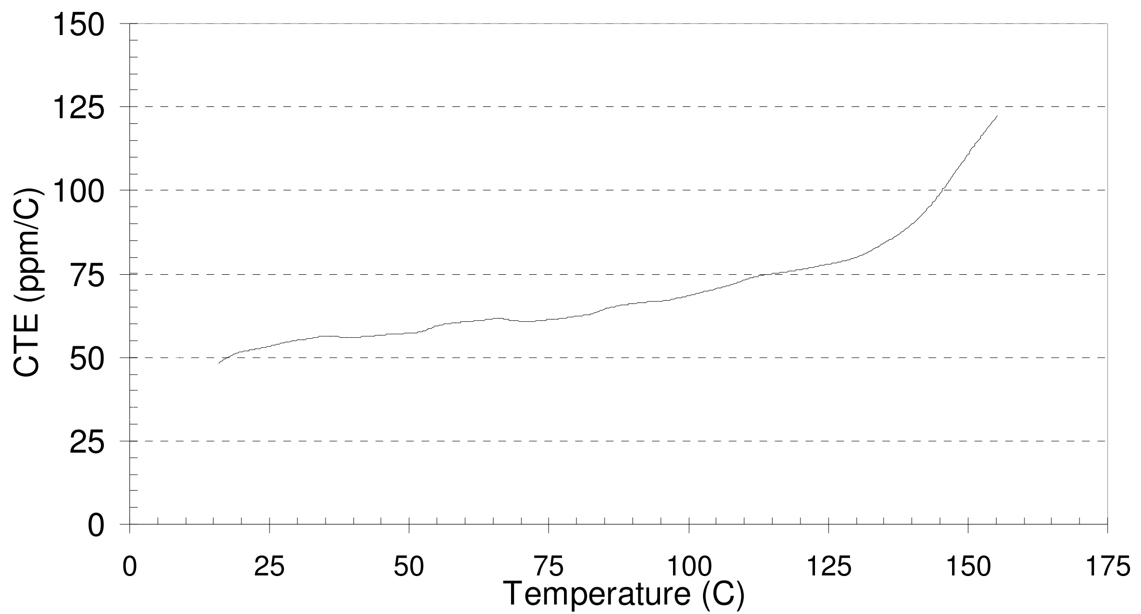

Figure 4.5 Temperature Dependent CTE of the Nano-filled Underfill

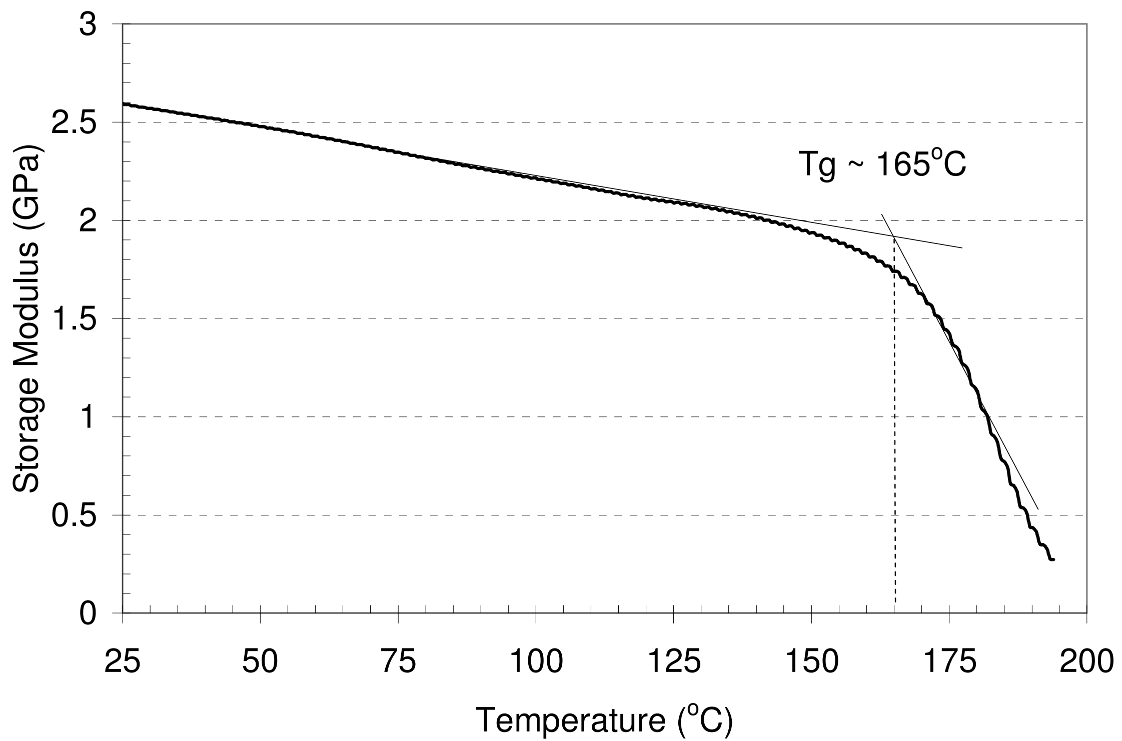

Figure 4.6 Temperature Dependent Modulus of the Nano-filled Underfill

As seen from Figures 4.6 and 4.7, the glass transition temperature of the underfill material was between 150° – 165°C. Separate differential scanning calorimetry (DSC) measurements confirmed that the glass transition temperature was around 155°C [Prabhakumar, 2004]. The temperature dependent properties of the underfill show that the thermoset underfill is stable and glassy in typical thermal cycling temperature ranges.

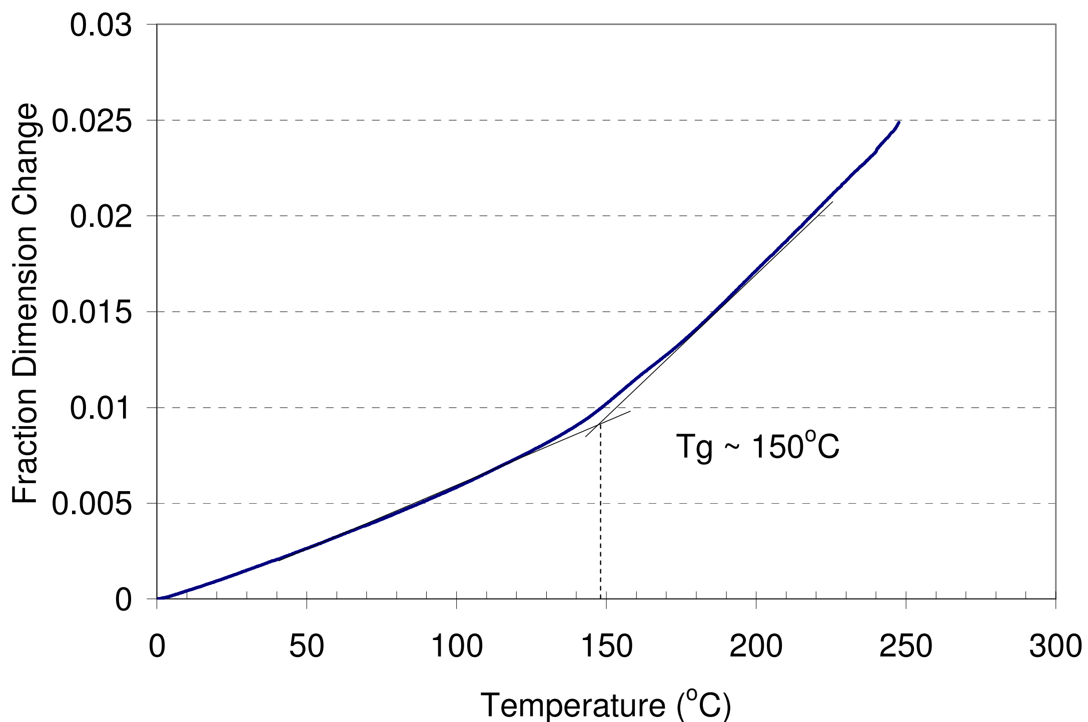

Figure 4.7 Glass Transition Temperature Measured by TMA

The glass transition temperature is the temperature where the underfill material changes from a hard, glassy state to a soft, rubbery state. TMA defines the glass transition in terms of the change in the dimensions of the sample as the NFU material transitions from the glassy to the rubbery state with an associated

change in free molecular volume. The rate of dimensional change of the NFU sample increases at the glass transition temperature and is seen in the form of a change in slope (Figure 4.7). Similarly, the rate of decrease of the modulus with temperature changes at the glass transition temperature (Figure 4.6). On the other hand, DSC defines the glass transition as a change in the heat capacity as the underfill material.

The glass transition temperature of the NFU material is higher than the temperature usually witnessed by the flip chip assembly under accelerated thermal testing. Within the range of the typical temperature shock test, the CTE of the underfill material increases from 50ppm/^{o}C at 25°C to 75ppm/^{o}C at 125°C while the modulus of the NFU material decreases from 2.6GPa at 25°C to 2.1GPa at 125°C. Since the change in NFU material properties when the flip chip assembly is subjected to thermal cycling is quite small, the reliability of the flip chip assembly is not adversely affected due to the change. In contrast, the glass transition temperature of unfilled no-flow underfill materials is typically 100-120°C. The CTE of such no-flow underfill materials increases from about 70ppm/^{o}C below glass transition temperature to more than 110ppm/^{o}C above the glass transition temperature and such a change can have an adverse effect on the reliability of the flip chip assembly. In the rest of this thesis, the temperature-dependent material properties characterized in this chapter are used in numerical simulations and other analyses.

CHAPTER 5

INTERFACIAL FRACTURE TOUGHNESS CHARACTERIZATION

5.1 Introduction

It is necessary to measure the interfacial fracture toughness to be able to predict the propagation of interfacial delamination under monotonic loading. The fracture toughness of an interface is the critical energy release rate for delamination propagation. The critical energy release rate is a measure of the minimum energy per unit area required for crack extension.

According to [Irwin, 1956], the energy needed to propagate a crack under a monotonic load comes from the potential energy of the body. Assuming that any inelastic dissipation at the crack tip is negligible, the energy release rate equals the change in potential energy of the body for a unit change in crack area [Anderson, 1995].

Mathematically,

$G = \frac{d\Pi}{dA} = \frac{dU}{dA} - \frac{dF}{dA}$ where

Π = Potential energy of the body

U = Strain energy stored in the body

F = Work done by external forces

When the available energy release rate exceeds the fracture toughness or the critical energy release of the interface, the crack propagates. In this work, the

term fracture toughness and critical energy release rate are used interchangeably.

Unlike cracks in homogenous materials, cracks along interfaces are inherently mixed mode in nature. This is due to the elastic mismatch between the two materials forming the interface. Unlike the solutions for mode I and mode II cracks in homogenous materials, the solution for the interfacial crack shows an oscillatory nature close to the crack tip [Williams, 1959; Erdogan, 1963; England, 1965]. Typically, the estimation of mode mixity and stress intensity factors for an interfacial crack is done with the help of finite element modeling. One such method, called the crack surface displacement (CSD) method is described in Appendix A and is used throughout this work to estimate mode mixity. Additional details on interfacial fracture mechanics are also described in Appendix A.

In this chapter, results from two different fracture toughness tests are presented. First, a single leg bending (SLB) test was used to estimate the fracture toughness of the underfill-passivation at a mode mixity of around -32°. Second, an innovative residual stress test is used to evaluate the fracture toughness of the underfill-passivation interface at a mode mixity close to 0°.

5.2 Single Leg Bending Test

As mentioned in Chapter 2, there are several existing methods to evaluate interfacial fracture toughness. The criteria that were used to select a test method were as follows - a) Ease of specimen preparation and fabrication b) Repeatability of the experiments c) Minimal effect of residual stress d) Small underfill consumption and e) Existence of an analytical solution. The first two requirements are self-explanatory. The importance of thermal residual stresses on fracture toughness testing is well known [Yao et al, 1999a; Nairn, 1999]. Since the underfill needs to be cured at 150°C, residual stresses are inevitable as the test specimen cools down from cure temperature to room temperature. The residual stresses can cause a change in the energy release rate as well as in the mode mixity of the crack. As the effect of residual stresses cannot be completely avoided, at best, it must be minimized and also appropriately accounted for in the computations. During this research, the quantity of nano-filled underfill available for use was limited and hence a specimen using a small amount of underfill material was sought. For many test specimens, analytical solutions exist in open literature. However, most of these solutions ignore the effect of residual stresses. Therefore, finite element modeling of the test specimen is required.

Based on the specific requirements listed above, the single-leg-bending (SLB) test was used to measure the fracture toughness of the SiN passivation-underfill interface. As seen in Figure 5.1, the passivated silicon strip and the NFU material are sandwiched between two steel bars and the starter crack is introduced in the

form of a Teflon™ film. The specimen is tested using the standard three-point bend setup as seen in Figure 5.1.

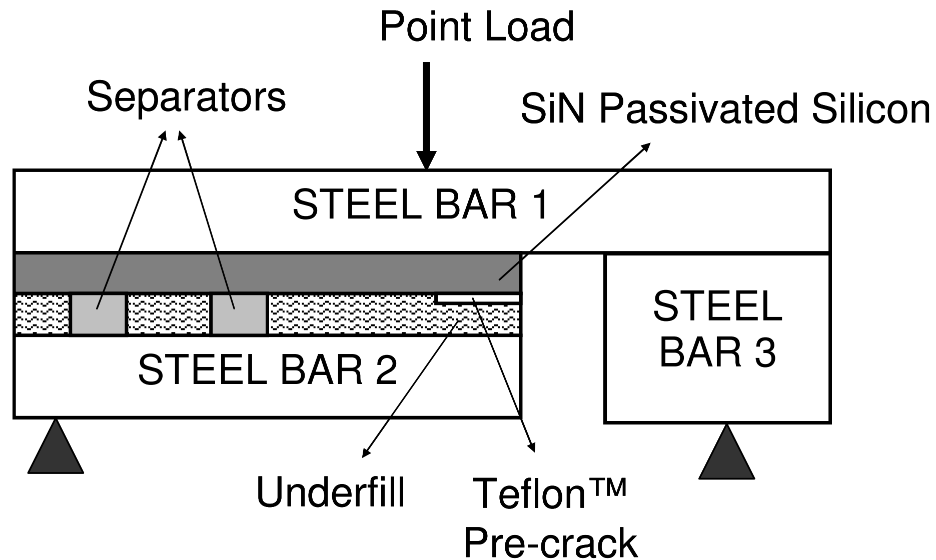

Figure 5.1 Single Leg Bending Test

5.2.1 Specimen Fabrication

A 4 inch silicon wafer having a 2 micron thick silicon nitride (SiN) passivation was diced into strips measuring 80mm long x 10mm wide x 0.5mm thick. Steel bars measuring 120mm long x 10mm wide x 5mm thick, 80mm long x 10mm wide x 5mm thick, and 20mm long x 10mm wide x 6mm thick were fabricated and phosphatized to improve adhesion to the underfill [Lord, 2004]. Small silicon supports measuring about 3mm long x 10mm wide x 0.5mm thick were cut from the corner of the diced wafers. All these parts were carefully cleaned using isopropyl alcohol in an ultrasonic bath and were wiped using lint-free cloth.

Subsequently, the silicon and steel strips were baked for one hour at 125°C to get rid of any moisture that may be present.

The long silicon strip (80mm x 10mm x 0.5mm) was adhered to steel bar 1 measuring 120mm x 10mm x 5mm using a thin layer of adhesive, as shown in Step 1, Figure 5.2. A 15mm long x 10mm wide x 15μm thick Teflon™ tape was then placed on to the edge of the silicon strip (Step 2 in Figure 5.2) and pressed firmly by hand into place. This Teflon™ tape will serve as the starter crack or pre-crack for the SLB test and the starter crack length was 15 mm in all specimens. As shown in Figure 5.2, steel bar 2, which measures 80mm x 10mm x 5mm was then placed on top of the silicon strip using two 3mm long x 10mm wide x 0.5mm thick silicon separators. The separators are intended to provide the necessary standoff height for the underfill. The silicon separators were placed at least 40mm away from the crack tip (the point where the Teflon™ pre-crack ends). Subsequently, steel bar 3 was adhered on steel bar 1, as shown in Step 3 of Figure 5.2 using a thin layer of adhesive. The entire setup was carefully placed on a hot plate, which was maintained about 100°C. The underfill was then dispensed near the edge of the assembly as shown in Step 4 of Figure 5.2 and the entire gap between the long silicon strip and steel bar 2 was filled with the underfill through capillary action. The entire assembly was cured in a hot air oven at 150°C for 2 hours.

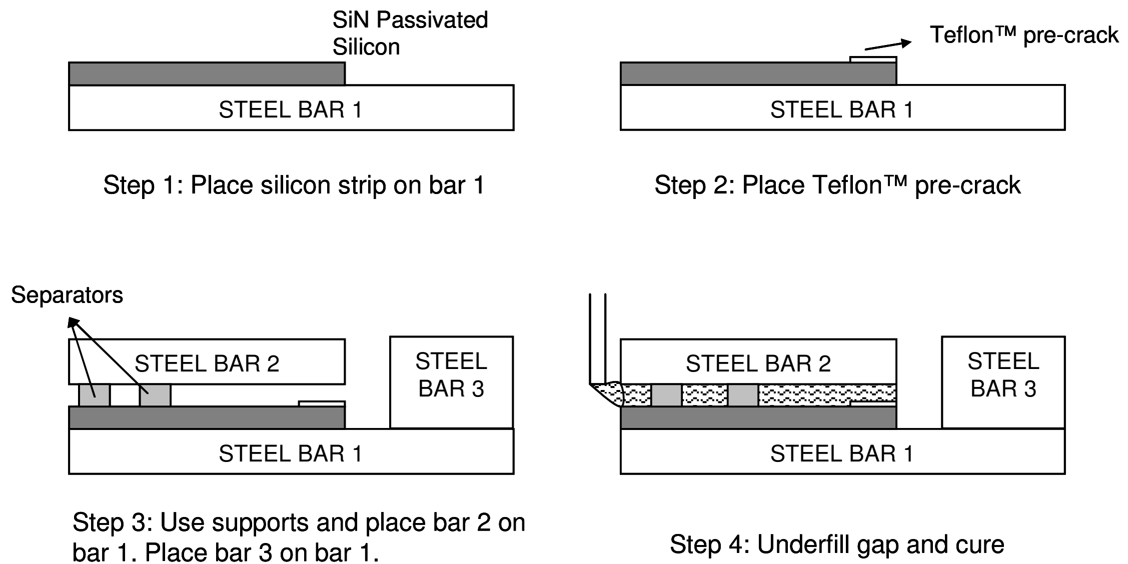

Figure 5.2 SLB Specimen Fabrication

5.2.3 Experimental Results

Eight specimens were prepared according to the method described above and tested on a Zwick™ mechanical testing system having a 1kN load cell. The test was displacement controlled and a loading rate of 0.1mm/minute was used. As shown in Figure 5.3, the load increases linearly with the displacement and when the crack propagates, the load drops. The test was stopped once the load dropped by 20%. The failure load varied between 240N to about 292N and the mean load to failure was about 265N (Table 5.2). Figure 5.4 shows an actual SLB specimen before and after testing. The separated upper (NFU) and lower (SiN) halves of the SLB specimen after testing are shown in Figure 5.4. It can be seen that the failure is purely interfacial and crack runs to an extent of about 20 mm along the interface.

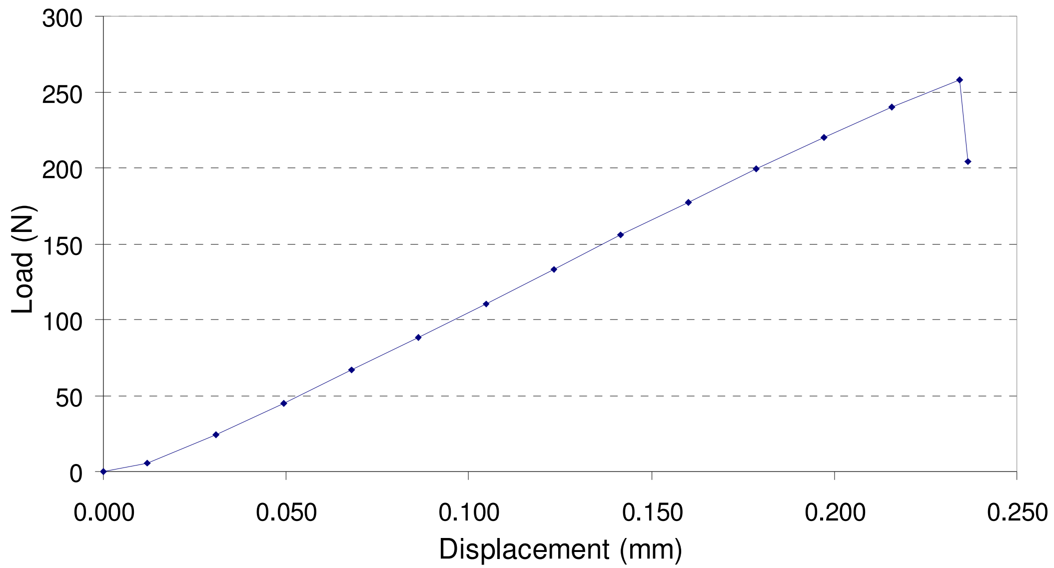

Figure 5.3 Typical Load-Displacement Curve

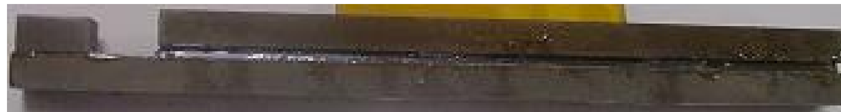

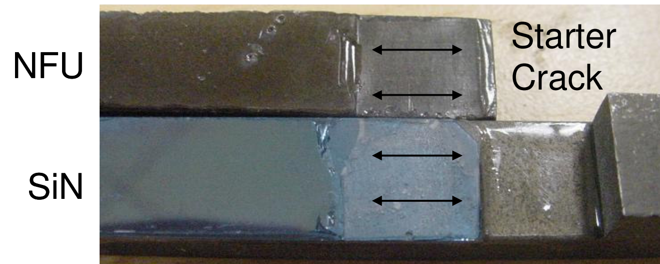

Figure 5.4 Single Leg Bending Test Specimen Before and After Testing

5.2.3 Extraction of Fracture Parameters

Except the separators, a 2D finite-element-model of the SLB test specimen was developed in ANSYS. The starter crack was simulated by having coincident nodes along the SiN-NFU interface and quarter-point elements were used at the

crack tip [Anderson, 1995]. Temperature dependent properties of the NFU material reported in Chapter 4 were used. Silicon, steel and SiN passivation were considered as temperature independent linear elastic materials (Table 5.1). In order to account for the residual stresses, the temperature change from the NFU cure temperature to room temperature was first simulated. The underfill cure temperature (150°C) was considered as the stress-free temperature. The boundary conditions for the first step was such that a set of nodes corresponding to a length of 0.5mm along the outer edge of steel bar 1 were prevented from moving in both X and Y directions (Figure 5.5).

Table 5.1 Properties of Materials Used in the SLB Test

Material	Elastic Modulus (GPa)	Poisson's Ratio	CTE (ppm/C)
Steel	210	0.32	16
Silicon	170	0.26	2.3
Silicon Nitride	300	0.25	2.8

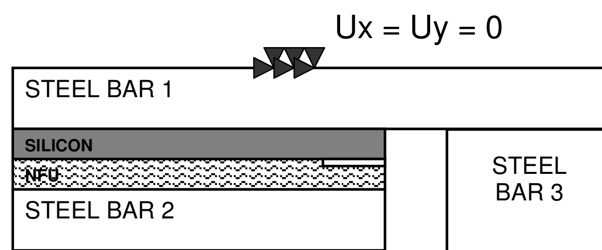

Figure 5.5 Boundary Conditions for Cooling Down from Cure Temperature to Room Temperature

At the end of the first step, residual shear and peel stresses were observed (Figures 5.6 and 5.7).

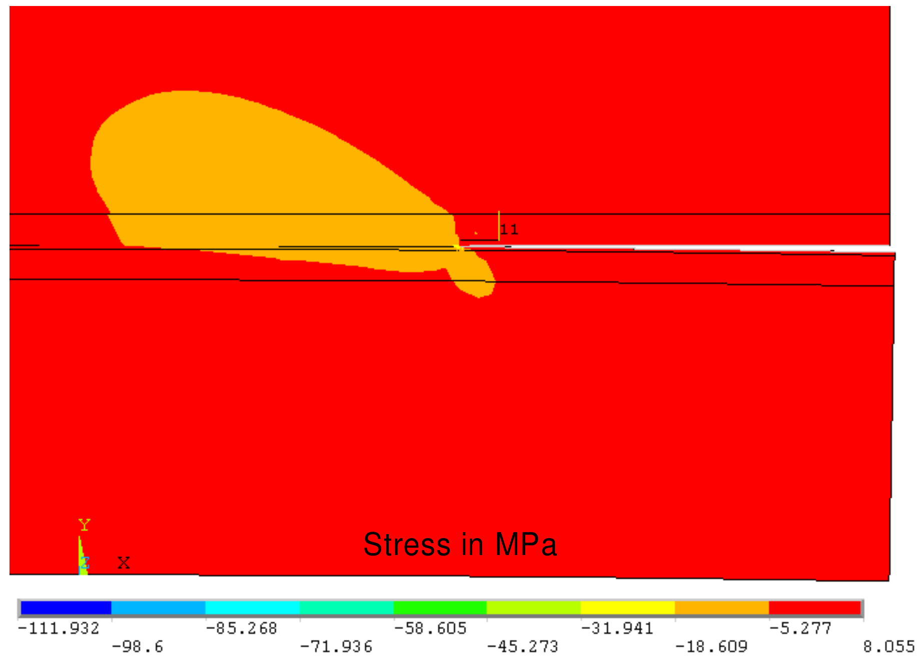

Figure 5.6 Contour Plot of Residual Shear Stresses Showing the Path for J Integral

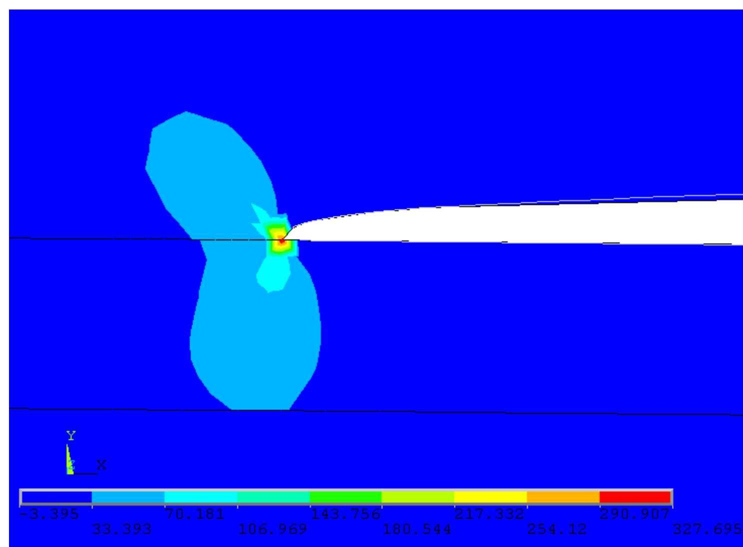

Figure 5.7 Contour Plot of Residual Peel Stresses

Following the cool down to room temperature, the critical load that caused the failure of the SLB specimen in the experiment was applied in the model. The boundary conditions are shown in Figure 5.1. The deformed shape of the SLB specimen after the application of the point load is shown in Figure 5.8.

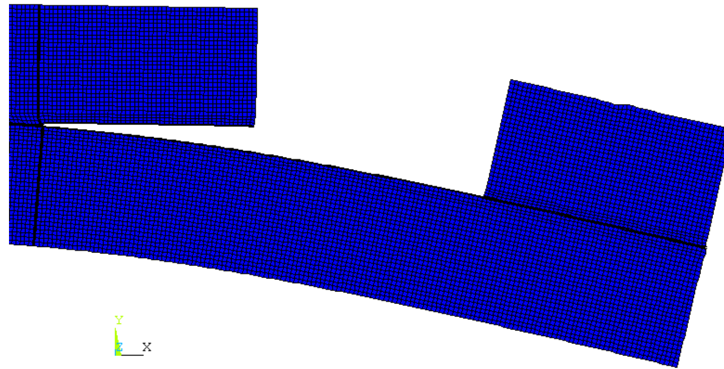

Figure 5.8 Deformed Shape of the SLB Specimen under Three-Point Bending

When the point load was applied, the peel stresses at the crack tip were larger than the residual stresses observed after the cool down (Figure 5.9).

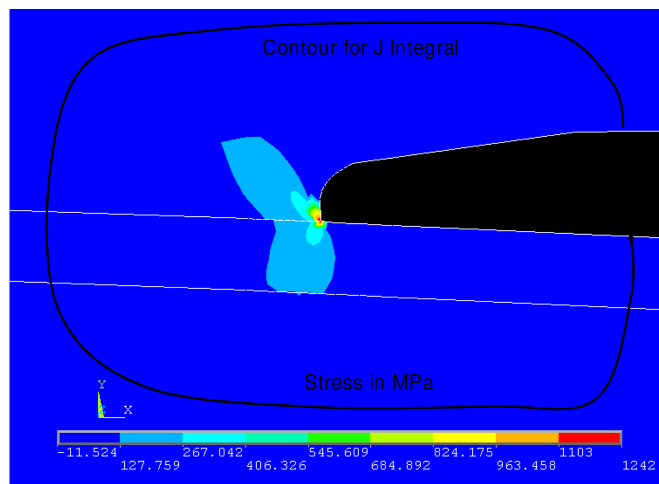

Figure 5.9 Peel Stresses Due to Three-Point Bending

The energy release rate (ERR) at the end of both the steps was calculated by performing the J integral over a suitable contour (Figure 5.9). The mode mixity was calculated by using the CSD method described in Appendix A.

The energy release rate due to residual stresses was about $30 J/m^2$ and the mode mixity of the crack was about -40°. The ERR due to three-point bending varied non-linearly with the load and is listed Table 5.2. The mode mixity of the crack under three-point bending was -32°. The ERR at the end of curing were less than 20% of the ERR when the point load was applied. Therefore, the specimen is quite insensitive to the residual stresses.

Table 5.2 Fracture Toughness of the SiN-NFU Interface – SLB Test

S No.	Failure load (N)	G (J/m^2)
1	240	109.5
2	252	115.2
3	267	122.4
4	280	128.9
5	292	135.0
6	249	113.7
7	283	130.4
8	257	117.6
Mean	265	121.6
Std. Dev.	17.3	8.5

As shown in Table 5.2, the mean fracture toughness of the NFU-SiN interface was $121.6 J/m^2$.

5.3 Residual Stress Induced Decohesion (RSID) Test

Thermal residual stresses are common in electronics packaging, primarily due to the processing of thermally mismatched materials under various temperature conditions. If one were to tailor the materials, dimensions, and curing profiles, it would be possible to propagate delamination through the presence of residual stresses alone, without the need for external load. Such a test will provide an easy way to measure the interfacial fracture toughness. Since the test relies upon the residual stresses, rather than external loads to drive the delamination, there are no corrections to be applied to the measured fracture toughness. The success of this test method, however, depends on the materials and the dimensions chosen to drive the delamination at the intended interface.

[Choi and Kim, 1992] have studied the spontaneous interfacial decohesion of a thin polyimide film on a glass substrate under a uniform temperature change. [Shaffer, 1994] developed the Edge-Liftoff-Test (ELT) based on the same principle. [Im et al, 2000] modified the ELT and introduced an epoxy backing layer to increase the energy release rate experienced by the specimen under a given temperature change. However, the test requires the use of a cryo-stage to cool the temperature of the specimen to below -70°C. It has been reported that cohesive failure of the polymer layer could occur at low temperatures and the failure need not be purely interfacial. The test also relies on the delamination occurring due to biaxial stresses, which can complicate the analysis of the test.

In this chapter, the mode I fracture toughness of the NFU-SiN passivation interface is measured using an innovative test method. However, in order to prevent problems associated with crack face contact and cohesive cracking of the underfill, the residual stresses are tailored by using a polycarbonate superlayer. The polycarbonate material is stable up to 150°C and possesses a CTE of 70ppm/^{o}C, which is higher than the CTE of the NFU material at room temperature. Therefore, when the specimen is cooled from the underfill cure temperature (150°C) to room temperature, the polycarbonate layer would have a tendency to peel the underfill layer away from the substrate. Further, since the CTE of silicon is quite low, the silicon strip is adhered to a steel bar, which has 7 times the CTE of silicon. The cumulative effect of this setup is that the NFU and passivated silicon are pulled away from each other by the polycarbonate and steel layers respectively.

5.3.1 Specimen Fabrication

As mentioned above, the specimen consists of four layers comprising of four different materials – steel, silicon with SiN passivation, underfill and polycarbonate (Figure 5.10). The thickness of the steel layer was about 5mm while the underfill and silicon layers were each 0.5mm thick. The thickness of the polycarbonate layer varied from 0.8mm to 4mm. All the layers were 60mm long and 13mm wide.

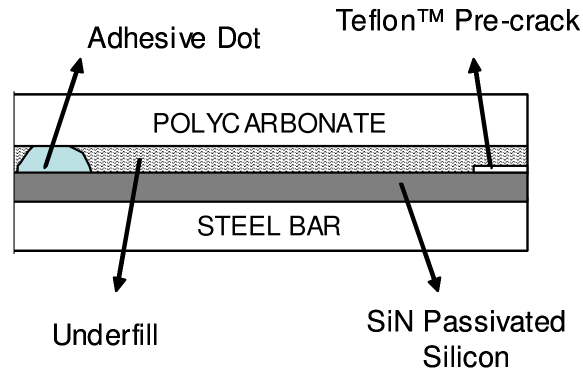

Figure 5.10 Residual Stress Induced Decohesion Test

The fabrication of the specimen was similar to the SLB test. The steel bar and silicon and polycarbonate strips were cleaned in an ultrasonically bath with isopropyl alcohol and were wiped using lint free cloth. Subsequently, the parts were baked for one hour at 125°C to drive out any moisture. The SiN passivated silicon strip measuring 60mm long x 13mm wide x 0.5mm thick was first adhered to the steel bar measuring 60mm long x 13mm wide x 5mm thick using a thin layer of adhesive, as shown in Step 1, Figure 5.11. A pre-crack in the form of a Teflon™ film, 15mm long x 13mm wide and 15µm thick was firmly pressed on the passivated face of the silicon strip as shown in Step 2, Figure 5.11. This Teflon™ strip will serve as the starter crack and the length of the starter crack in all specimens was 15mm. As discussed under the SLB test, a spacer strip of 40mm long x 13 mm wide and 0.5 mm thick was then placed on the silicon strip and a 10 mm dot of standard Araldite™ was placed at the far left side of the

specimen. The 60mm long, 13mm wide, and 0.8 – 4.0 mm thick polycarbonate strip was then placed on top supported by the spacer and the Araldite™ as illustrated in Step 3, Figure 5.11. The entire assembly was then placed on a hot plate and Araldite™ dot was cured at 100°C for about 10 minutes. The curing temperature and time for Araldite™ were based on vendor specifications. Once the Araldite™ was fully cured, the spacer strip was removed carefully and the NFU material was dispensed in the gap between the polycarbonate layer and silicon and the NFU material filled the gap completely by capillary action. The assembly was placed in a hot air oven for 2 hours at 150°C to cure the underfill (Figure 5.11).

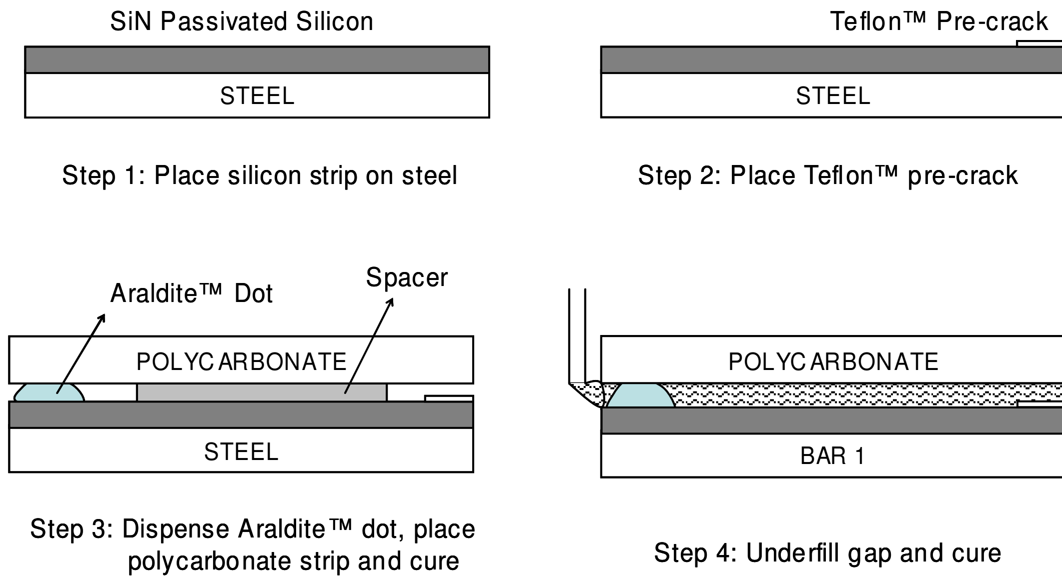

Figure 5.11 Fabrication of Residual Stress Induced Decohesion Test Specimen

5.3.2 Experimental Results

The specimens were allowed to cool to about 35°C (ambient temperature) at less than 1°C per min. Due to the residual stresses that develop as the specimen cools down, it was found that the underfill-passivation interface had delaminated completely starting at the Teflon™ pre-crack. As mentioned earlier, several polycarbonate layers with different thicknesses were used. It was seen that the all polycarbonate strips thicker than 0.8mm would provide enough energy to propagate the interfacial delamination. Figure 5.12 shows interfacial delamination in a specimen with 1mm thick polycarbonate strip.

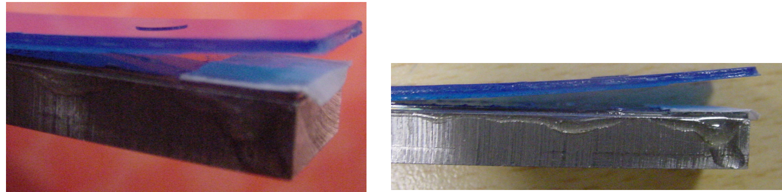

Figure 5.12 Residual Stress Driven Interfacial Delamination

Since the ambient temperature in this particular lab (35°C) was higher than the normal room temperature (20-25°C), it was conjectured that the specimen with 0.8mm thick polycarbonate layer did not witness enough temperature change to cause interfacial delamination. Therefore, it was decided to subject the samples with a 0.8mm thick polycarbonate layer to a larger temperature change. In order to prevent delamination due to a rapid change in temperature, the specimens were first cooled to about 35°C from the underfill cure temperature at less than 1°C/min. Subsequently, in order to cool the specimens below the ambient

temperature, the specimens were placed on a steel block that had been cooled to about 5°C. A linear displacement sensor and a thermocouple were placed on top of the polycarbonate layer, exactly above the pre-crack (Figure 5.13). The linear displacement sensor would record any change in displacement as an equivalent change in voltage. The voltage from the linear displacement sensor and the temperature from the thermocouple were continuously monitored and the data was acquired using a computer aided data acquisition system.

When the temperature dropped below 22°C, the delamination between the underfill and passivation propagated and the polycarbonate layer lifted up. Figure 5.14 shows the plot of temperature of the polycarbonate layer against the voltage recorded by the linear displacement sensor. A sudden change in voltage from 3.6V to 4.25V occurred at the same instant as the temperature dropped below 22°C. The test was repeated for 7 specimens with 0.8mm thick polycarbonate strips and the interfacial delamination propagated when the temperature dropped to about 22-25°C (Table 5.4).

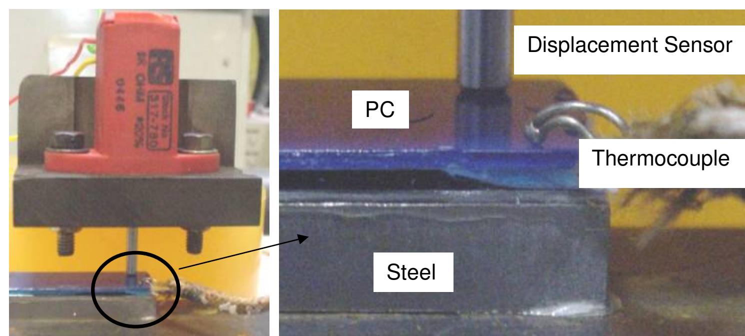

Figure 5.13 Residual Stress Test Setup

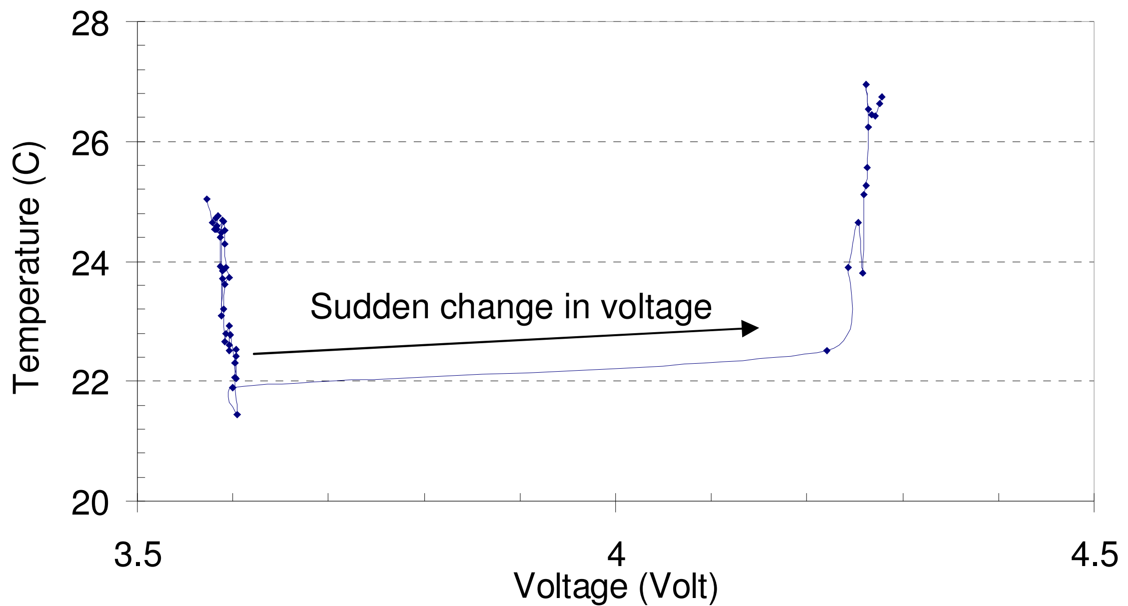

Figure 5.14 Residual Stress Test - Temperature Vs. Voltage

5.3.3 Extraction of Fracture Parameters

A 2D finite element model of the residual stress induced decohesion test was developed in ANSYS and the energy release rate and the mode mixity were calculated for a temperature change experienced by the specimens in the actual test (Figure 5.15). The temperature dependent properties of the NFU material reported in Chapter 4 were used. In the mode, silicon, silicon nitride, steel and polycarbonate were specified as temperature independent linear elastic materials (Table 5.3). The cure temperature of the NFU material (150°C) was set as stress-free temperature. Nodes along a 0.5mm length along the outer edge of the steel bar were constrained in X and Y directions in the model. A uniform temperature change corresponding to the experiment was applied.

Table 5.3 Material Properties

Material	Elastic Modulus (GPa)	Poisson's Ratio	CTE (ppm/C)
Steel	210	0.32	16
Silicon	170	0.26	2.3
Silicon Nitride	300	0.25	2.8
Polycarbonate	2.4	0.35	70

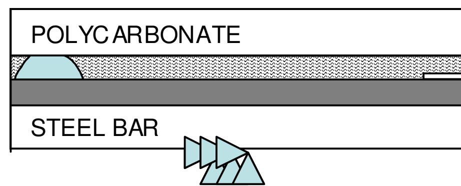

Figure 5.15 Boundary Conditions in the Finite-Element Model

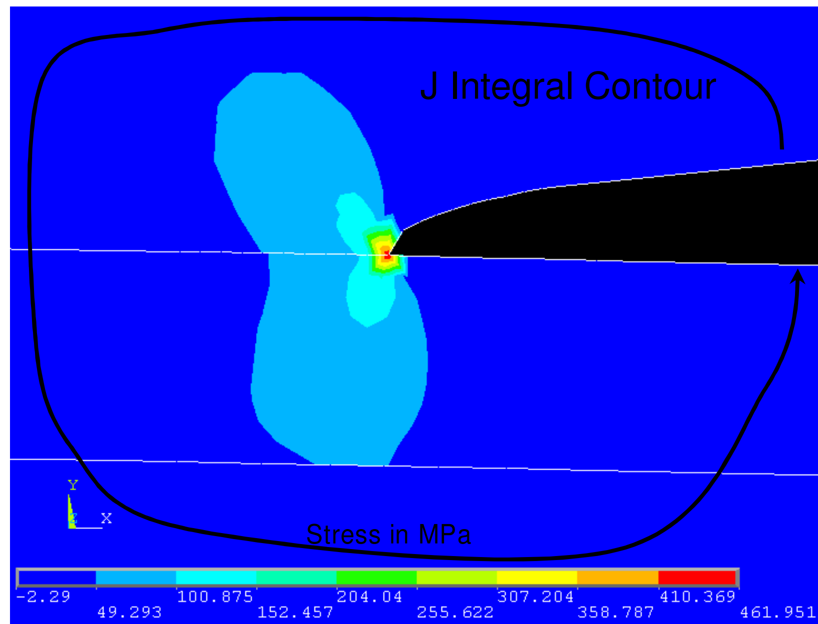

Figure 5.16 Peel Stresses Close to the Crack Tip

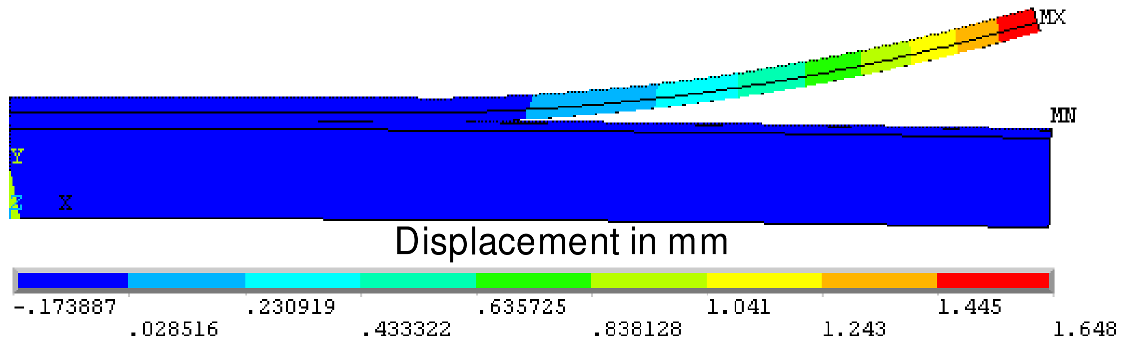

Figure 5.17 Vertical Displacement Due to Residual Stresses

The peel stresses close to the crack tip are shown in Figure 5.16. The average voltage change due to the progress of delamination in the experiment was about 0.6V, which translates to a mean displacement of 1.4mm for the sensor probe. From finite element modeling, the displacement of the tip of the polycarbonate layer was found to be about 1.65mm (Figure 5.17) for a temperature change of 125°C. The smaller value in the experiment is due to the resistance offered by the sensor probe.

The energy release rate for the test was found by performing the J integral along a suitable path around the crack tip (Figure 5.15). The ERR values for the test are shown in Table 5.4 The mode mixity was evaluated using the CSD method described in Appendix A and was -0.1^{o}. The mean fracture toughness of the SiN-NFU interface at a mode mixity of -0.1^{o} is 77J/m^{2}.

Table 5.4 Fracture Toughness of the SiN-NFU Interface – Residual Stress Induced Decohesion Test

S. No	Temperature (C)	ΔT (C)	ERR (J/m^2)
1	24	126	76.4
2	25.4	124.6	74.7
3	23.4	126.6	77.1
4	22.5	127.5	78.2
5	24.3	125.7	76.0
6	22.9	127.1	77.7
7	22	128	78.8
	Mean	126.5	77.0
	Std. Deviation	1.16	1.4

To ensure that the energy release rates determined through finite element models are in the same range as predicted by analytical models, certain simplified analytical models were used for calculating the interface fracture parameters. One such model is due to [Suo and Hutchinson, 1990] where they have shown an analytical expression for energy release rate for crack propagation for a two-layer strip under thermal loading. As the current test set-up consists of four layers, certain simplifications were made to reduce it to two layers.

The underfill and the polycarbonate have similar properties (high CTE and low modulus) (Table 5.3) and therefore, can be treated as a single layer. On the other hand, silicon and steel have similar modulus of elasticity. As the modulus of these two materials are close to each other and are nearly two orders of magnitude greater than underfill and polycarbonate, it is reasonable to treat them as a single material with a combined thickness of 5.5mm. Between steel and

silicon, as the thickness of steel is one order of magnitude greater than silicon, the properties of steel will dominate the interfacial delamination propagation, and therefore, calculations have been made with steel as the bottom layer with a combined thickness of 5.5 mm. It should be stated that the purpose of these analytical calculations is to compare with the finite-element results and therefore, any simplifying assumption that leads to conservative estimate of the interfacial fracture toughness is acceptable. Thus, when steel's CTE is used in the analytical calculations, the results will be conservative, and as seen in Figure 5.18, the results from the analytical solution are lower than the finite-element results. The details of the analytical calculations are presented in Appendix B. The mode mixity based on the analytical solution increases from -1° and -1.3° as the polycarbonate layer thickness increases from 0.8mm to 4mm. According to the FEM solution, the mode mixity increases from -0.1° to 5.1° as the polycarbonate layer thickness increases from 0.8mm to 4mm.

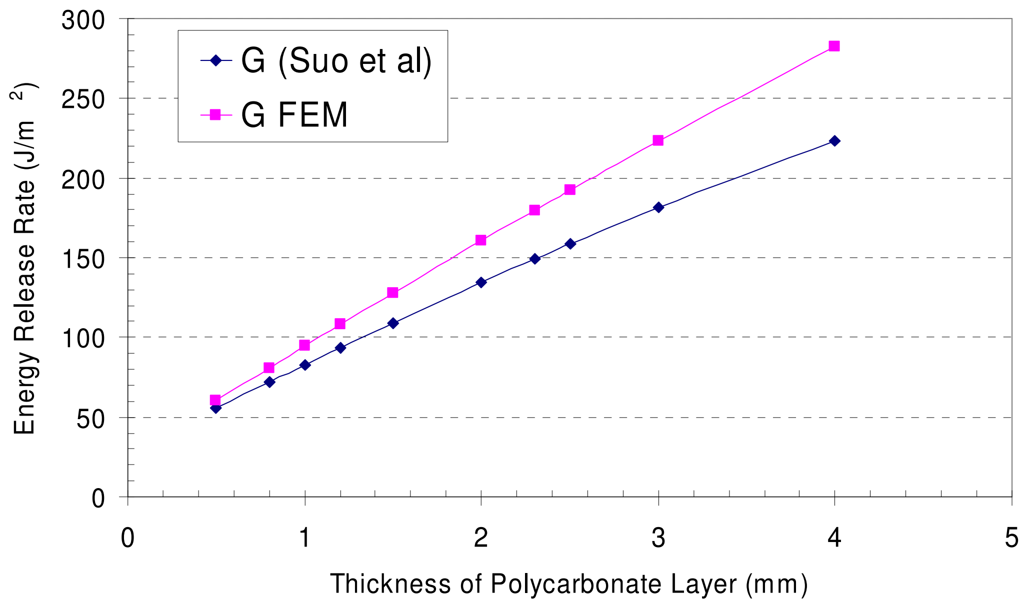

Figure 5.18 Effect of Polycarbonate Layer Thickness on ERR

5.4 Discussion

From the SLB test it was established that the mean fracture toughness of the underfill-passivation interface was about 120J/m^2 at a mode mixity of -32° and as expected, the fracture toughness of the interface close to mode I was lower. Both the tests have their unique advantages. The SLB test is well suited to evaluate fracture toughness at different mode mixities. However, the residual stresses that occur during specimen fabrication have to be considered in the analysis of the specimen. The residual stress induced decohesion test, on the other hand, relies on residual stresses caused by temperature change to propagate the crack and it offers a unique way to evaluate the mode I fracture toughness of the interface. By changing the geometry or the materials involved in the test, it is possible to

achieve different mode mixities. However, rapid temperature changes must be avoided and the temperature must be measured as close to the crack tip as possible. The effect of temperature variation across the specimen could play an important role on the outcome of the test. In the test, both steel and silicon have higher thermal conductivity than the underfill or polycarbonate. This means that a temperature gradient across the underfill-passivation interface can occur and such gradients must be minimized. In order to get conservative estimates of the fracture toughness, the temperature on top of the polycarbonate layer was measured because it would be higher than the temperature at any other location in the same. A higher temperature would mean a smaller temperature change and hence smaller fracture toughness. In the actual test, the cooling rate after the specimen was placed on the cooled steel block was about 3°C/min, which is not a thermal shock. At any point during the test, the temperature of the steel block was about 5°C less than the temperature of the polycarbonate layer. This is comparable to the variation in temperature at which the delamination propagated.

CHAPTER 6

COHESIVE ZONE MODELING

6.1 Introduction

Conventional fracture mechanics needs a pre-existing crack and extensive calculations for mode mixity calculations when applied to interfacial problems. As an alternative, the cohesive zone modeling (CZM) of this problem has been explored in this research and the details are presented in the following paragraphs. The 2D models were developed using ANSYS 7.1 and some of the limitations that arise due to this restriction are discussed.

Linear elastic fracture mechanics suggests that the stresses are singular at the crack tip. Infinite stresses cannot be physically sustained by the material and are alleviated by the occurrence of damage in the material surrounding the crack tip. In metals, this damage results from void formation and coalescence due to plastic deformation. In polymers, the molecular chains slide past each other in a manner similar to dislocation motion in metals and leads to permanent damage. In brittle materials, the damage is due to the formation of micro-cracks, which reduces the energy available for crack growth. Though the actual mechanism of the process is different, the stresses in all these cases are lowered due to the damage occurring ahead of the crack tip. The region around crack tip in which this damage occurs is known as a cohesive zone. The extent of this zone depends on the material/interface [Anderson, 1995; Feng and You, 1996].

The use of models having a cohesive zone or a damage zone is becoming more and more popular in the simulation of fracture processes [Zou et al, 2003; Petrossian et al, 1998; Needleman, 1988; Mohammed et al, 2000; Rahul Kumar, 1999; Borg et al, 2001]. The use of cohesive zone models dates back to [Dugdale, 1962] and [Barenblatt, 1960] who used it to estimate the extent of plastic deformation in ductile materials. In brittle materials, a similar damage zone does exist, although smaller in size [Wang and Shen, 1993].

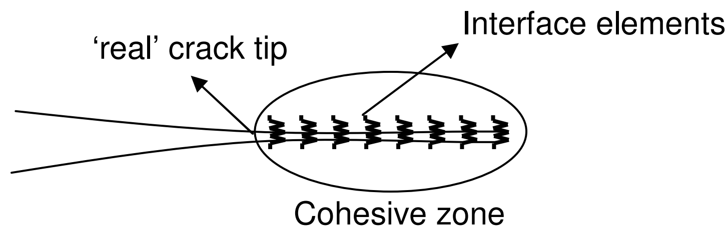

Figure 6.1 Cohesive Zone

The fundamental feature of a CZM is to incorporate cohesive interface elements ahead of the crack tip and accurately predict the propagation of the crack based on the deformation occurring in the damage/cohesive zone (Figure 6.1). A well-defined cohesive law relates the traction and displacement for the interface element. When the area under the traction-displacement curve equals the critical fracture energy, the tractions reduce to zero and the crack is said to have progressed. Various traction-displacement laws have been explored – cubic/exponential [Needleman, 1989], bilinear [Reedy et al, 1997; Mi et al, 1998], trapezoidal [Tvergaard et al, 1992] and perfectly plastic [Cui et al, 1993] (Figure 6.2). The cohesive interface elements can be implemented ahead of a pre-

existing crack as well as in regions where there is no pre-existing crack. In other words, the CZM can be used to study not only crack propagation but also crack initiation.

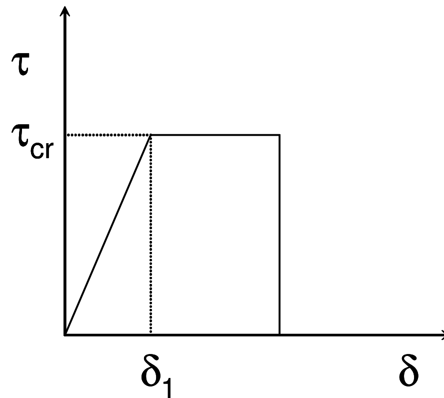

Figure 6.2 Traction Displacement Curve Used by [Cui et al, 1993]

With the advent of high speed computing, the implementation of CZM has become considerably easier. In the finite element models, the future path(s) of the crack are laced with non-linear spring like elements, which obey a given traction-displacement law. These elements have zero thickness and exist between coincident nodes that move away as the load is applied. The maximum traction that can be sustained by these elements is related to the strength of the material/interface in which the crack exists [Tomar et al, 2004]. The parameters that define the traction-displacement law are derived by matching modeling results to available interfacial decohesion experimental data. Since the fracture toughness of the underfill-passivation interface was measured using the Residual Stress Induced Decohesion (RSID) test and Single-Leg Bending (SLB) test, the cohesive law parameters were extracted from these same experimental data.

The cohesive zone element is represented as non-linear spring element with a multi-linear traction-displacement law, which can include softening. These elements are placed between coincident nodes and have one displacement degree of freedom, either in the normal (*Y*) or in the tangential direction (*X*). In a mixed-mode problem, both normal and tangential displacements have to be accounted for, and in such cases, two springs can be used between the same pair of coincident nodes. One spring acts in the tangential direction while the other spring acts in the normal direction. The behavior of the springs is non-linear elastic and though the traction law includes softening, the damage is only notional. When the springs are unloaded, they retrace the traction law in the reverse direction without any hysterisis.

In the published literature, a single variable λ usually defines the state of the interface element in a mixed mode problem. λ is usually defined as,

$$\lambda = \sqrt{\left[(\frac{u_n}{u_n^c})^2 + (\frac{u_t}{u_t^c})^2 \right]} \quad \text{where} \qquad 6.1$$

u_n is the normal displacement

u_n^c is the critical normal displacement

u_t is the tangential displacement

u_t^c is the critical tangential displacement

The traction-displacement law for the interface element is specified between the non-dimensional λ and interfacial stress. The trapezoidal law developed by [Tvergaard and Hutchinson, 1992] (Figure 6.3), the triangular laws used by [Borg et al, 2003] and [Tomar et al, 2004] are good examples. As seen, the interface is assumed to have broken when λ reaches unity and the cohesive element can no longer sustain traction. This implies that the failure of the interface, i.e., the progression of the crack will take place when λ reaches unity. This also means that the individual displacements in the two directions need not reach their critical values in order to cause failure. It should be pointed out that although the term "traction-displacement" is used to describe the cohesive element behavior, it is usually represented as "stress vs. non-dimensionalized displacement" as shown in Figures 6.3.

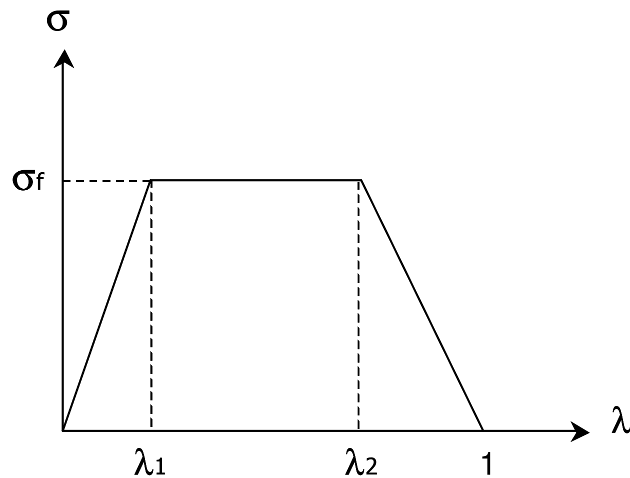

Figure 6.3 Trapezoidal Traction-Displacement Law

6.2 Derivation of the Cohesive Law

The cohesive law parameters are derived by fitting the results from the residual stress induced decohesion (RSID) test and the single-leg bending (SLB) test, described in Chapter 5. Since the mode mixity for the RSID test was -0.1°, only one spring acting in the normal direction was used in the model. However, for the SLB test, the mode mixity was close to -32° and hence both normal and tangential springs were used. A triangular traction-displacement law was used (Figure 6.4). The point of maximum interfacial stress was defined by parameter λ_1, as seen in Figure 6.4. Since the NFU-SiN interfacial fracture toughness was characterized at room temperature, which is much lower than the glass transition temperature of the NFU material, it is reasonable to expect very little softening behavior. Therefore, λ_1 was kept constant at 0.95 in all the models. The same shape of the traction-displacement law was used for both the normal and tangential springs though the critical tangential and normal parameters were different. The area under the curve equals the critical energy release rate for the particular mode.

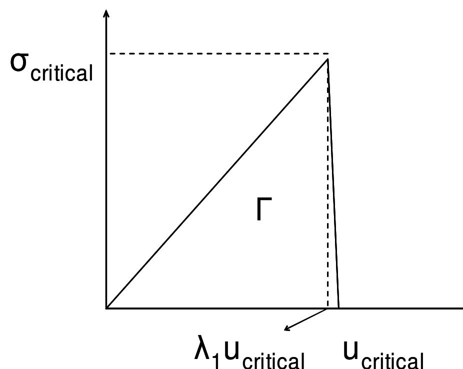

Figure 6.4 Triangular Traction-Displacement Law

6.2.1 Characterization of Normal Cohesive Element using RSID Test

The RSID test was used to measure the mode I fracture toughness of the NFU-SiN interface. Therefore, in the cohesive zone model of the test, springs acting in the normal direction were introduced in the cohesive zone.

The peel stresses at the NFU-SiN interface in the RSID test were tensile to an extent of 0.2mm from the crack tip (please refer to Figure 5.15, Chapter 5) and it was assumed that the damage would be restricted to this region. Therefore, cohesive elements were introduced along this region between coincident nodes at the NFU-SiN interface. As the load is applied, the cohesive elements act as non-linear springs coupling NFU and SiN solid elements across the crack face.

In ANSYS, the traction-displacement law for the non-linear spring elements had to be specified in force and displacement units. Therefore, the critical interfacial stress had to be translated into a critical traction for the spring element. This was done by using the technique of weighted element area employed by [Borg et al, 2001]. In the 2D model, the weighted area for each spring element equals the product of the width of the specimen and the distance between two adjacent spring elements. It is important to note that all of the normal springs in cohesive zone had the same magnitude of critical normal stress and critical normal displacement. For this simulation, the distance between adjacent springs was maintained at 2.5µm.

Boundary conditions and material properties were the same as the RSID test described in Chapter 5. A uniform temperature change from NFU cure temperature (150°C) to room temperature (25°C) was simulated. The propagation of delamination was said to occur when the spring, closest to the crack tip is at the point of failure. Since the delamination in the RSID propagated under the uniform temperature change, the problem is reduced to finding the value of critical normal interfacial traction that would cause the spring closest to the crack tip to fail. Two criteria could be used to determine the cohesive law used for the springs: 1) the energy release rate associated with the breaking of the first spring closest to the crack tip and this value should be close to the experimentally measured mode I fracture toughness. 2) λ should approach 1 for the first spring closest to the crack tip, and this is consistent with the definition given in equation 6.1.

Using these two criteria, the cohesive law for the normal springs was obtained are:

u_n^c = 2.6μm

σ_n = 55MPa

It may be pointed out that the area under the traction-displacement law (Figure 6.3) equals the mode I critical energy release. In other words,

$$\Gamma_y = \frac{1}{2}\sigma_n u_n^c$$

σ_n is the critical normal interfacial stress

u_n^c is the critical normal displacement

Γ_y is the Mode I fracture toughness

6.2.2 Characterization of Tangential Cohesive Element using SLB Test

Now that the normal cohesive element has been characterized, the tangent cohesive element was characterized using the SLB test. The SLB test was used to evaluate the fracture toughness of the NFU-SiN interface at a mode mixity of -32°. Since this is a mixed-mode problem, two springs between the same pair of coincident nodes were introduced. The extent of cohesive zone for this test was found to be 4mm (please refer to Figure 5.9, Chapter 5). The normal springs were represented with the cohesive law obtained from the RSID test. In order to calibrate the tangential springs, either the mode II fracture toughness or the critical tangential interfacial stress needs to be known. Following [Mohammed and Liechti, 1999], who also use two separate springs to handle the mixed-mode problem, the critical tangential interfacial stress was set to be equal to the critical normal interfacial stress. As mentioned earlier, for the propagation of mixed-mode crack, the individual displacements in the two directions need not reach their critical values.

The boundary conditions and material properties for the cohesive zone model of the SLB test are the same as shown in Chapter 5. As in the previous case, the distance between adjacent springs was maintained at 2.5μm. In order to achieve parity with the fracture mechanics analysis of the SLB test, the temperature

change from the NFU cure temperature (150°C) to room temperature (25°C) was first simulated. As before, two criteria could be used to determine the cohesive law used for the springs: 1) the energy release rate associated with the breaking of the first pair of normal and tangential springs closest to the crack tip and this value should be close to the experimentally measured mixed-mode fracture toughness. 2) λ should approach 1 for this first pair of normal and tangential springs closest to the crack tip, and this is consistent with the definition given in Eqn. 1. Using these two criteria, the critical tangential displacement was obtained as 6.3μm.

The uniqueness of the CZM parameters that were deduced in this chapter cannot be asserted due to the limited number of experiments from which the parameters were derived. In open literature, there are a number of approaches to CZM leading to equally different results. While many of them claim that the CZM parameters that were deduced worked well when extrapolated, it is difficult to use the same set of parameters in another work, though applied to the same material system.

The objective of this work was to explore the possibility of using CZM for modeling underfill delamination. The development of sophisticated finite-element code for the interface element behavior was beyond the scope of this work. Therefore, commercially available finite-element code, ANSYS was used. As a consequence, the cohesive modeling approach presented here is different from the approach usually presented in open literature where cohesive zone models

are developed using special finite-element routines. Nevertheless, the cohesive zone model developed here is used in Chapter 8 to predict the delamination behavior of a flip chip assembly under monotonic loading.

CHAPTER 7

EXPERIMENTAL CHARACTERIZATION OF FATIGUE CRACK PROPAGATION

In addition to interfacial crack propagation under monotonic load, it is necessary to study the interfacial crack propagation under cyclic or fatigue loading. This is because the underfill in flip-chip assemblies typically delaminates after a few hundred thermal cycles and such delamination propagates with thermal cycling. Once the delamination starts to grow, the underfill is no longer able to provide its intended mechanical support to the solder bumps, and the solder bumps could crack and fail prematurely. Therefore, it is important to study the growth of underfill delamination under fatigue loading, and it is equally important that the characterization is done using thermo-mechanical loads, not mechanical fatigue loads at room temperature. Such a characterization is especially important for a novel nano-filled underfill material. In this chapter, a model for the growth of NFU delamination under thermo-mechanical fatigue loading is developed.

7.1 Experiment

Typical fatigue crack propagation studies involve the use of an optical system to monitor crack growth under fatigue loading [Xie, 2001]. Such tests are usually conducted at room temperature and use mechanical fatigue loads, and do not account for the effect of temperature on crack propagation. In this work, the interface crack propagation was studied using thermo-mechanical fatigue loading

on a test specimen representative of flip-chip assemblies in terms of materials, and dimensions.

The test specimen consists of three layers – a microscopic glass slide measuring 76mm long x 25mm wide x 1mm thick, an underfill layer and a SiN passivated silicon strip measuring 40mm long x 5mm wide x 0.5mm thick (Figure 7.1). The glass slide and the silicon strips were cleaned in an ultrasonic bath of isopropyl alcohol and wiped clean using lint free cloth. Subsequently, they were baked for one hour at 125°C to get rid of any moisture that may be present.

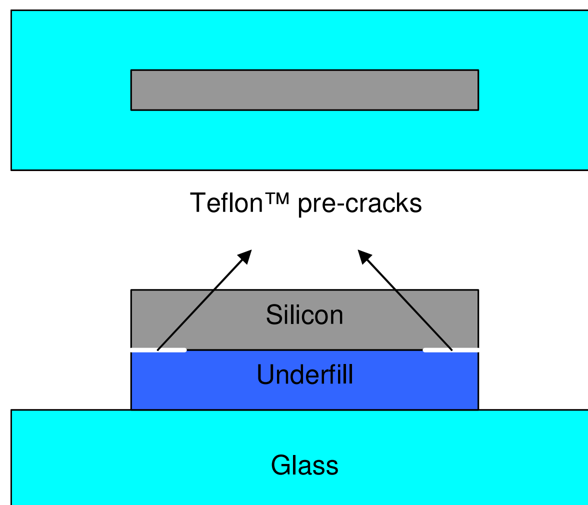

Figure 7.1 Fatigue Testing Specimen

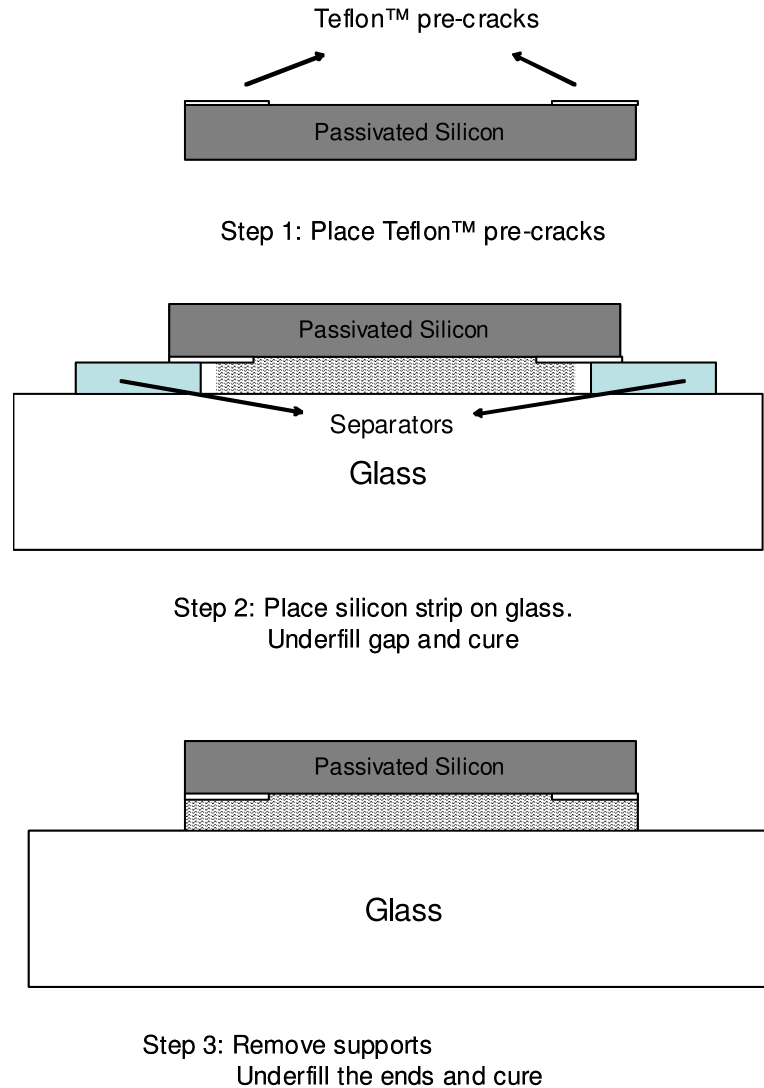

Figure 7.2 Fatigue Specimen Fabrication

First, 5mm long, xxx wide, and 15μm thick Teflon™ strips were placed on both edges of the silicon strip as pre-cracks (Step 1 in Figure 7.2) by firmly pressing by hand. The silicon strip was placed on the glass slide by using 0.15mm thick microscopic cover slips as supports. The setup was placed on a hotplate about 100°C and the NFU was dispensed carefully between the silicon strip and the glass slide (Step 2 in Figure 7.2). The NFU filled the gap between the glass slide

and silicon strip by capillary action. Care was taken to ensure that the underfill did not touch the cover slips. It must also be noted that the underfill covered a part of the pre-crack extents at either end (Figure 7.2). The setup was placed in a hot air oven at 150°C for 2 hours to cure the underfill. Subsequently, the cover slips were removed and the underfill was dispensed in their place (Step 3 in Figure 7.2). The setup was again placed in a hot air oven at 150°C for 2 hours to cure the additional underfill dispensed near the edges. Care was taken to ensure that there were no underfill fillets along the edges of the assembly as fillets tend to crack during thermal cycling tests and delamination would be initiated from the sides of the specimen. Four underfill thicknesses (0.15mm, 0.3mm, 0.45mm and 0.6mm) were considered in this study using appropriately-sized cover slips and two samples for each underfill thickness were fabricated.

7.2 Results

The specimens were subjected to air to air thermal shock testing between -55°C and 125°C with a dwell of five minutes at each extreme. The underfill-passivation interface was scanned using C mode scanning acoustic microscopy (CSAM) after every 300-500 cycles to monitor the progress of delamination (Figure 7.3). Since the nano-filled underfill was transparent, the extent of delamination could be seen from the bottom (glass) side as well (Figure 7.4). In the absence of delamination, light is reflected from the underfill-passivation interface. However, in the presence of delamination, there are two reflections – one from the underfill and one from the passivation surface. The resulting interference between the two

reflections becomes clear as the specimen is inspected optically by slightly tilting the specimen. This is shown in the right hand side picture of Figure 7.4.

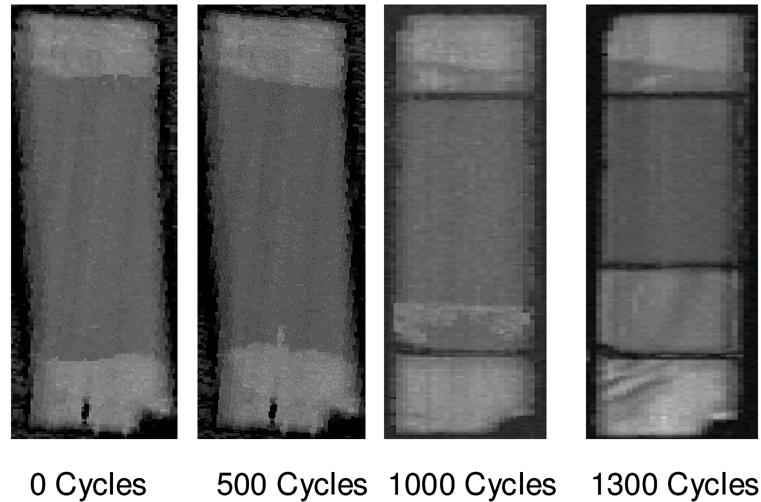

Figure 7.3 Progress of Delamination

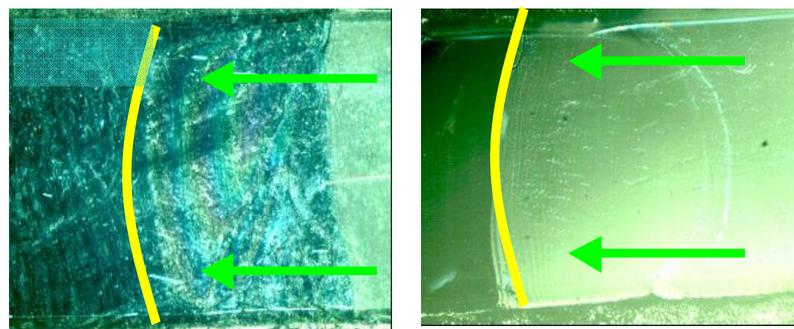

Figure 7.4 Optically Visible Delamination

7.3 Analysis

A 2D, half-symmetric finite-element model of the fatigue test specimen was developed in ANSYS (Figure 7.5). The mesh close to the crack tip was particularly fine (Figure 7.5) and quarter-point elements were used at the crack

tip to simulate the singularity. The right edge of the specimen was constrained in the X direction and one node at the bottom right corner was constrained in the Y direction as well (Figure 7.5). Contact elements were introduced between the crack faces to prevent interpenetration during the simulation of thermal shock testing [Figiel and Kaminski, 2003]. The temperature dependent properties of the NFU material, reported in Chapter 4, were used. Glass, silicon and silicon nitride passivation were all considered as temperature independent linear elastic materials (Table 7.1). The cure temperature of the underfill material (150°C) was considered as the stress-free temperature for the model.

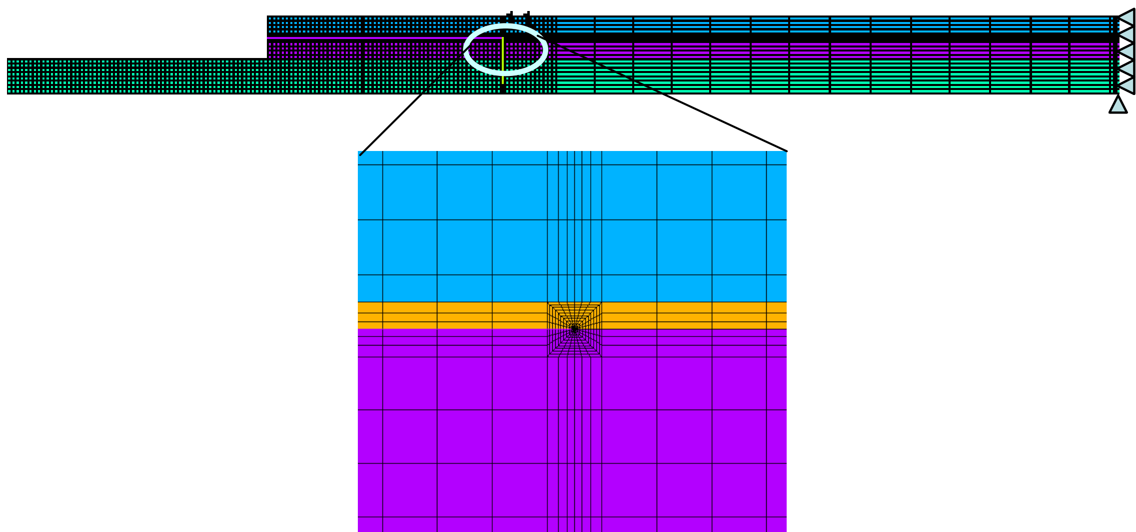

Figure 7.5 Finite Element Model of the Fatigue Specimen

Table 7.1 Material Properties

Material	Elastic Modulus (GPa)	Poisson's Ratio	CTE (ppm/C)
Steel	210	0.32	16
Silicon	170	0.26	2.3
Silicon Nitride	300	0.25	2.8
Glass	62.75	0.2	3.3

A thermal shock cycle between -55°C and 125°C was simulated for all the thicknesses of the underfill layer used in the experiment. The peel stresses close to the crack tip at -55°C for an underfill thickness of 0.15mm are shown in Figure 7.6. The energy release rate (ERR) was calculated at both the extreme temperatures of the cycle by performing the J integral around a suitable contour (Figure 7.6)

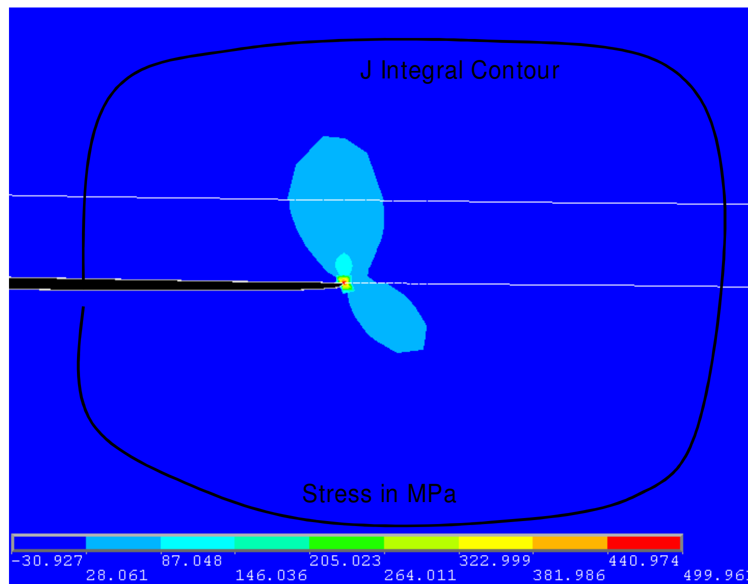

Figure 7.6 Peel Stresses Around the Crack Tip at -55°C

The mode mixity of the crack was evaluated at both the extreme temperatures using the CSD method described in Appendix A. Table 7.2 lists the ERR and mode mixity values for the different thicknesses of the underfill layer.

Table 7.2 Energy Release Rate and Mode Mixity in Fatigue Testing

Underfill	Energy Release Rate			Mode Mixity		
Thickness (mm)	-55C	125C	ΔG	-55C	125C	%ΔΨ
0.15	3.01	0.06	2.95	-70.1	-67.6	4%
0.3	12.18	0.23	11.95	-63	-58.7	7%
0.45	20.91	0.40	20.51	-57.2	-53.5	6%
0.6	43.12	0.82	42.30	-51	-49.4	3%

To ensure that the energy release rates determined through finite element models are reasonable, the analytical solution due to [Gaudette et al, 2000] was used to predict the range of energy release rate in the fatigue test specimen for a temperature change from -55°C and 125°C. This three-layer solution is applicable to cases where the outer two layers are made of the same material and the middle layer is made of a different material, and the crack is assumed to exist between the top two layers similar to the silicon and underfill in the fatigue test specimen. However, as the analytical solution assumes that two layers sandwiching the middle layer are made of the same material, the analytical model differs from the current test specimen where the top layer is silicon and the bottom layer is glass. Glass and silicon have very similar CTE while the elastic modulus of silicon is about 2.5 times that of glass (Table 7.1). In order to compare the results of the finite element model with the analytical solution, two cases were studied using the analytical solution. In the first case, silicon was assumed to exist on either side of the underfill layer (labeled 'G Si' in Figure 7.7) and in the second case, glass was assumed to exist on either side of the underfill layer (labeled 'G Glass' in Figure 7.7). It is important to note that the thickness of

the silicon replacing the glass substrate in the first case is the same as the thickness of the glass substrate. Similarly, the thickness of the glass replacing the silicon in the second case is the same as the thickness of silicon. As seen in Figure 7.7, the finite-element solution predicts a similar dependence for ΔERR on the thickness of the underfill layer.

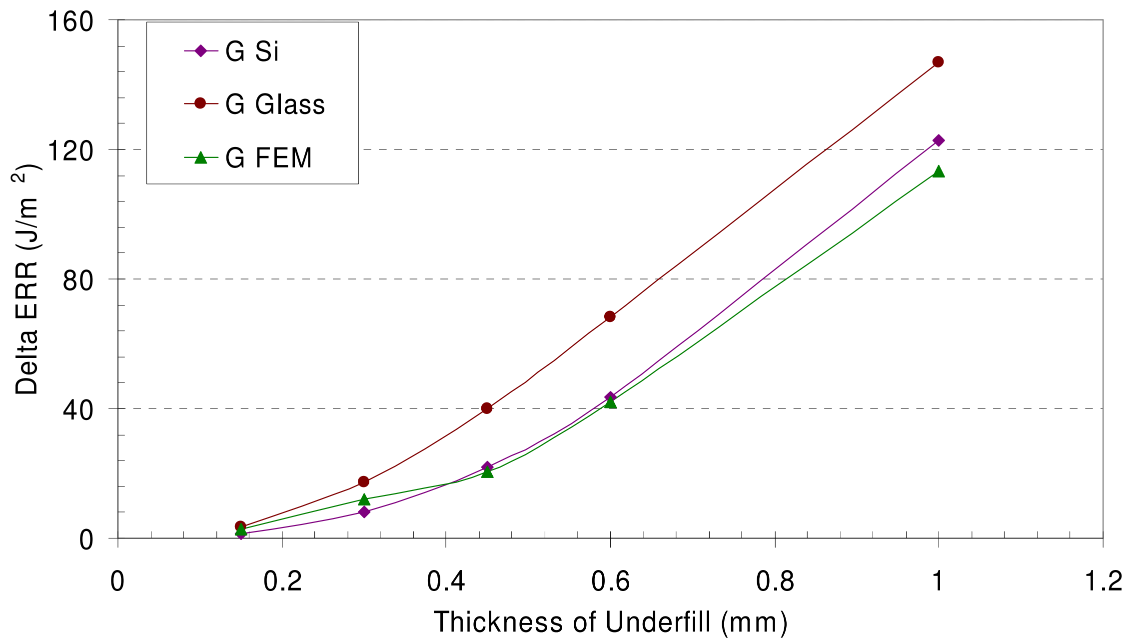

Figure 7.7 Comparison Between Finite-Element Model and Analytical Model

While the analytical solution agrees with the FEM solution well, the energy release rate for a specimen with glass on either side is higher than a specimen with silicon on either side. Since the elastic modulus of silicon higher than that of glass, the energy release rate of a specimen with silicon on both sides is expected to be higher under a uniform temperature change. In fact, the analytical solution for a crack between two layers [Suo and Hutchinson, 1990] used to

analyze the residual stress test in Chapter 5 shows increase in energy release rate with increase with elastic modulus or CTE of one of the layers (Appendix B).

The reason for this anomaly in the result can be explained as follows. The elastic modulus has opposite effects on cracked and uncracked bimaterial strips. The energy release rate (ERR) of a cracked specimen increases with increase in elastic modulus. However, in an uncracked strip, a higher elastic modulus means smaller radius of curvature and hence lower compliance. Since the analytical solution assumes that the materials on either side of the underfill layer are the same, an increase in elastic modulus of that layer causes two competing effects. The ERR increases in the cracked part and at the same time, the overall ERR decreases due to reduced compliance of the uncracked part.

Just as the analytical solution, the finite element model also showed that both the mode mixity and the ERR were independent of the crack length. This is very useful because the conditions for crack propagation do not change as the crack propagates and the rate of crack propagation can be calculated based on the crack lengths that are more than a few hundred cycles apart.

Since each specimen had two crack fronts and two specimens were cycled for a given thickness of underfill, a total of four data points were obtained for the extent of delamination for a given value of ΔG. From the extent of delamination for each crack front, the rate of crack propagation ($\frac{da}{dN}$) was obtained based on a least

square fit (Figure 7.8). A good linear fit was obtained for the rate of crack propagation.

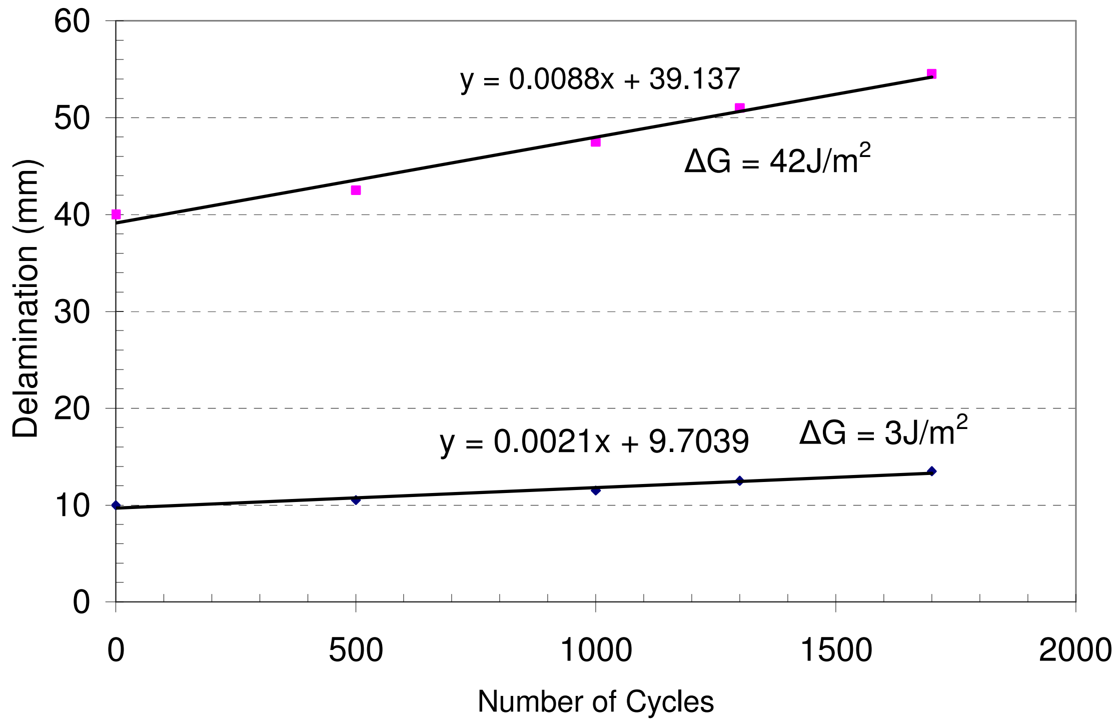

Figure 7.8 Rate of Crack Propagation

A Paris law between $\frac{da}{dN}$ and the range of energy release rate was fitted (Figure 7.9) based on the least square method.

$$\frac{da}{dN} = 0.0006(\Delta G)^{0.8786}$$

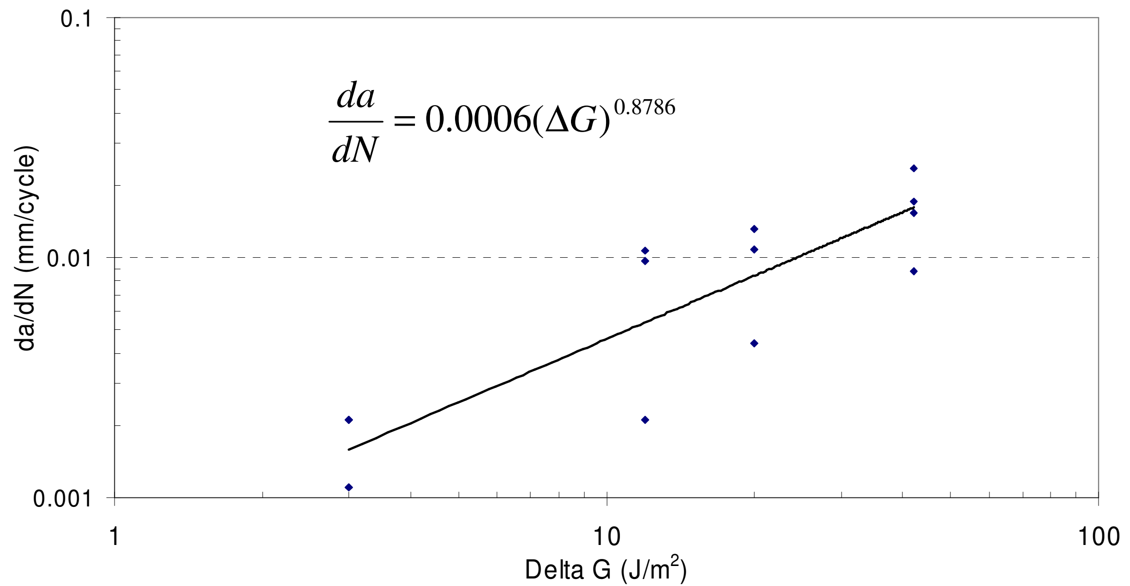

Figure 7.9 Paris Law for Underfill Delamination

[Xu et al, 2004] have fit a similar law for underfill delamination propagation based on testing of flip chip packages and according to their work, the exponent in the Paris law is around 0.60 and the pre-exponential constant is 4.0×10^{-5}. The values for the exponent and the pre-exponent constant in the present work are higher because samples were subjected to thermal shock cycles between -55°C and 125°C whereas [Xu et al, 2004] have employed a thermal cycling test. In the present thermal shock tests, it took about 90 seconds for the temperature to change between the extremes whereas it took about 5 minutes for thermal cycling tests [Xu et al., 2004].

The fatigue crack propagation at the NFU-SiN interface was characterized using a thermo-mechanical test and a Paris law was fitted to the experimental results. Together with the fracture toughness of the interface, evaluated in Chapter 5, the integrity of NFU-SiN interface in actual flip chip assemblies can be studied.

CHAPTER 8

RELIABILITY OF FLIP CHIP ASSEMBLIES WITH NANO-FILLED UNDERFILL MATERIAL

Flip chip assemblies underfilled with the NFU material under typical accelerated thermal cycling tests in important to qualify the NFU material for commercial use. In this chapter, the reliability of flip chip assemblies with the NFU material is assessed under a thermal shock test between -40°C and 125°C and the delamination occurring at the NFU-SiN passivation interface is monitored. Finite-element models of the flip chip assembly are developed and the results are correlated to the interfacial fracture studies reported in Chapters 5, 6 and 7.

8.1 Experiment

A total of 30 flip chips measuring 5mm x 5mm x 0.5mm were assembled on a 6.5mm x 6.5mm x 1.5mm FR4 substrate (Figure 8.1). There were 88 solder bumps along the periphery of the chip and the bump pitch was 200μm. The no-flow assembly process with a standard eutectic-solder reflow profile was used to assemble the chip using the NFU material. To ensure that the underfill is fully cured, the flip chip assemblies were placed in a hot oven for one hour at 150°C after the reflow process.

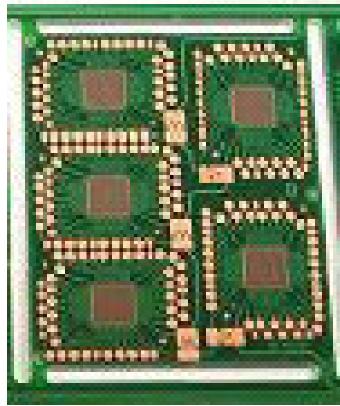

Figure 8.1 Test Vehicle

As a baseline, the underfill-passivation interface was scanned using CSAM immediately after assembly and no voiding or delamination was detected. The solder joints in the flip chip were daisy-chained and the electrical resistance of the solder joints can be monitored via the test pads. The flip chip assemblies were tested in air-to-air thermal shock between -40°C and 125°C. The packages were held at the extreme temperatures for 10 minutes during each cycle. The samples were inspected under C-mode Scanning Acoustic Microscopy (CSAM) for delamination between the underfill and passivation at regular intervals. The electrical resistance of the solder joints was also monitored. Since the assemblies had to be dipped in water for CSAM, the assemblies were baked for 2 hours at 125°C before the resumption of thermal shock testing. This was done to remove any moisture that may have seeped in during CSAM.

Cracks in underfill fillets were observed after 1000 cycles of testing (Figure 8.2). It is believed that these cracks later lead to delamination of the passivation-

underfill interface. After 1000 cycles, all the flip chip assemblies were electrically continuous and there was little delamination along the passivation-underfill interface. The solder joints in the flip chip assemblies started failing by 1200 cycles and by 1800 cycles, all the flip chip assemblies were electrically open. At this point, there was a significant amount of delamination at the underfill-passivation interface, mostly starting from the corner of the chip as seen in Figure 8.3. Due to the no-flow assembly process, the corner of the chips had very thin fillets unlike the edges. Fillets are known to offer protection against premature underfill delamination [Mahalingam, 2001]. Added to the thin fillets, the stress concentration caused by the chip corner resulted in the underfill-passivation delamination starting at the corner.

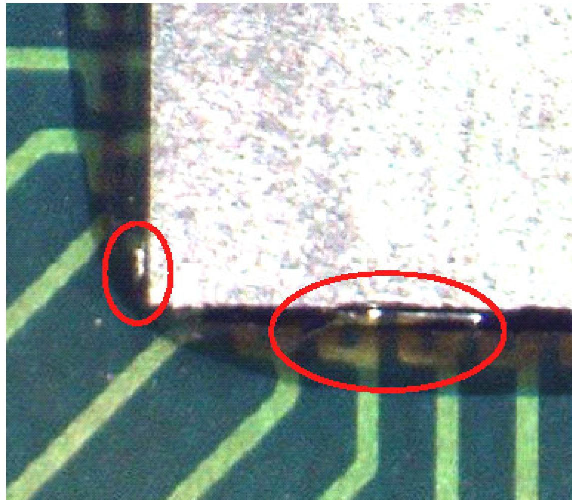

Figure 8.2 Underfill Fillet Cracking

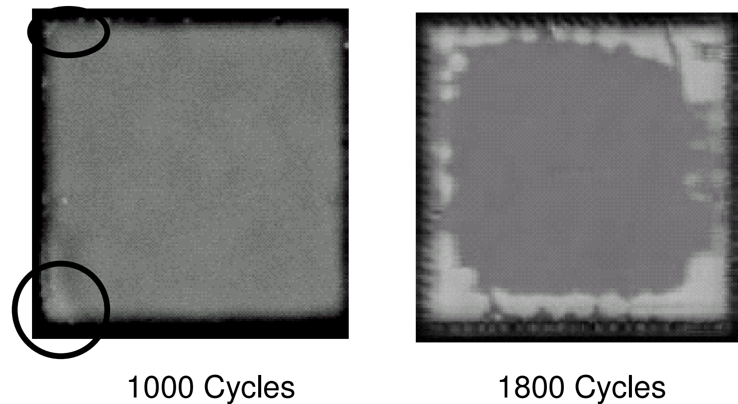

Figure 8.3 Delamination of the Underfill-Passivation Interface

8.2 Analysis of Delamination in Flip Chip Assembly

A half-symmetric 2D plane stress model of the flip chip test vehicle was developed in ANSYS (Figure 8.4). The left edge of the model was constrained in the *X* direction and one node at the left bottom edge of the model was constrained in the *Y* direction as well (Figure 8.4). The crack was assumed to exist at the NFU-SiN passivation interface with complete separation of the chip-fillet interface. Quarter-point elements were used at the crack tip to simulate the singularity and an initial crack length of 3μm was used (Figure 8.5) [Anderson, 1995]. The temperature dependent properties of the underfill material, presented in Chapter 4, were used. Eutectic solder was modeled as an isotropic, elastic-plastic material obeying the bilinear kinematically hardening law (Figure 8.6) and the FR4 substrate was modeled as a linear orthotropic material. Silicon, silicon nitride and the solder mask were modeled as linear elastic materials (Table 8.1). Except the solder and NFU material, all the other materials were specified with temperature independent properties. Since the flip chip assembly was placed in a

hot air oven at 150°C for two hours to completely cure the NFU material, this post-cure temperature was taken as the stress-free temperature for the analysis.

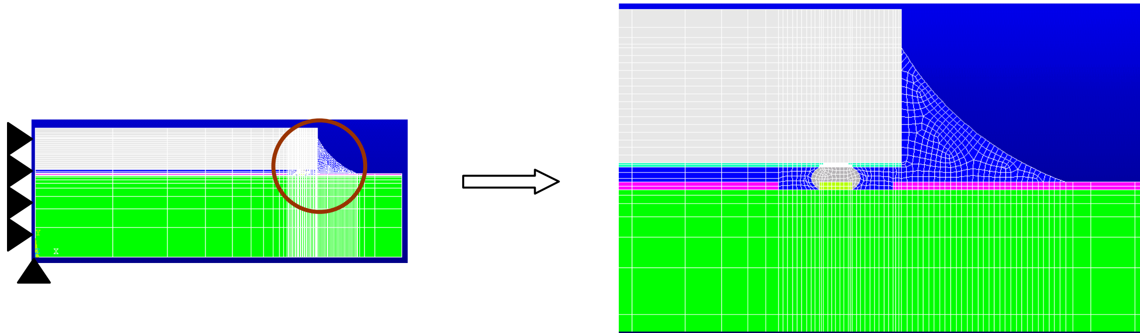

Figure 8.4 Finite Element Model of Flip Chip Assembly

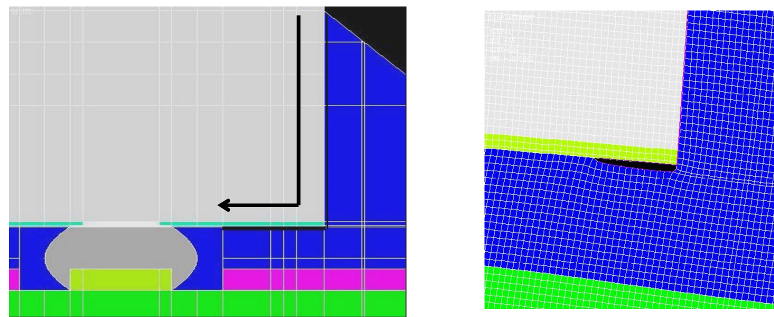

Figure 8.5 Model of Underfill Delamination

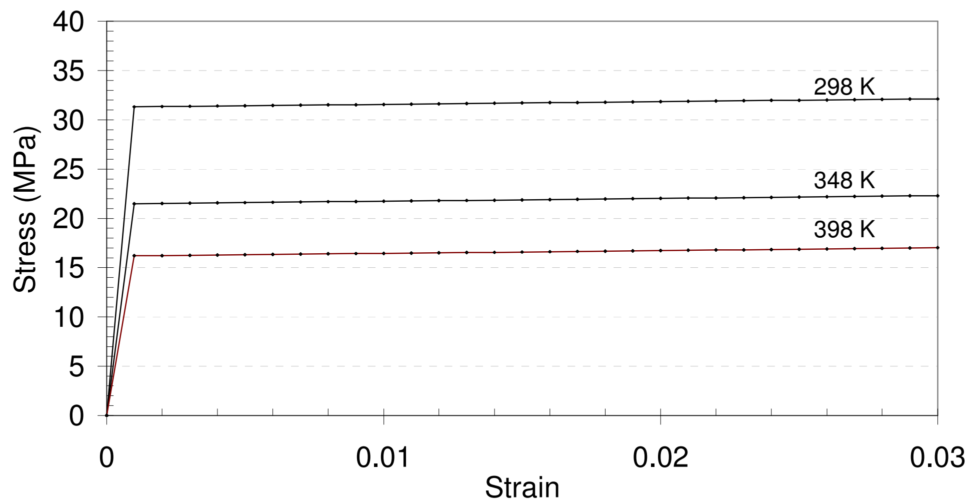

Figure 8.6 Elastic-Plastic Properties of Eutectic Solder

Table 8.1 Material Properties

Material	Elastic Modulus (GPa)	Poisson's Ratio	CTE (ppm/C)
Silicon	170	0.26	2.3
Silicon Nitride	300	0.25	2.8
FR4	24.4 in-plane 1.5 out-of-plane	0.136 in-plane 0.14 out-of-plane	16.2 in-plane 54 out-of-plane
Solder Mask	4	0.38	36

8.2.1 Monotonic Loading

A uniform temperature decrease from the underfill cure temperature (150°C) to room temperature (25°C) was first simulated. The energy release rate was evaluated by performing the J integral along a suitable contour. The mode mixity was evaluated using the CSD method described in Appendix A. The energy release rate and mode mixity for the uniform temperature change was 0.7J/m^2 and 48° respectively. This is much smaller than even the mode I fracture toughness of the NFU-SiN interface. Therefore, the NFU-SiN interface will not delaminate due to the residual stresses that develop as the flip chip cools down to room temperature after the assembly process.

In the same model, normal and tangential cohesive elements were introduced ahead of the crack tip. The cohesive law parameters that were calculated in Chapter 6 were employed and a uniform temperature decrease from 150°C to 25°C was simulated. The energy release rate associated with the spring closest to the crack tip was evaluated as 5.04J/m^2, which is much lower than even the mode I fracture toughness of the NFU-SiN interface. Like conventional fracture mechanics, the cohesive zone model of underfill delamination indicates that

interfacial delamination will not propagate even under large monotonic changes in temperature. However, this value is higher than the value predicted by conventional fracture mechanics. The CZM parameters were derived from two fracture toughness tests, one at mode I and another at mode mixity close to -32°. Clearly, when extrapolated to larger mode mixities, the CZM parameters do not perform as well as linear elastic fracture mechanics.

8.2.2 Fatigue Loading

In order to understand the propagation of delamination under fatigue loading, a thermal shock cycle between -40°C and 125°C was simulated on the finite-element model developed earlier. Contact elements were used between the crack faces to prevent interpenetration during the simulation [Figiel and Kaminski, 2003]. The mode mixity at the two extreme temperatures was calculated using the CSD method, described in Appendix A. The mode mixity was calculated using the CSD method and was found to be 49.2^{o} and 47.1^{o} at -40°C and 125°C respectively and this is slightly higher than the mode mixity of the delamination studies in the fatigue test. The energy release rate (ERR) was calculated by performing the J integral around a suitable contour and the range of ERR (ΔG) was calculated as the difference between the ERR at the two extreme temperatures. The ERR was found to be 1.6J/m^2 and 0.03J/m^2 at –40°C and 125°C respectively.

According to the Paris law developed in Chapter 7, the rate of crack propagation for a ΔG of 1.57J/m^2 is 0.86μm per cycle. At this rate, the crack length at the end of 1800 cycles would be 1.54mm. Assuming the delamination grows in a circular shape where the radius is defined by the crack length (Figure 8.7), the extent of delamination at the end of 1800 cycles is about 30% of the chip area. The extent of delamination in the flip chip assemblies that were tested under thermal shock varied between 2 and 25% and the average extent of delamination was about 7% of the total chip area (Figure 8.8). The Paris model predicts much faster delamination in actual flip chip packages.

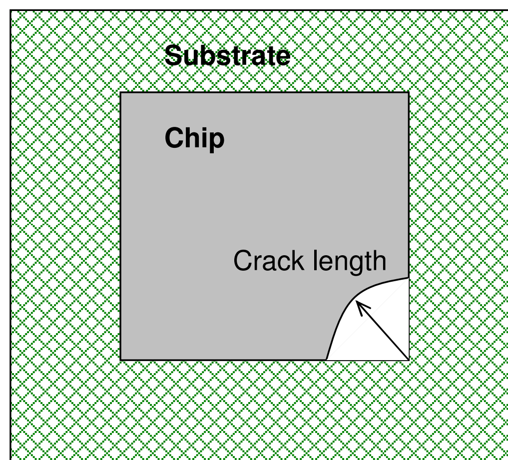

Figure 8.7 Growth of Delamination in Flip Chip Assembly

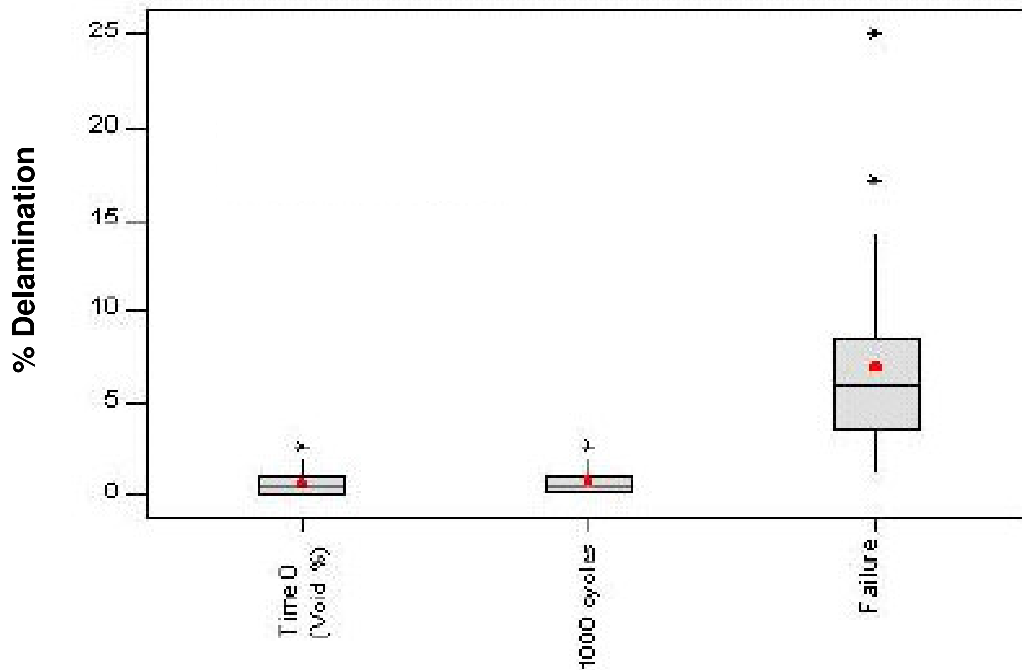

Figure 8.8 NFU-SiN Interfacial Delamination in Flip Chip Assemblies

Unlike the flip chip assembly, the finite-element model assumes the presence of initial delamination. In the actual flip chip assemblies, it took about 1000 cycles for the delamination to initiate and this is not accounted in the prediction based on the Paris law. Therefore, the delamination in the flip chip assemblies propagated only over 800 cycles and not for the entire duration of 1800 cycles and the crack length of at the end of 1800 cycles would then be 0.68mm, which translates to a delamination of about 6% of the chip area. When compared to the flip chip assemblies, this is a reasonable estimate of the extent of delamination.

CHAPTER 9

GUIDELINES FOR UNDERFILL DESIGN

In the previous chapters, the behavior of the underfill-passivation interface under monotonic and fatigue loading was studied. It was shown that while the delamination may not progress under monotonic loading, it may delaminate under thermal cycling. Based on the experiments and models developed thus far, general guidelines for NFU material design are developed and presented in this chapter.

9.1 Interfacial Delamination

In this chapter, different types of delamination occurring in flip chip assemblies are studied using finite-element models and the effect of underfill material properties is emphasized (Figure 9.1). In particular, three delamination patterns were analyzed:

a) A crack along the chip-fillet interface
b) A crack along the underfill-passivation interface with complete separation at the chip-fillet interface (called L crack)
c) A crack only along the underfill-passivation interface (called corner crack)

The 2D model consisted of the diagonal section of a peripheral array, 5mm x 5mm flip chip assembled on a 6.5mm x 6.5mm, 1.5mm thick FR4 substrate (please refer to Figure 8.4, Chapter 8). The parameters of interest were the

energy release rate (ERR) and mode mixity of the crack, and were evaluated using the J integral and the CSD method respectively (Appendix A). Plane stress conditions were assumed to give conservative estimates of ERR. Half-symmetry boundary conditions as shown in Figure 8.4 in Chapter 8 were considered.

Solder was considered as an isotropic, temperature dependent elastic-plastic following the bilinear kinematically hardening law for plasticity. The substrate material, FR4, was modeled as a linear orthotropic material. Silicon, silicon nitride and solder mask were considered as temperature independent linear elastic materials (please refer to Table 8.1, Chapter 8).

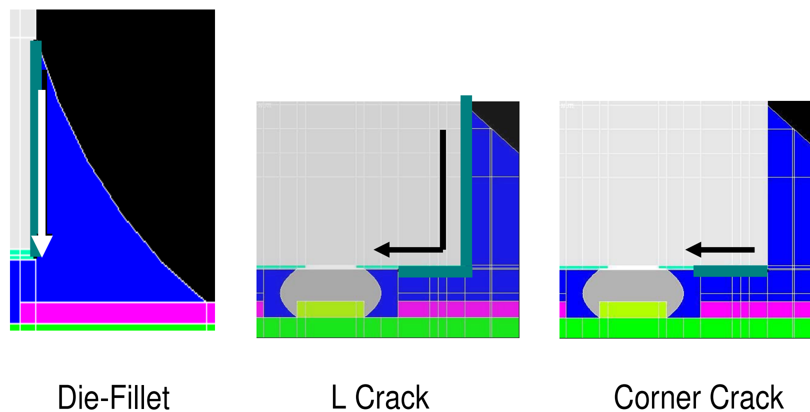

Figure 9.1 Delamination Patterns

The cracks lengths were normalized to the maximum length of the crack that was possible. Three levels of underfill modulus – 3, 6 and 9GPa and three levels of underfill CTE – 25, 50 and 75ppm/^{o}C were simulated. For all the models, the post cure temperature of the NFU material (150°C) was taken as the stress free

temperature for the model. In order to simulate the worst case, a temperature change from 150°C to –55°C was studied.

9.2 Chip-Fillet Interface

Figure 9.2 shows the model of a crack between the underfill fillet and the vertical edge of the chip. The energy release rate (ERR) for the chip-fillet crack increases with increase in modulus and CTE (Figure 9.3). While the dependence on modulus appears to be linear, the dependence on CTE is non-linear. This is expected since the energy release rate depends using on the square of the load, which is proportional to $\Delta\alpha\Delta T$ [Gurumurthy et al, 1998b]. The effect of underfill material properties on the mode mixity at the chip fillet interface is shown in Figure 9.4. Unlike the energy release rate, the pre-dominant effect here is one of the crack length itself. As the crack opens, it approaches mode I and as it was shown in Chapter 5, the mode I fracture toughness is usually smaller than the mode II fracture toughness. While it may seem that the crack would get arrested, the mode mixity of the crack and hence the fracture toughness decrease with crack length. Therefore, the crack can continue to grow even though ERR decreases.

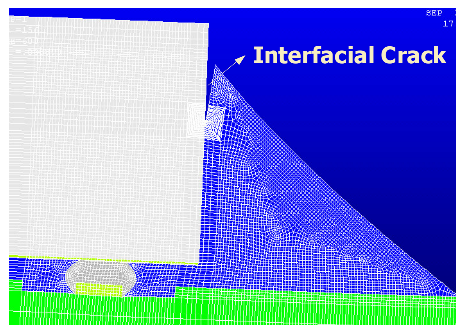

Figure 9.2 Finite Element Model of the Chip-Fillet Crack

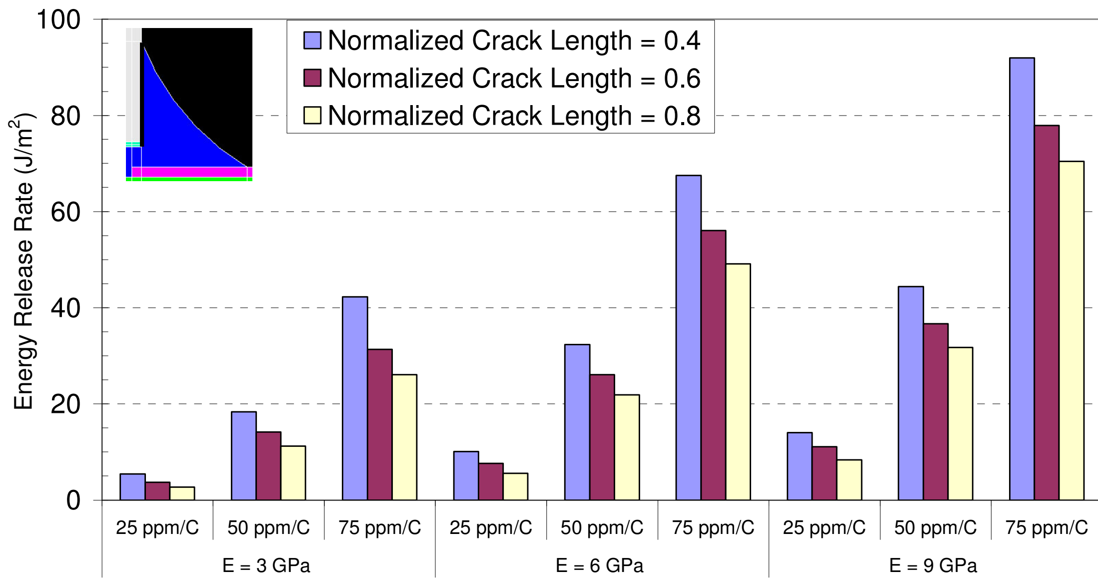

Figure 9.3 Effect of Underfill Properties on the ERR for the Chip-Fillet Crack

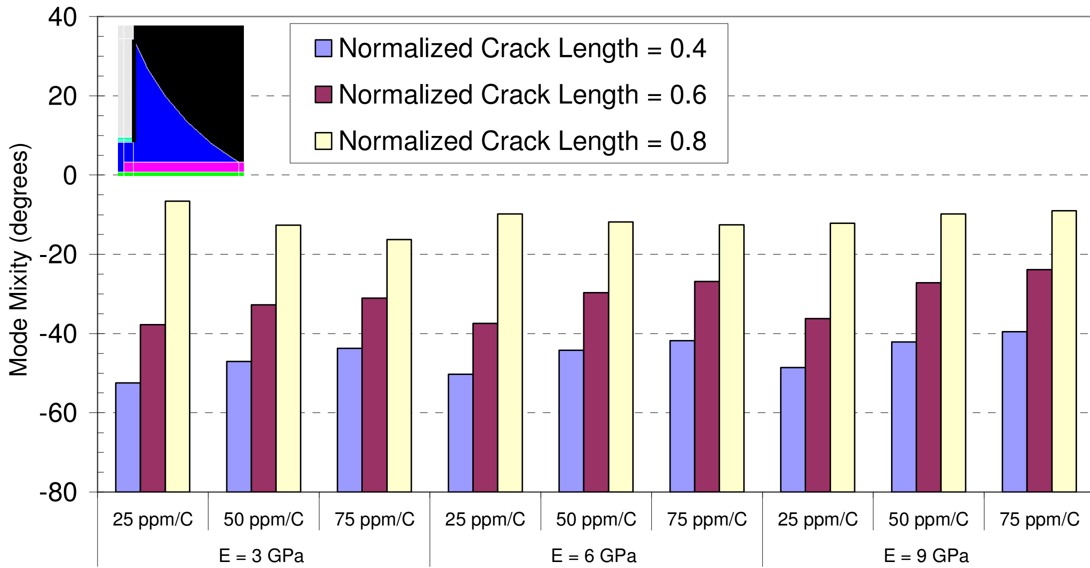

Figure 9.4 Effect of Underfill Properties on the Mode Mixity for the Chip-Fillet Crack

9.3 Crack Deflection

Once the crack grows through the entire length of the chip-fillet interface, there are many paths the crack can deflect into. Five such options, $\theta = 0^o, 45^o, 90^o$, 135° and 180°, were explored (Figure 9.5) and the energy release rate and mode mixity in all these cases were calculated. It is to be noted that in four of the five options investigated, the crack changes from being an interfacial crack into a crack purely in the underfill material. For these cases, calculation of ERR and mode mixity was achieved through the displacement extrapolation method built within ANSYS. The underfill modulus and CTE were 6GPa and 50ppm/^{o}C respectively for all the simulations. The crack length in all the directions was assumed to be 50µm and a temperature change from 150°C to –55°C was applied to the model in all the cases.

The ERR for the five options are shown in Figure 9.6. The criterion for crack deflection suggested by [He et al, 1989] is that between two options, A and B, for the crack to grow into, the crack would deflect into path A if the following criterion were satisfied.

$[G/G_c]_A > [G/G_c]_B$ where

G is the energy release rate and G_c is the critical energy release rate for that path.

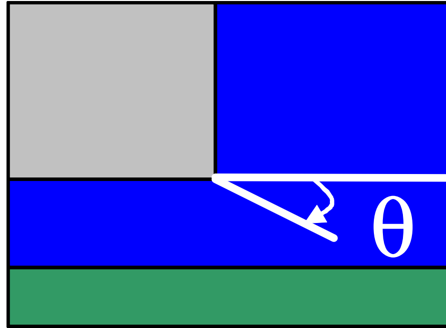

Figure 9.5 Paths for Crack Deflection

Based on this criterion, it seems most likely that the crack would get deflected into the underfill-passivation interface as is normally observed in flip chip assemblies.

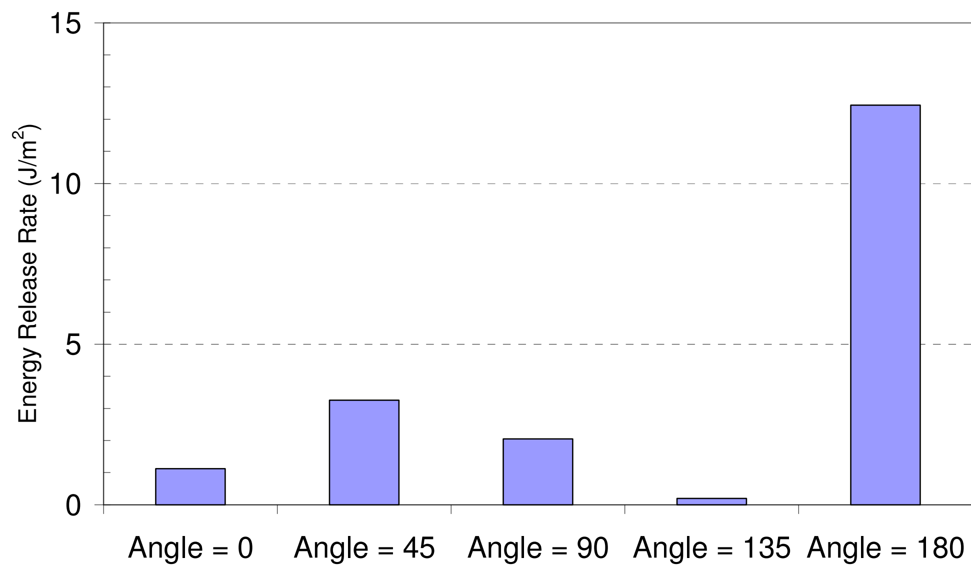

Figure 9.6 Comparison of ERR for Different Crack Paths

9.4 L Crack

The effect of underfill properties on the ERR for the L crack is shown in Figure 9.7. It is clear that the ERR is not as high as the previous case. Higher underfill CTE leads to higher ERR. However, there is not a strong effect of the modulus of the underfill material. The ERR seems to increases steadily with the crack length as well. The mode mixity for all cases varies between 45 and 55 degrees and there is no clear trend in terms of the underfill properties or the crack length (Figure 9.8).

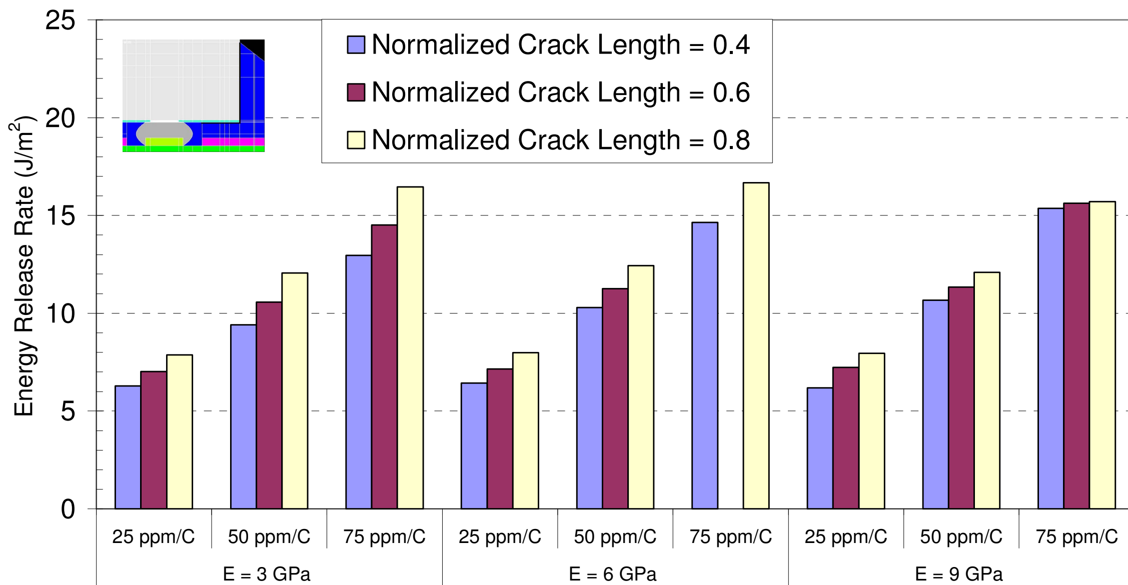

Figure 9.7 Effect of Underfill Properties on the ERR for the L Crack

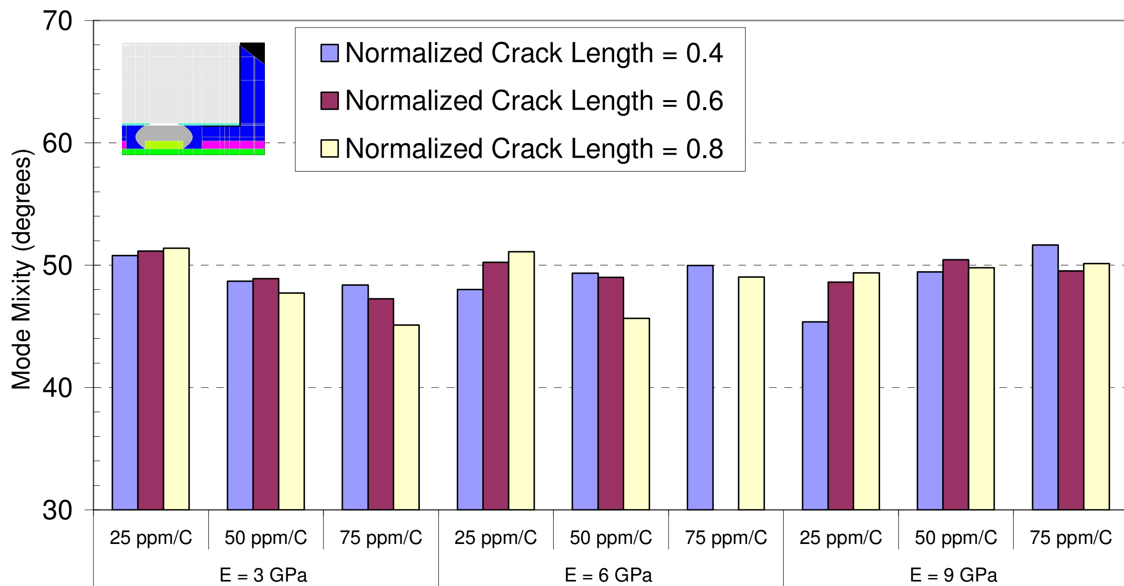

Figure 9.8 Effect of Underfill Properties on the Mode Mixity for the L Crack

9.5 Corner Crack

The effect of underfill properties on ERR for the corner crack is shown in Figure 9.9. Compared to the L crack configuration, the corner crack is less prone to delamination because the entire length of the chip-fillet interface has not delaminated and this is reflected in the slightly lower values of energy release rate. Like the L crack, the underfill CTE has a strong effect on the ERR experienced at the crack tip compared to the underfill modulus. The mode mixity of the crack tip is higher than the L crack configuration indicating that the corner crack configuration may be less prone to delamination (Figure 9.10). However, there is no clear effect of the underfill material properties on the mode mixity of the corner crack configuration.

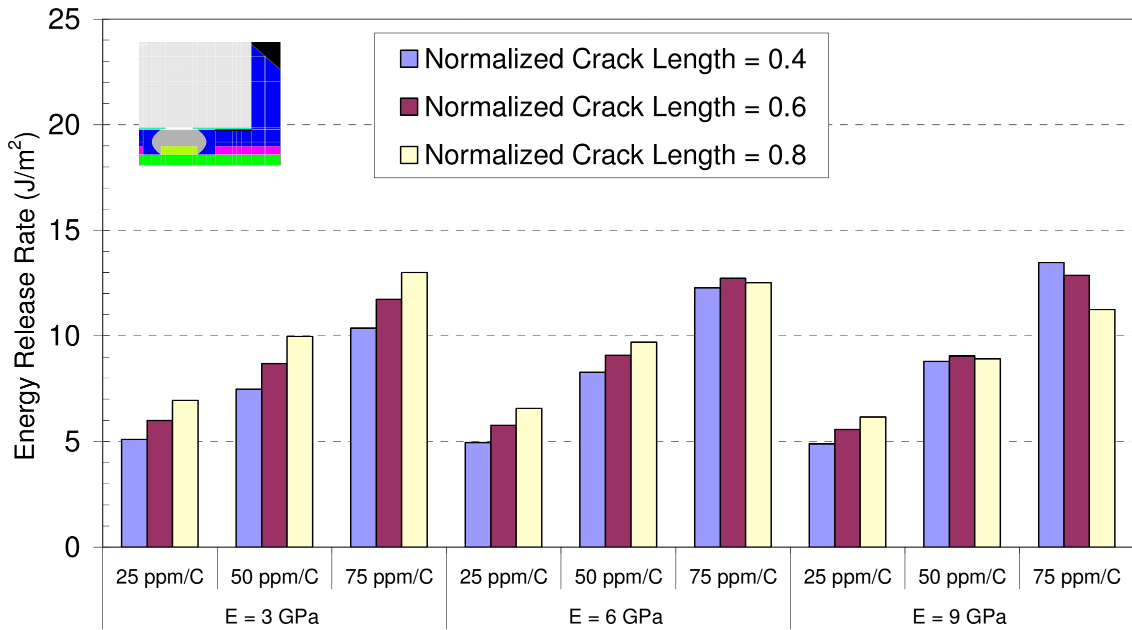

Figure 9.9 Effect of Underfill Properties on the ERR for the Corner Crack

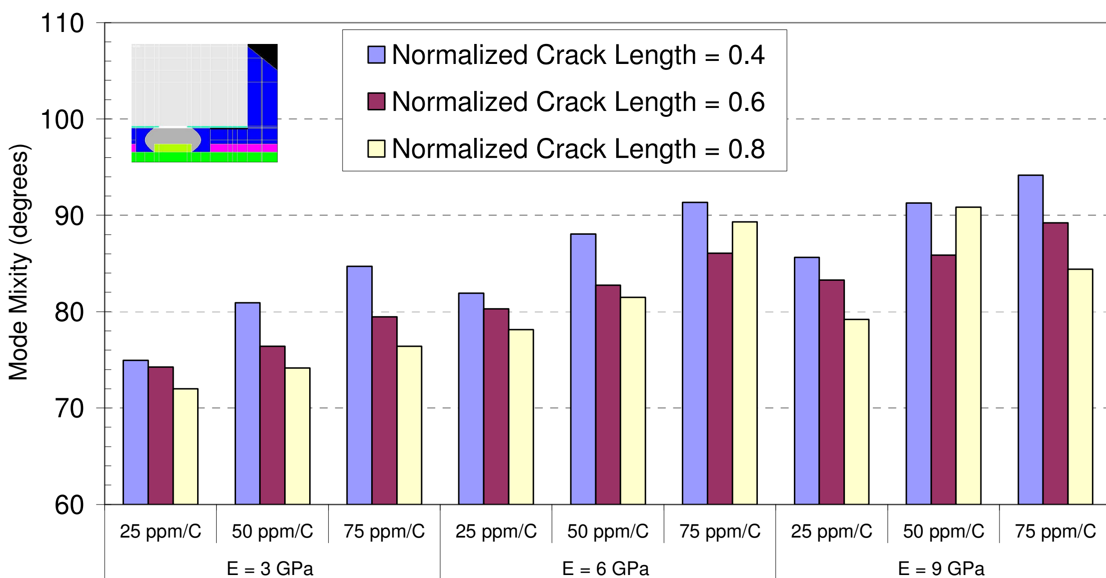

Figure 9.10 Effect of Underfill Properties on the Mode Mixity for the Corner Crack

9.6 Underfill Fillet Crack

Besides the 2D models, a 3D model of an assembly with a crack in the underfill fillet at the chip corner was also modeled (Figure 9.11). A 3D quarter symmetry model of the flip chip was developed and a crack in the underfill fillet starting the corner of the chip was introduced. The solder joint, solder mask and the silicon nitride passivation were not included in the model. Silicon and underfill were modeled as temperature independent linear elastic materials while the FR4 substrate was modeled as a linear orthotropic material. Since this is not an interfacial crack, 3D quarter point elements were used and the extraction of fracture parameters was done using the displacement extrapolation method built within ANSYS. The crack length was normalized against the fillet height and three crack lengths, 0.3, 0.5, and 0.7 were examined. Three levels of underfill CTE, 25, 50 and 75ppm/^{o}C and two levels of modulus, 3 and 5GPa were simulated.

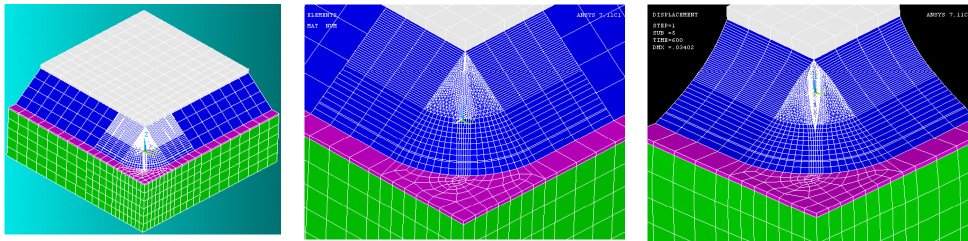

Figure 9.11 3D Model of a Flip Chip with a Fillet Crack at the Corner

The effect of underfill material properties on ERR is shown in Figure 9.12. It is clear that the ERR increases with increase in modulus and CTE. The effect of crack length seems insignificant though it does increase slightly for the higher CTE underfills. For all these cases, the crack was purely mode I. The G_{II} and G_{III}

values were three orders of magnitude smaller than the value of G_I. This is expected since the corner crack is symmetric along the diagonal of the chip.

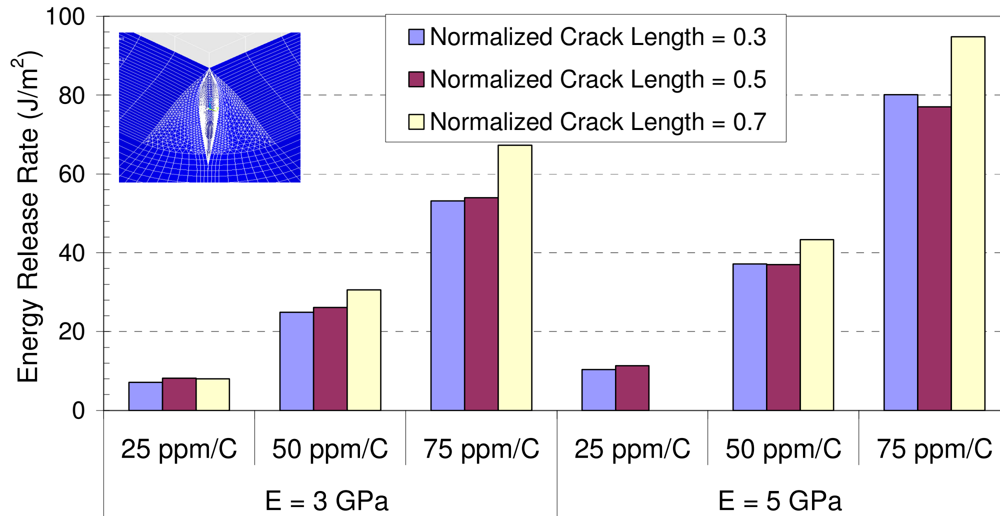

Figure 9.12 Effect of Underfill Properties on the ERR for the Corner Fillet Crack

9.7 Design Guidelines

The energy release rate for the L-crack and corner crack configurations were much smaller than the mode I fracture toughness of the NFU-SiN fracture toughness measured in Chapter 5. Therefore, it is unlikely that delamination at the underfill-passivation interface will propagate under monotonic thermal loading. However, the ERR for the die-fillet interface crack and the crack in underfill fillet were much higher. Though the fracture toughness is not known, it is possible for small, pre-existing flaws along the die-fillet interface or in the underfill fillet to propagate under a uniform temperature change. The ERR for all types of delamination increased with the CTE of the underfill material and in some cases,

the ERR also increased with the modulus of the underfill material. In order to prevent the propagation of delamination, the energy available for crack growth needs to be minimized and lower modulus and CTE values are required to achieve this objective. Since it is not possible to decrease both the modulus and the CTE of the underfill material at the same time and since CTE has a stronger effect on the propagation of delamination, it is recommended that the CTE be given more emphasis in designing the underfill material against delamination.

As mentioned earlier, underfill delamination in flip chip assemblies propagates under thermal excursions. The range of energy release rate or ΔG was used to calculate the rate of crack propagation in Chapter 8. Like monotonic loading, lower modulus and CTE of the underfill material lead to lower values of ΔG for the same thermal shock cycle, and the propagation of underfill delamination can be delayed.

CHAPTER 10

CONCLUSIONS, RESEARCH CONTRIBUTIONS AND FUTURE WORK

10.1 Conclusions

The next generation of electronic packaging may truly be the era of nano-composites. Using materials at the nano-size presents certain unique advantages and some tough challenges. Traditional dispense-and-cure underfills add time and process cost, and also cannot be effectively used with the continued reduction in the flip-chip solder bump pitch. On the other hand, nano-filled underfills have a great potential as no-flow underfills and could enhance the overall reliability of solder bumps. In addition, nano-filled underfill materials are excellent candidates for the wafer level underfilling process because of their optical translucence. This eliminates the need for capillary as well as no-flow underfilling. However, as it was shown, the formulation of nano-filled underfill (NFU) materials is a challenging task.

Based on the work that was presented in this thesis, the following conclusions can be drawn.

1) The viscosity of NFU materials increases dramatically when the filler content is above 50% by weight. For an efficient no-flow underfill process, it is estimated that the viscosity of the underfill has to be less than 10Pa.s.

2) The CTE of the underfill can be decreased by increasing the filler content. However, any additional decrease in CTE by having filler content beyond 30% is not substantial and therefore it is recommended that

3) The NFU be filled with 30% of 20nm silica particles by weight. The viscosity of such an NFU material is about 2Pa.s and the CTE is about 50ppm/^{o}C at room temperature.

4) The glass transition temperature of an underfill filled with 30% by weight with 20nm silica particles is about 150°C. This glass transition temperature is higher than the typical temperature witnessed by the flip chip package in field-use conditions as well as most accelerated thermal cycling conditions. This implies that the underfill remains glassy during such thermal excursions and will provide sufficient mechanical support to enhance solder bump reliability.

5) The fracture toughness of the NFU-passivation interface is about 120J/m^2 at a mode mixity of 32° and about 79J/m^2 at a mode mixity of -0.1^{o}.

6) The energy release rate experienced by the NFU-SiN interface at the end of curing and cool down to room temperature as well during thermal cycling is much smaller than the fracture toughness of the interface. This means that the interface will not delaminate due to the thermal stresses resulting from the assembly process. This is confirmed by both traditional fracture mechanics approach as well as CZM.

7) The fatigue crack propagation along the NFU-passivation interface follows a power law and is given by $\frac{da}{dN} = 0.0006(\Delta G)^{0.8786}$. According to this law , 6% of the NFU-SiN interface in a standard 5mm x 5mm flip chip would have delaminated by 1800 cycles. Experimental results show that the delamination varies from 2 to 25% between samples and the average delamination was about 6%.

8) Flip chip assemblies using the NFU material lasted more than 1000 thermal shock cycles. The first solder bump failure occurred at 1200 cycles and all the assemblies were electrically discontinuous by 1800 cycles.

9) Finite element modeling of delamination occurring in a flip chip package indicates that the energy release rate increases linearly with the elastic modulus of the underfill and non-linearly with the CTE of the underfill. The driving force or energy release rate for delamination propagation can be reduced by reducing the CTE of the underfill and/or the modulus of the underfill.

10) Cohesive zone modeling can be used to study underfill delamination. There was good agreement between the results from CZM and linear elastic fracture mechanics. However, the results are quite sensitive to the CZM parameters and it is recommended that these parameters be derived based on a number of experiments conducted at different mode mixities.

10.2 Research Contributions

The following contributions have been made by this research.

1) This research has contributed toward the fundamental understanding of interfacial delamination in NFU through both experiments and models. In particular, this work

   a. Has characterized the properties of a nano-filled underfill material, and based on process and reliability requirements, has recommended an optimal filler content of 30% to satisfy competing requirements.

   b. Has developed an innovative residual stress induced decohesion (RSID) test and used the test to measure the interfacial fracture toughness of NFU-SiN interface at a mode mixity of -0.1^{o}. This research has also characterized the same interface at a higher mode mixity -32° using the single-leg bending (SLB) test.

   c. Has conducted comprehensive thermo-mechanical fatigue delamination test to create a model for delamination propagation under thermo-mechanical fatigue loading. Such thermo-mechanical fatigue characterization for underfills is different from isothermal mechanical fatigue tests reported in literature, and the developed characterization is representative of typical thermal excursions in flip chip assemblies.

   d. Has applied the developed models to flip-chip assemblies under thermal cycling conditions, predicted the delamination propagation

under thermal cycling, and have validated the results with experimental data. Such an approach is rarely found in literature, and is the first for nano-filled underfills.

e. Has successfully used CZM to model and study interfacial fracture in flip chip assemblies, and such an application of CZM is unique.
f. Has made design guidelines to enhance the reliability of flip-chip assemblies based on the experimental data and predictive models.

10.3 Recommendations for Future Work

The following are some recommendations for future work in this area.

1) With the pending regulations toward moving to environmentally friendly lead-free solder alloys, the development of nano-filled, no-flow underfill materials for lead-free flip chip assembly would be a logical extension to this work. There are significant challenges in terms of material development because of the higher reflow temperature of the lead-free solder. The thermal stresses will be higher and the interfacial integrity will be crucial to ensure reliability of lead-free assemblies.
2) The effect of moisture on the behavior of the NFU materials under monotonic and fatigue loading conditions will complete the picture of delamination under different environmental conditions. At present, the physics of moisture penetration in nano-filled underfills is not known.

3) The effect of temperature on the fracture toughness of underfill related interfaces is not known. Cracks tend to grow or initiate at low temperatures not only because the residual stresses are high but also because the fracture toughness of the interfaces are usually lower at lower temperatures.

4) In general, the uniqueness of the cohesive zone parameters developed in this work cannot be emphasized because of the extensive use of finite element modeling. The physical relevance of the cohesive law parameters can only be qualitatively argued and their relevance to underlying material behavior will need extensive experimentation.

APPENDIX A

INTERFACIAL FRACTURE MECHANICS

In this work, interfacial delamination is considered as an interfacial crack and the calculation of the interfacial fracture parameters such as energy release rate and mode mixity can be achieved in a number of methods. [Williams, 1959], [Erdogan, 1963], and [England, 1965] have provided elasticity solutions for bimaterial fracture. These solutions demonstrate the oscillatory nature of the singularity close to the crack tip. This can be represented as,

$$\sigma_{yy} + i\sigma_{xy} = \frac{Kr^{i\varepsilon}}{\sqrt{2\pi r}} = \frac{(K_I^* + iK_{II}^*)r^{i\varepsilon}}{\sqrt{2\pi r}} \qquad (1)$$

where

$\varepsilon = \frac{1}{2\pi}\log[\frac{\frac{\mu_1}{\kappa_1}+\frac{1}{\kappa_2}}{\frac{\mu_2}{\kappa_2}+\frac{1}{\kappa_1}}]$ is the oscillation index

$\kappa_i =$ shear modulus of the ith material

$\mu_i = \frac{3-\nu_i}{1+\nu_i}$ for plane stress and $3-4\nu_i$ for plane strain and

ν_i is the Poisson's ratio of the ith material

Due to the elastic mismatch of the materials involved in the interface, an interface crack experiences both a peel and a shear mode, even if the remote loading is strictly mode I. Therefore, mode mixity, which is a measure of the relative magnitudes of the in plane shear and peel stresses, has to be considered in any

interfacial crack problem. Since the elasticity solution is oscillatory in nature, the ratio of modes varies with the distance from the crack tip.

The mode mixity and stress intensity factors are extracted using the Crack Surface Displacement (CSD) method [Matos et al, 1989]. The method is based on deriving fracture mechanics parameters from the relative displacements of the nodes along the crack surface that were initially coincident. The development of this method is as follows.

Based on equation 1, the displacements also exhibit an oscillatory character,

$$\Delta u_y + i\Delta u_x = \mathrm{H}\frac{(K_1^* + iK_2^*)r^{i\varepsilon}}{(1+i2\varepsilon)\cosh\pi\varepsilon}\sqrt{\frac{r}{2\pi}} \qquad (2)$$

where

$$H = 2[\frac{(1-\nu_1^2)}{E_1} + \frac{(1-\nu_2^2)}{E_2}] \text{ for plane strain}$$

$$= [\frac{1}{E_1} + \frac{1}{E_2}] \text{ for plane stress}$$

and r is the distance from the crack tip

The symbol Δ is used to signify the relative displacements in the corresponding direction between two initially coincident nodes along the crack surface. Equation (2) can be expressed as

$$|\Delta u| e^{i\phi} = \alpha \sqrt{r} |K| e^{i\left[\hat{\psi} + \varepsilon \ln(\frac{r}{\hat{r}}) - \beta\right]}$$

where

$$\alpha = \frac{\mathrm{H}}{\sqrt{2\pi(1+4\varepsilon^2)} \cosh(\pi\varepsilon)}$$

$|\Delta u|$ and ϕ are the modulus and argument of the complex number $\Delta u_y + i\Delta u_x$

β is the principal argument of the complex number $1 + i2\varepsilon$

It can therefore be written that

the phase angle, $\hat{\psi} = \phi - \varepsilon \ln(\frac{r}{\hat{r}}) + \beta$ and

the modulus of stress intensity factor, $|K| = \frac{|\Delta u| \sqrt{2\pi(1+4\varepsilon^2)} \cosh(\pi\varepsilon)}{H\sqrt{r}}$ (3)

where

$\hat{r}$ is the characteristic dimension.

The modulus of the complex stress intensity factor can now be related to the energy release rate, G as follows.

$$|K| = 2\sqrt{\frac{2G}{H}} \cosh(\pi\varepsilon) \qquad (4)$$

The “global” energy release rate is calculated using the J integral. Other techniques to calculate the energy release rate exist and are discussed in [Harries et al; Rybicki et al, 1977; Aslantas, 2003; Bjerken et al, 2001; Venkatesha et al, 1996]. The “local” energy release rate is given by equation 3 and is based on the CSD method. Using an appropriate choice of $\hat{r}$, the characteristic dimension, the values of mode mixity and stress intensity factors are calculated at the node where the “global” and “local” values of the energy release rate are equal to each other. The characteristic dimension does not influence the mode mixity values much if the value of the oscillation index ε is small. This is typically the case in the interfaces that are studied in this work. The characteristic dimension for all the mode mixity calculations done in this work was chosen as the thickness of the solder mask layer, which is 25 microns.

In all the cases, the “global” value of the energy release rate was calculated by using the path independent J integral. For the linear elastic case, there is no difference between the global energy release and the J integral.

Global Energy Release Rate $G = J = \int_{\Gamma}(Wdy - T_i \frac{\partial u_i}{\partial x} ds)$ where W, T_i and u_i are strain energy density, nodal tractions and displacements respectively and are reported in any finite element solution [Harries and Sitaraman, 2001].

APPENDIX B

CRACK IN A BILAYER UNDER UNIFORM TEMPERATURE CHANGE

[Suo and Hutchinson, 1990] have presented a general solution for a crack between two elastic layers under a given edge loading. They use superposition to reduce the problem and the energy release rate is given in terms of force P and moment M (Figure A2.1).

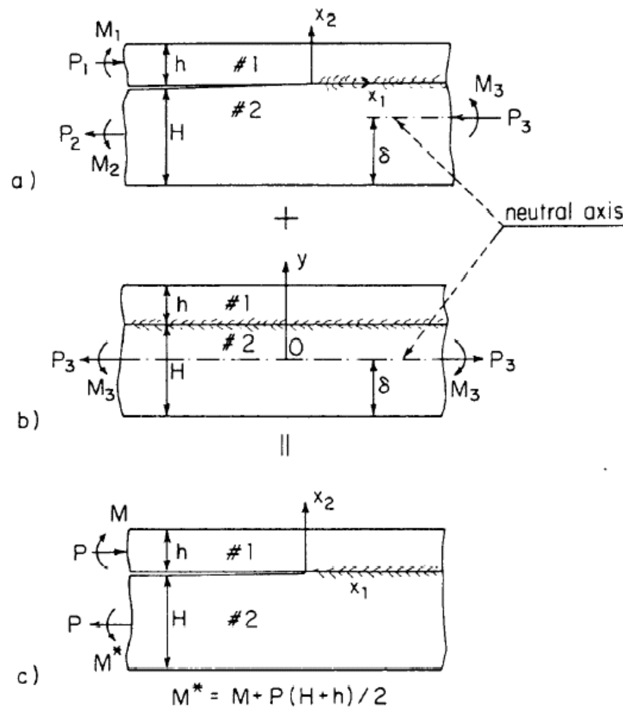

Figure A2.1 Crack between Two Elastic Layers – Superposition [Suo and Hutchinson, 1990]

The case of the residually stressed thin film on a substrate is exactly equivalent to the following load combinations shown in Figure A1.1a.

$$P_1 = P_3 = \sigma^T h$$

$$M_3 = \sigma^T h\left(H - \delta + \frac{h}{2}\right)$$

$$M_1 = 0$$

Therefore,

$$P = \sigma^T h\left[1 - C_1 - C_2(\frac{1}{\eta} - \Delta + \frac{1}{2})\right]$$

$$M = -\sigma^T h^2 C_3\left(\frac{1}{\eta} - \Delta + \frac{1}{2}\right)$$

where

$\sigma^T = \dfrac{8\Delta\alpha\Delta T}{c_1}$ is the misfit stress between the two layers

$\Delta\alpha$ is the difference in CTE between the two layers

ΔT is the uniform temperature change

$$C_1 = \frac{\Sigma}{A_o}$$

$$C_2 = \frac{\Sigma}{I_o}\left(\frac{1}{\eta} - \Delta + \frac{1}{2}\right)$$

$$C_3 = \frac{\Sigma}{12 I_o}$$

$$A_o = \frac{1}{\eta} + \Sigma$$

$$I_o = \frac{1}{3}\left\{\Sigma\left[3\left(\Delta - \frac{1}{\eta}\right)^2 - 3\left(\Delta - \frac{1}{\eta}\right) + 1\right] + 3\frac{\Delta}{\eta}\left(\Delta - \frac{1}{\eta}\right) + \frac{1}{\eta^3}\right\}$$

$$\frac{\delta}{h} = \Delta = \frac{1 + 2\Sigma\eta + \Sigma\eta^2}{2\eta(1 + \Sigma\eta)}$$

$$\Sigma = \frac{1+\alpha}{1-\alpha}$$

$$\eta = \frac{h}{H}$$

h = thickness of the thin film layer

H = thickness of the substrate

$$\alpha = \frac{\Gamma(\kappa_2 + 1) - (\kappa_1 + 1)}{\Gamma(\kappa_2 + 1) + (\kappa_1 + 1)}$$

$$\beta = \frac{\Gamma(\kappa_2 - 1) - (\kappa_1 - 1)}{\Gamma(\kappa_2 + 1) + (\kappa_1 + 1)}$$

are the Dundurs parameters

The oscillation index is

$$\varepsilon = \frac{1}{2\pi} \ln \frac{1-\beta}{1+\beta}$$

$$c_1 = \frac{\kappa_1 + 1}{\mu_1}$$

$$c_2 = \frac{\kappa_2 + 1}{\mu_2}$$

where

$$\Gamma = \frac{\mu_1}{\mu_2}$$

$\kappa_i = 3 - 4\nu_i$ for plane strain

$\kappa_i = \dfrac{3-\nu_i}{1+\nu_i}$ for plane stress

μ_i and ν_i are the shear modulus and Poisson's ratio of the respective layers (Figure A2.1a)

The energy release rate can be computed by taking the difference of the energy stored in the structure far ahead and far behind the crack tip.

$$G = \frac{c_1}{16}\left[\frac{P^2}{Ah} + \frac{M^2}{Ih^3} + 2\frac{PM}{h^2\sqrt{AI}}\sin\gamma\right]$$

where

$$A = \frac{1}{1+\Sigma(4\eta + 6\eta^2 + 3\eta^3)}$$

$$I = \frac{1}{12(1+\Sigma\eta^3)}$$

and

$$\sin\gamma = 6\Sigma\eta^2(!+\eta)\sqrt{AI}$$

The mode mixity is given by

$$\psi = \tan^{-1}\left[\frac{\lambda\sin\omega - \cos(\omega+\lambda)}{\lambda\cos\omega - \sin(\omega+\lambda)}\right]$$

where

$$\lambda = \frac{Ph}{M}\sqrt{\frac{I}{A}}$$

and ω is a function of α, β and η

[Suo and Hutchinson, 1990] have published values of ω for various combinations of α, β and η. In all the cases encountered, ω varied between -55° and -53°.

APPENDIX C

CRACK IN A TRILAYER UNDER UNIFORM TEMPERATURE CHANGE

[Gaudette et al, 2000] have presented the solution for energy release rate for a crack existing between the top two layers in a three layered structure under uniform temperature change (Figure A3.1).

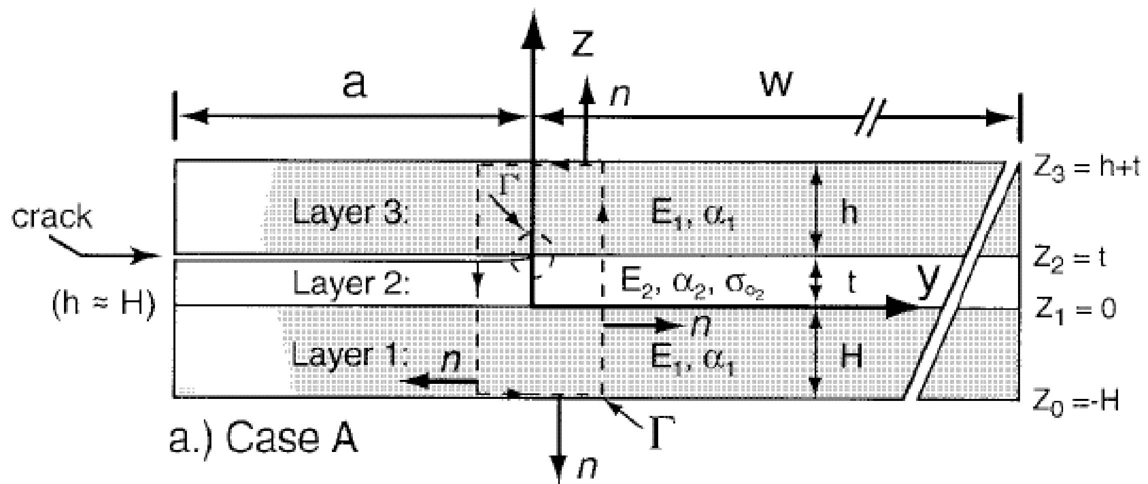

Figure A3.1 Crack in a Tri-layer Structure [Gaudette et al, 2000]

The approach taken here is very similar to the approach taken by [Suo and Hutchinson, 1990] described in Appendix 2. The energy release rate is calculated as the difference between the energy stored ahead of the crack tip and energy stored ahead of the crack tip.

The energy stored ahead of the crack tip is first estimated by solving for the strain at the interface between layers 1 and 2 and the radius of curvature of the uncracked tri-layer structure.

$$\varepsilon_o = \alpha_2 \Delta T \left(\frac{4\lambda_3\lambda_4 - 3\lambda_2\lambda_5}{4\lambda_1\lambda_3 - 3\lambda_2^2} \right)$$

$$\kappa = \frac{6\alpha_2 \Delta T}{t} \left(\frac{\lambda_1\lambda_5 - \lambda_2\lambda_4}{4\lambda_1\lambda_3 - 3\lambda_2^2} \right)$$

where

α_i is the CTE of the ith layer (Figure A3.1)

ΔT is the uniform change in temperature

$$\lambda_1 = X\varsigma + Z\eta + 1$$
$$\lambda_2 = -X\varsigma^2 + Z\left((\eta+1)^2 - 1\right) + 1$$
$$\lambda_3 = X\varsigma^3 + Z\left((\eta+1)^3 - 1\right) + 1$$
$$\lambda_4 = XY\varsigma + ZW\eta + 1$$
$$\lambda_5 = -XY\varsigma^2 + ZW\left((\eta+1)^2 - 1\right) + 1$$

and

$$\eta = \frac{h}{t}$$
$$\varsigma = \frac{H}{t}$$

$$X = \frac{E_1}{E_2}$$
$$Z = \frac{E_3}{E_2}$$

$$Y = \frac{\alpha_1}{\alpha_2}$$
$$W = \frac{\alpha_3}{\alpha_2}$$

E_i is the Young's modulus of the ith layer

For the case (A) described in the paper, the material properties of the layer 1 and 3 are assumed to be the same. This simplifies a number of the equations.

The energy ahead of the crack is given by:

$$\overline{U} = \frac{1}{6E_2 t(\Delta T(\alpha_2 - \alpha_1))^2}\begin{Bmatrix} X\varsigma\left[3(C_1-1)^2 - 3C_2\varsigma(C_1-1) + (C_2\varsigma)^2\right] + \left[3C_1^2 + 3C_1C_2 + C_2^2\right] + \\ X\eta\left[3(C_1 - 1 + C_2)^2 + C_2\eta(C_1 - 1 + C_2) + (C_2\eta)^2\right] \end{Bmatrix}$$

where

$$C_1 = \frac{\varepsilon_o - \alpha_2 \Delta T}{\Delta T(\alpha_1 - \alpha_2)} \text{ and}$$

$$C_2 = \frac{t\kappa}{\Delta T(\alpha_1 - \alpha_2)}$$

The energy stored in the wake of the crack is calculated by assuming the crack to exist between a substrate comprising of layer 1 and 2 and layer 3. The solution of [Suo and Hutchinson, 1990] with η = 0 (Appendix 1) is used. This gives

$$\overline{U}^* = (E_2 t(\Delta T(\alpha_1 - \alpha_2))^2\left[\frac{X\varsigma(X\varsigma^3 + 1)}{2\xi}\right]$$

where

$$\xi = X\varsigma(X\varsigma^3 + 4\varsigma^2 + 6\varsigma + 4) + 1$$

The energy release is given by

$$G = \overline{U} - \overline{U}^*$$

REFERENCES

Anderson, T. L., “Fracture Mechanics: Fundamentals and Applications”, Second Edition, CRC Press LLC, 1995.

ANSYS Theory Reference, ANSYS Inc., 2003.

Ashcroft, I. A. and Shaw, S. J., “Mode I Fracture of Epoxy Bonded Composite Joints 2. Fatigue Loading”, International Journal of Adhesion and Adhesives, Vol. 22, pp. 151-167, 2002.

Ashcroft, I. A., Adbel Wahab, M. M., Crocombe, A. D., Hughes, D. J. and Shaw, S. J., “The Effect of Environment on the Fatigue of Bonded Composite Joints Part 1: Testing and Fractography”, Composites: Part A 32, pp. 45-58, 2001.

Aslantas, K., “A Different Approach for Calculation of Stress Intensity Factors in Continuous Fiber Reinforced Metal Matrix Composites”, International Journal of Solids and Structures, Vol. 40, pp. 7475-7481, 2003.

Auersperg, J., Kieselstein, E., Schubert, A. and Michel B., “Delamination Risk Evaluation for Plastic Packages Based on Mixed Mode Fracture Mechanics Approaches”, Transactions of ASME – Journal of Electronic Packaging, Vol. 124, pp. 318-322, 2002.

Awaji, H. and Sato, S., “Combined Mode Fracture Toughness Measurement by the Disk Test”, Journal of Engineering Materials and Technology, Vol. 100, pp. 175-182, April 1978.

Ayhan, A. O. and Nied, H. F., “Finite Element Analysis of Interface Cracking in Semiconductor Packages”, IEEE Transactions on Components and Packaging Technology, Vol. 22, No. 4, pp. 503-511, December 1999.

Ayhan, A. O. and Nied, H. F., “Finite Element Modeling of Interface Fracture in Semiconductor Packages: Issues and Applications”, Proceedings of the InterSociety Conference on Thermal Phenomena, pp. 185-192, 1998.

Ayhan, A. O., Ph.D. Dissertation, Mechanical Engineering and Mechanics Department, Lehigh University, Bethlehem, PA 18015.

Bagchi A, Lucas GE, Suo Z, Evans AG, “A New Procedure For Measuring The Decohesion Energy For Thin Ductile Films On Substrates”, Journal of Material Research, Vol. 9, No. 7, pp. 1734–41, 1994.

Barenblatt, G. I., “The Mathematical Theory of Equilibrium Cracks in Brittle Fracture”, Advances in Applied Mechanics, Vol. VII, Dryden, H. L. and von Karman (Editors), Academic Press, New York, pp. 55-129, 1962.

Bjerken, C. and Persson, C., "A Numerical Method for Calculating Stress Intensity Factors for Interface Cracks in Bimaterials", Engineering Fracture Mechanics, Vol. 68, pp. 235-246, 2001.

Borg, R., Nilsson, L. and Simonsson, K., "Simulation of Delamination in Fiber Composites With a Discrete Cohesive Failure Model", Composites Science and Technology, Vol. 61, No. 5, pp. 667-677, 2001.

Borgesen, P., "Flip Chip on Organic Substrates", SMTA International – Proceedings of the Technical Program, Chicago, IL, 2000, pp. 121-127

Chandra, N., "Evaluation of Interfacial Fracture Toughness Using Cohesive Zone Model", Composites: Part A, Vol. 33, pp. 1433-1447, 2002.

Chandra, N., and Shet, C., "A Micromechanistic Perspective to Cohesive Zone Approach in Modeling Fracture", www.fsu.edu, 2004.

Cheng, Z., Xu, B., Zhang, Q., Cai, X., Huang, W. and Xie, X., "Underfill Delamination Analysis of Flip Chip on Low Cost Board", Proceedings of the International Symposium on Electronic Materials and Packaging, pp. 280-285, 2001.

Cheuk, P. T., Tong, L., Wang, C. H., Baker, A. and Chalkley, P., "Fatigue Crack Growth in Adhesively Bonded Composite Metal Double Lap Joints", Composite Structures, Vol. 57, pp. 109-115, 2002.

Chowdhury, S. R. and Narasimhan, R., "A Finite Element Analysis of Quasistatic Crack Growth in a Pressure Sensitive Constrained Ductile Layer", Engineering Fracture Mechanics, Vol. 66, pp. 551-571, 2000.

Cui, W. and Wisnom, M. R., "A Combined Stess-based and Fracture Mechanics Based Model for Predicting Delamination in Composites", Composites, Vol. 24, pp. 467-474, 1993.

Darbha, K., Okura, J., Shetty, S., Dasgupta, A., Reinikainen, T., Zhu, J., and Caers, J., "Thermomechanical Durability Analysis of Flip Chip Solder Interconnects: Part 2 – With Underfill", Transactions of ASME – Journal of Electronics Packaging, Vol. 121, December 1999, pp. 237-24.

Davidson, B. D. and Sundararaman, V., "A Single Leg Bending Test for Interfacial Fracture Toughness Determination", International Journal of Fracture, Vol. 78, 193-210, 1996.

De, D. and Narasimhan, R., “Analysis of an Interface Fracture Specimen For Adhesively Bonded Joints”, International Journal of Fracture, Vol. 92, pp. L35-L40, 1998.

Dessureault, M. and Spelt, J. K., “Observations of Fatigue Crack Initiation and Propagation in an Epoxy Adhesive”, International Journal of Adhesion and Adhesives, Vol. 17, pp. 183-195, 1997.

Ducept, F., Gamby, D. and Davies, P., “A Mixed Mode Failure Criterion Derived from Tests on Symmetric and Asymmetric Specimens”, Composites Science and Technology, Vol. 59, 609-619, 1999.

Dudek, R., Schubert, A., and Michel, B., “Analyses of Flip Chip Attach Reliability”, Proceedings of the 4th International Conference on Adhesive Joining and Coating Technology in Electronics Manufacturing, San Francisco, CA, 2000, pp. 77-85.

Dugdale, D. S., “Yielding in Steel Sheets Containing Slits”, Journal of Mechanics and Physics of Solids, Vol. 8, pp. 100-104, 1960.

England, A. H., “A Crack Between Dissimilar Media”, Journal of Applied Mechanics, Vol. 32, pp. 400-402, 1965.

Erdogan, F., “Stress Distribution in a Non-homogenous Elastic Plane With Cracks”, Journal of Applied Mechanics, Vol. 30, pp. 232-236, 1963.

Fan, X. J., Wang, H. B. and Lim, T. B., “Investigation of the Underfill Delamination and Cracking in Flip Chip Modules Under Temperature Cyclic Loading”, Proceedings of the Electronic Components and Technology Conference, pp. 994-1000, 1999.

Feng, X. -Q., “Analyses of Damage Localization at Crack Tip in a Brittle Damaged Material”, Engineering Fracture Mechanics, Vol. 53, No. 2, pp. 169-177, 1996.

Fernlund, G. and Spelt, J. K., “Failure Load Prediction of Structural Adhesive Joints Part 2: Experimental Study”, International Journal of Adhesion and Adhesives, Vol. 11, No. 4, 221-227. 1991.

Figiel, L., and Kamiski, M., “Mechanical And Thermal Fatigue Delamination Of Curved Layered Composites”, Computers & Structures, Vol. 81, No. 18-19, pp. 1865-1873, 2003.

Gaudette, F. G., Giannapoulos, A. E., and Suresh, S., “Interface Cracks in Layered Materials Subjected to Uniform Temperature Change”, International Journal of Fracture, Vol. 110, pp. 325-349, 2001.

Goh, T., "Thermal and Mechanical Reliability Loading Effects on the Reliability of Organic Flip Chip Package", ASME Journal of Electronic Packaging, Vol. 123, No. 1, 2001, pp. 83-87.

Goyal, V. K., Johnson, E. R., Davilla, C. G. and Jaunky, N., "An Irreversible Constitutive Law for Modeling the Delamination Process Using Interface Elements", American Institute of Aeronautics and Astronautics, No. 2002-1576, 2002.

Gross, K., Hackett, S., Schultz, W., Thompson, W., Zhang, Z., Fan, L., and Wong, C.P., "Nanocomposite Underfills for Flip Chip Applications", Proceedings of the Electronic Components and Technology Conference, New Orleans, LA, pp. 951-956, 2003.

Gu, Yu., Nakamura, T., Chen, W. T. and Cotterell, B., "Interfacial Delamination Near Solder Bumps and UBM in Flip Chip Packages", Transactions of ASME – Journal of Electronic Packaging, Vol. 123, pp. 295-301, September 2001.

Guo, Ya-Jun, Weitsman, Y. J., "A Modified DCB Specimen to Determine Mixed Mode Fracture Toughness of Adhesives", Engineering Fracture Mechanics, Vol. 68, 1647-1668, 2001.

Gurumurthy, C. K., C. K., Norris, L. G., Hui, C. –Y. and Kramer, E. J., "Characterization of Underfill/Passivation Interfacial Adhesion for Direct Chip Attach Assemblies Using Fracture Toughness and Hydro-Thermal Fatigue Measurements", Proceedings of the Electronic Components and Technology Conference, pp. 721-728, 1998a.

Gurumurthy, C. K., Jiao, J., Norris, L. G., Hui, C. –Y. and Kramer, E. J., "A Thermo-Mechanical Approach to Fatigue Testing of Polymer Bimaterial Interfaces", Transactions of ASME – Journal of Electronic Packaging, Vol.120, pp. 372-378, December 1998b.

Harries R. and Sitaraman, S. K., "Numerical Modeling of Interfacial Delamination Propagation in a Novel Peripheral Array Package", IEEE Transactions on Components and Packaging Technologies, Vol. 24, No. 2, pp. 256-264, June 2001.

Harris, J. A. and Fay, P. A., "Fatigue Life Evaluation of Structural Adhesives for Automotive Applications", International Journal of Adhesion and Adhesives, Vol. 12, No. 1, pp. 9-18, 1992.

He, M. E. and Hutchinson, J. W., "Kinking of a crack out of an interface," Journal of Applied Mechanics, Vol. 56, pp. 270-278, 1989.

Huang, Y., Liu, C. and Stout, M. G., “A Brazilian Disk for Measuring Fracture Toughness of Orthotropic Materials”, Acta Materialia, Vol. 44, No. 3, pp. 1223-1232, 1996.

Im., J –H., Shaffer, E. O., Stokich T., Jr., Strandjord, A., Hetzner, J., Curphy, J., Karas, C., Meyers, G., Hawn, D., Chakrabarti, A., and Froelicher, S., “On the Mechanical Reliability of Photo-BCB Based Thin Film Dielectric Polymer for Electronic Packaging Applications”, Journal of Electronic Packaging – Transactions of ASME, Vol. 122, pp. 28-33, March 2000

ITRS Roadmap for Semiconductors – 2002 Update, public.itrs.net

Kenane, M. and Benzeggagh, M. L., “Mixed Mode Delamination Fracture Toughness of Unidirectional Glass-Epoxy Composites Under Fatigue Loading”, Composite Science and Technology, Vol. 57, pp. 597-605, 1997.

Klingbeil, N. W. and Beuth, J. L., “Interfacial Fracture Testing of Deposited Metal Layers Under Four Bending”, Engineering Fracture Mechanics, Vol. 56, No. 1, pp. 113-126, 1997.

Kook, S. –Y., Snodgrass, J.M., Kirtikar, A. and Dauskardt, R. H., “Adhesion and Reliability of Polymer/Inorganic Interfaces”, Transactions of ASME – Journal of Electronic Packaging, Vol.120, pp. 328-334, December 1998.

Krenk, S., Jonsson, J. and Hansen, L. P., “Fatigue Analysis and Testing of Adhesive Joints”, Engineering Fracture Mechanics, Vol. 53, No. 6, pp. 859-872, 1996.

Lai, Y. –H., Rakestraw, M. D. and Dillard, D. A., “The Cracked Lap Shear Specimen Revisited – A Closed Form Solution”, International Journal of Solids and Structures, Vol. 33, No.12, pp. 1725-1743, 1996.

Lam, W. K., Yeung, T. S., Teng, A. and Yuen, M. M. F., “A Method for Evaluating Delamination Between Epoxy Moulding Compunds and Different Plated Leadframes”, Proceedings of the International Symposium on Electronic Materials and Packaging, pp. 214-219, 2000.

Lau, J. H. and Lee, R. S. –W., “Effects of Underfill Delamination and Chip Size on the Reliability of Solder Bumped Flip Chip on Board”, The International Journal of Microcircuits and Electronic Packaging, Vol. 23, No. 1, pp. 33-39, 2000b.

Lau, J. H., Lee, R, S. –W. and Chang, C., “Effects of Underfill Material Properties on the Reliability of Solder Bumped Flip Chip on Board with Imperfect Underfill Encapsulants”, IEEE Transactions on Components and Packaging Technologies, Vol. 23, No. 2, pp. 323-333, June 2000a.

Le Gall, C. A., Qu, J. and McDowell, D. L., “Delamination Cracking in Encapsulated Flip Chips”, Proceedings of the Electronic Components and Technology Conference, pp. 430-434, 1996.

Lefebvre, D. R. and Dillard, D. A., “A Stress Singularity Approach for the Prediction of Fatigue Crack Initiation in Adhesive Bonds Part 1: Theory”, Journal of Adhesion, Vol. 70, pp. 119-138, 1999.

Lefebvre, D. R. and Dillard, D. A., “A Stress Singularity Approach for the Prediction of Fatigue Crack Initiation in Adhesive Bonds Part 2: Experimental”, Journal of Adhesion, Vol. 70, pp. 139-154, 1999.

Liechti, K. M. and Chai, Y. S., “Biaxial Loading Experiments for Determining Interfacial Fracture Toughness”, ASME Journal of Applied Mechanics, Vol. 58, pp. 680-687, 1991.

Liu, C., Huang, Y. and Stout, M. G., “Enhanced Mode II Fracture Toughness of an Epoxy Resin Due to Shear Banding”, Acta Materialia, Vol. 46, No. 16, pp. 5647-5661, 1998.

Liu, C., Huang, Y., Lovato, M. L. and Stout, M. G., “Measurement of the Fracture Toughness of a Fiber Reinforced Composite Using the Brazilian Disk Geometry”, International Journal of Fracture, Vol. 87, pp. 241-263, 1997.

Lu, H., Bailey, C., and Cross, M., “Reliability Analysis of Flip Chip Designs Via Computer Simulation”, ASME Journal of Electronic Packaging, Vol. 122, No. 3, 2000, pp.214-219.

Madenci, E., Shkarayev, S. and Mahajan, R., “Potential Failure Sites in a Flip Chip Package With and Without Underfill”, Transactions of ASME – Journal of Electronic Packaging, Vol. 120, pp. 336-341, December 1998.

Madhusudhana, K. S., and Narasimhan, R., “Experimental and Numerical Investigations of Mixed-Mode Crack Growth Resistance of a Ductile Adhesive Joint”, Engineering Fracture Mechanics, Vol. 69, pp. 865-883, 2002.

Mahalingam, S., “Flip Chip Reliability – Issues in Underfill Selection”, Masters Thesis, State University of New York at Binghamton, Binghamton, NY 13902, 2001.

Matos, P. P. L., McMeeking, R. M., Charalambides, P. G. and Drory, M. D., “A Method for Calculating Stress Intensities in Bimaterial Fracture”, International Journal of Fracture, Vol. 40, pp. 235-254, 1989.

Mercado, L. L., Sarihan, V. and Hauck, T., “An Analysis of Interface Delamination in Flip Chip Packages”, Proceedings of the Electronic Components and Technology Conference, pp. 1332-1337, 2000.

Mi, Y., Crisfield, M. A. and Davies, G. A. O., “Progressive Delamination Using Interface Elements”, Journal of Composite Materials, Vol. 32, pp. 1246-1272, 1998.

Modi, M., and Sitaraman, S. K., “Interfacial Fracture Toughness Measurement For Thin Film Interfaces”, Engineering Fracture Mechanics, Vol. 71, No. 9-10, pp. 1219-1234, 2004.

Mohammed, I. and Liechti, K. M., “Cohesive Zone Modeling of Crack Nucleation at Bimaterial Corners”, Journal of Mechanics and Physics of Solids, Vol. 48, pp. 735-764, 2000.

Nagarajan, K. and Dauskardt, R. H., “Adhesion and Reliability of Underfill/Substrate Interfaces in Flip Chip BGA Packages: Metrology and Characterization”, Proceedings of SEMICON West, pp. 206-214, 2002.

Nairn, J. A., “Energy Release Rate Analysis for Adhesive and Laminate Double Cantilever Beam Specimens Emphasizing the Effect of Residual Stresses”, International Journal of Adhesion and Adhesives, 1999.

Needleman, A., “An Analysis of Decohesion Along an Imperfect Interface”, International Journal of Fracture, Vol. 42, pp. 21-20, 1990.

Nguyen, L. and Nguyen, H., “Effect of Underfill Fillet Configuration on Flip Chip Package Reliability”, Proceedings of SEMICON West, pp. 291-303, 2002.

O’Dowd, N. P., Shih, C. F., and Stout, M. G., “Test Geometries for Measuring Interfacial Fracture Toughness”, International Journal of Solids and Structures, Vol. 29, pp. 571-589, 1992.

Okura, J. H., Shetty, S., Ramakrishnan, B., Dasgupta, A., Caers, J. F. J. M. and Reinikainen, T., “Guidelines to Select Underfills for Flip Chip on Board Assemblies and Compliant Interposers for Chip Scale Package Assemblies”, Microelectronics Reliability, July 2000, Vo. 23, No.2, pp. 86-92.

Pang, H. L. G., Zhang, X. R., Lim, C. H., Shi, X. Q. and Wang, Z. P., “Interfacial Fracture Toughness Test Methodology for Flip Chip Underfill Encapsulant”, Proceedings of the Electronic Components and Technology Conference, pp. 1640-1644, 2002.

Pang, H. L. J., Bong, S. N., Shi, X. Q. and Wang Z. P., “Mixed Mode Fracture Toughness Characterization for Interface and Interlayer Cracks in Adhesive

Bonded Joints", Proceedings of the International Symposium on Electronic Materials and Packaging, pp. 197-200. 2000.

Pearson, R. A. and McAdams, B. J., "Initiation and Propagation of Delaminations Underfill/Passivation Interface in Flip Chip Assemblies", Proceedings of the Ninth International Symposium on Advanced Packaging Materials, pp. 280-283, 2004.

Pearson, R., Ayhan, A., and Nied, H., "Modeling the Mechanical Behavior of Underfill Resins and Predicting Their Performance in Flip-Chip Assemblies", Proceedings of the International Symposium on Advanced Packaging Materials, Boston, MA, 2000, pp. 63-67.

Petrossian, Z. and Wisnom, M. R., "Prediction of Delamination Initiation and Growth from Discontinuous Plies Using Interface Elements", Composites: Part A, Vol. 29A, pp. 503-515, 1998.

Popelar, S., "A Parametric Study of Flip Chip Reliability Based on Solder Fatigue Modeling: Part II – Flip Chip on Organic", Proceedings of the International Symposium on Microelectronics, San Jose, CA, 1998, pp. 497-504.

Prabhakumar, A., Rubinsztajn, S., Buckley, D., Campbell, J., Sherman, D., Esler, D., Fiveland, F., Chaudhuri, A. and Tonapi, S., "Development of Novel No-flow Underfill Material for Flip Chip Applications", Proceedings of the 5th Electronic Packaging Technology Conference, pp. 429-434, 2003.

Prabhakumar, A., "System Based Materials Design for Wafer Level Underfills", Ph.D. Dissertation, State University of New York at Binghamton, 2004.

Prabhakumar, A., GE Global Research, private communication, 2005

Prasad, R., "Surface Mount Technology – Principles and Practice", Second Edition, Kluwer Academic Publishers, ISBN: 0412129213, 1997.

Qu, J. and Kuhl, A. M., "Interfacial Fracture Toughness Between Copper and Several Underfill Materials", from http://www.me.gatech.edu/jianmin.qu/Publication%20List.htm

Qu. J., and Wong, C. –P., "Effective Elastric Modulus for Underfill Material for Flip Chip Applications", IEEE Transactions On Components And Packaging Technologies, Vol. 25, No. 1, pp. 53-55, March 2002.

Rahul-Kumar, P., Jagota, A., Bennison, S. J. and Saigal, S., "Interfacial Failures in a Compressive Shear Strength Test of a Glass/Polymer Laminates", International Journal of Solids and Structures, Vol. 37, pp. 7281-7305, 2000.

Rahul-Kumar, P., Jagota, A., Bennison, S. J., Saigal, S. and Muralidhar, S., "Polymer Interfacial Fracture Simulations Using Cohesive Elements", Acta Materialia, Vol. 47, pp. 4161-4169, 1999.

Reedy, E. D., Mello, F. J. and Guess, T. R., "Modeling the Initiation and Growth of Delaminations in Composite Structures", Journal of Composite Materials, Vol. 31, pp. 812-831, 1997.

Ritter, J. E., Jacome, G. S., Pelch, J. R., Russell, T. P. and Lardner, T. J., "Controlling Subcritical Crack Growth at Epoxy/Glass Interfaces", Transactions of ASME – Journal of Electronic Packaging, Vol.124, pp. 328-333, December 2002.

Roe, K. L. and Siegmund, T., "An Irreversible Cohesive Zone Model for Interface Fatigue Crack Growth Simulation", Engineering Fracture Mechanics, Vol. 70, 209-232, 2003.

Rubinsztajn, S., Campbell, J.R., Buckley, D., Sherman, D.M., Prabhakumar, A., Fiveland, E., Esler, D., and Tonapi, S., "Development of a Novel Filler Technology for No-Flow and Wafer Level Underfills", Proceedings of 3rd International IEEE Conference on Polymers and Adhesives in Microelectronics and Photonics, Montereux, Switzerland, 2003.

Rybicki, E. F. and Kanninen, M. F., "A Finite Element Method of Stress Intensity Factors by a Modified Crack Closure Integral", Engineering Fracture Mechanics, Vol. 9, pp. 931-938, 1977.

Rzepka, S., Feustel, F., Meusel, E., Korhonen, M. A. and Li, C. –Y., "The Effect of Underfill Imperfections on the Reliability of Flip Chip Modules: FEM Simulations and Experiments", Proceedings of the Electronic Components and Technology Conference, pp. 362-370, 1998.

Saitoh, T., Matsuyama, H. and Toya, M., "Linear Fracture Mechanics Analysis on Growth of Interfacial Delamination in LSI Plastic Packages Under Temperature Cyclic Loading", IEEE Transactions on Components, Packaging and Manufacturing Technology – Part B, Vol. 21, No. 4, pp. 422-427, November 2000a.

Saitoh, T., Matsuyama, H. and Toya, M., "Linear Fracture Mechanics Analysis on Growth of Interfacial Delamination in LSI Plastic Packages Under Temperature Cyclic Loading – Part 2: Material Properties and Package Geometry Factors", IEEE Transactions on Advanced Packaging, Vol. 23, No. 3, pp. 554-560, August 2000b.

Saponara, V. L., Muliana, H., Haj-Ali, Rami and Kardomateas, G. A., "Experimental and Numerical Analysis of Delamination Growth in Double

Cantilever Laminated Beams", Engineering Fracture Mechanics, Vol. 69, pp. 687-699, 2002.

Shaffer, E. O., Sikorski, S. A., McGarry F. J., in Materials Reliability in Microelectronics IV, edited by Borgesen, P., and Coburn, J. C., Sinchez, J. E. Jr., Rodbell, K. P., and Filter, W. F., Mater. Res. Soc. Symp. Proc. 338, Pittsburgh, PA, 1994, pp.541-551.

Shetty, D. K., Rosenfield, A. R. and Duckworth, W. H., "Mixed Mode Fracture in Biaxial Stress State: Application of the Diametral Compression (Brazilian Disk) Test", Engineering Fracture Mechanics, Vol. 26, No. 6, pp. 825-840, 1987.

Shi, S., Yao, Q., Qu, J., and Wong, C. P., "Study on the Correlation of Flip-Chip Reliability With Mechanical Properties of No-Flow Underfills", Proceedings of the International Symposium on Advanced Packaging Materials, San Francisco, CA, 2000, pp. 271-277.

Shi, X. Q., Wang, Z. P. and Pickering, J. P., "A New Methodology for the Characterization of Fracture Toughness of Filled Epoxy Films Involved in Microelectronics Packages", Microelectronics and Reliability, Vol. 43, No. 7. pp. 1105-1115, 2003.

Shim, J., Ahn, E., Cho, T., Moon, H., and Chung, T., "Mechanisms of Die and Underfill Cracking in Flip Chip PBGA Package", Proceedings of the International Symposium on Advanced Packaging Materials, San Francisco, CA, 2000, pp. 201-205.

Smith, B., Thorpe, R., and Baldwin, D., "A Reliability and Failure Mode Analysis of No Flow Underfill Materials for Low Cost Flip Chip Assembly", Proceedings of the Electronic Components and Technology Conference, Orlando, FL, 2000, pp. 1719-1730.

Snodgrass, J. M., Pantelidis, D., Jenkins, M. L., Bravman, J. C. and Dauskardt, R. H., "Subcritical Debonding of Polymer/Silica Interfaces Under Monotonic and Cyclic Loading", Acta Materialia, No. 50, pp. 2935-2411, 2002.

Sundararaman, V. and Davidson, B. D., "An Unsymmetric Double Cantilever Beam Test for Interfacial Fracture Toughness Determination", International Journal of Solids and Structures, Vol. 34, No. 7, pp. 799-817, 1997.

Sundararaman, V. and Davidson, B. D., "An Unsymmetric End-Notched Flexure Test for Interfacial Fracture Determination", Engineering Fracture Mechanics, Vol. 60, No. 3, pp. 361-377, 1998.

Sundararaman, V. and Sitaraman, S. K., “Determination of Fracture Toughness of Metal/Polymer Interfaces”, Transactions of ASME – Journal of Electronic Packaging, Vol. 121, pp. 275-281, December 1999.

Sundararaman, V., Harries, R. and Sitaraman, S. K., “Fracture Mechanics Based Delamination Growth Prediction in the Very Small Peripheral Array (VSPA) Package”, Proceedings of the IEEE-CPMT Electronics Packaging Technology Conference, pp. 160-169.

Suo, Z. and Hutchinson, J. W., “Interface Crack Between Two Elastic Layers”, International Journal of Fracture, Vol. 43, pp. 1-18, 1990.

Suo, Z. and Hutchinson, J., “Sandwich Test Specimens for Measuring Interface Crack Toughness”, Material Science and Engineering, A107, pp. 135-143, 1989.

Suryanarayana, D., Hsiao, R., Gall, T. P., and McCreary, J. M., “Enhancement of Flip-Chip Fatigue Life by Encapsulation”, IEEE Transactions on Components, Hybrids, and Manufacturing Technology, Vol. 4, No. 1, 1991, pp. 218-223.

Swadener, J. G., Liechti, K. M. and de Lozanne, A. L., “The Intrinsic Toughness and Adhesion Mechanisms of a Glass/Epoxy Interface”, Journal of the Mechanics and Physics of Solids, Vol. 47, 223-258, 1999.

Tomar, V., “Bounds for Element Size in a Variable Stiffness Cohesive Finite Element Model”, International Journal of Numerical Methods in Engineering, Vol. 61, 2004.

Tsukada, Y., Nishimura, H., Sakane, M., and Ohnami, M., “Fatigue Life Analysis of Solder Joints in Flip Chip Bonding”, ASME Journal of Electronic Packaging, Vol. 122, No. 3, 2000, pp. 207-213.

Tvergaard, V. and Hutchinson, J. W., “Toughness of an Interface Along a Thin Ductile Layer Joining Elastic Solids”, Philisophical Magazine A, Vol. 70, No. 4, pp. 641-656, 1994.

Tvergaard, V. and Hutchinson, J., “The Relation Between Crack Growth Resistance and Fracture Parameters in Elastic-Plastic Solids”, Journal of Mechanics and Physics of Solids, Vol. 40, No. 6, pp. 1377-1397, 1992.

Tvergaard, V. and Hutchinson, S. W., “On the Toughness of Ductile Adhesive Joints”, Journal of Mechanics and Physics of Solids, Vol. 44, No. 5, pp. 789-800, 1996.

Venkatesha, K. S., Ramamurthy, T. S. and Dattaguru, B., “Generalized Modified Crack Closure Integral (GMCCI) and Its Application to Interface Crack Problems”, Computers and Structures, Vol. 60, No. 4, pp. 665-676, 1996.

Wang, J, -S., and Suo, Z., "Experimental Determination of Interfacial Toughness Curves Using Brazil Nut Sandwiches", Acta Metallurgica Materialia, Vol. 38, No. 7, 1279-1290, 1990.

Wang, J., Lu, M., Ren, W., Zou, D. and Liu, Sheng., "A Study of the Mixed Mode Interfacial Fracture Toughness of Adhesive Joints Using a Multiaxial Fatigue Tester", IEEE Transactions on Electronics Packaging Manufacturing, Vol .22, No. 2, pp. 166-173, April 1999.

Wang, L. and Wong, C.P. ,"Recent Advances in Underfill Technology for Flip Chip, Ball Grid Array, and Chip scale Package Applications", Proceedings of International Symposium on Electronic Materials and Packaging, Braselton, GA, pp. 224- 31, 2001.

Wang, J., Zou, D., Lu, M., Ren, W. and Liu, S., "Evaluation of Interfacial Fracture Toughness of a Flip Chip Package and a Bimaterial System by a Combined Experimental and Numerical Method", Engineering Fracture Toughness, Vol. 64, pp. 781-797, 1999.

Wang, X. –M., "The Dugdale Crack on Bimaterial Interface", International Journal of Fracture, Vol. 59, pp. R25-R32, 1993.

Williams, M. L., "The Stresses Around a Fault or a Crack in Dissimilar Media", Bulletin of the Seismological Society of America, Vol. 49, No. 2, pp. 199-204, 1959.

Wu, D., Su, B., Lee, Y. C. and Dunn, M. L., "Prediction of Fatigue Crack Initiation Between Underfill Epoxy and Substrate", Proceedings of Electronic Components and Technology Conference, pp. 646-649, 2000.

Xie, W. and Sitaraman, S. K., "An Experimental Technique to Determine Critical Stress Intensity Factors for Delamination Initiation", Engineering Fracture Mechanics, Vol. 70, 1193-1201, 2003.

Xu, A. Q. and Nied, H. F., "Finite Element Analysis of Stress Singularities in Attached Flip Chip Packages", Transactions of ASME – Journal of Electronic Packaging, Vol. 122, pp. 301-305, December 2000.

Xu, X. X., Crocombe, A. D. and Smith, P. A., "Mixed Mode Fatigue and Fracture Behavior of Joints Bonded with Either Filled or Filled and Toughened Adhesive", International Journal of Fatigue, Vol. 17, No. 4, pp. 27-286, 1995.

Xu, B., Cai, X., Huang, W., and Cheng, Z., "Research of Underfill Delamination in Flip Chip by the J Integral Method", Transactions of the ASME - Journal of Electronic Packaging, Vol. 126, No. 1, pp. 94-99, March 2004.

Yao, Q. and Qu, J., “Effect of Thermal Residual Stresses on the Apparent Interfacial Fracture Toughness of Polymer/Metal Interface”, Proceedings of the Electronic Components and Technology Conference, pp. 365-368, 1999a.

Yao, Q. and Qu, J., “Quantitative Characterization of Underfill/Substrate Interfacial Toughness Enhancement by Silane Additives”, Proceedings of the Electronic Components and Technology Conference, pp. 1079-1082, 1999b.

Yeung, D. T. S., Lam, D. C. C. and Yuen, M. M. F., “Specimen Design for Mixed Mode Interfacial Fracture Properties Measurement in Electronic Packages”, Transactions of ASME - Journal of Electronic Packaging, Vol. 122, pp. 67-72, March 2000.

Zavattieri, P. D. and Espinosa, H. D., “Grain Level Analysis of Crack Initiation and Propagation in Brittle Materials”, Acta Materialia, Vol. 49, pp. 4291-4311, 2001.

Zhai, C. J., Sidharth, Blish II, R. C. and Master, R. N., “Investigation and Minimization of Underfill Delamination in Flip Chip Packages”, Proceedings of the International Symposium of Advanced Packaging Materials, 2004.

Zhang, J., “Fatigue Crack Propagation Behavior of Underfill Materials in Microelectronics Packaging”, Material Science and Engineering, A314, pp. 194-200, 2001.

Zou, Z., Reid, S. R. and Li, S., “A Continuum Damage Model for Delaminations in Laminated Composites”, Journal of the Mechanics and Physics of Solids, Vol. 51, pp. 333-356, 2003.

VITA

Sakethraman Mahalingam was born in the coastal town of Cuddalore in the state of Tamil Nadu, India on October 7, 1977. He completed his Bachelor of Engineering degree from Coimbatore Institute of Technology in June 1998. After working for Baan Company as a software engineer for a year, he moved to the State University of New York, Binghamton to pursue his Masters degree in Industrial Engineering. In August 2001, he started pursuing his doctoral studies under the guidance of Dr. Suresh Sitaraman at the G. W. Woodruff School of Mechanical Engineering, Georgia Institute of Technology. At Georgia Tech., he was involved in research with the Microsystems Packaging Research Center (PRC) focusing on the reliability of Printed Wiring Boards (PWB). He spent his time between Summer 2003 to Spring 2005 at the General Electric Global Research Center in Bangalore, India as an intern. During this time, he focused on the reliability of novel, nano-filled no-flow underfill materials for flip chip packaging. He received his Ph.D. in August 2005.